The Study of a Hybrid-SELEX Method for the Development and Characterisation of an Aptamer to the Dendritic Cell Surface Receptor: Clec9A

Thesis submitted in partial fulfilment of the requirements for the degree of

Master of Science in Biotechnology

Rebecca Susan Jestin Palmer

School of Biological Sciences

Victoria University of Wellington

Te Herenga Waka

2022

ABSTRACT

Current immunotherapies utilise antibodies to inhibit or aid immunological functions, or as delivery vehicles capable of targeting therapeutic drugs to the immune system. However, the limitations of antibodies compromises the growth of the field of immunotherapy and thus investigations into new avenues should be fast-tracked. One potential avenue is the use of aptamers. Aptamers are single stranded pieces of DNA that, through the formation of unique 3D-structures specific to the sequence, have the capacity to bind virtually any molecule of interest due to their creation through systematic evolution of ligands by exponential enrichment, or SELEX. They have shown to exhibit great potential for immunotherapies and specifically, mitigate the limitations presented by antibodies. Aptamers can be developed to bind cell surface receptors that play a role in the immunological response. Furthermore, direct conjugation with immunostimulants such as antigenic peptides or adjuvants could elicit direct and tailored responses. A receptor of interest is the class V C-type lectin receptor, Clec9A. Clec9A is found on a small subset of dendritic cells and its restricted nature makes it highly desirable for targeted antigen delivery.

In this study, I hypothesised that a novel Hybrid-SELEX approach would generate aptamers with high affinity and specificity to their cognate target. This was tested by utilising the Hybrid-SELEX to develop a DNA aptamer to Clec9A. This was achieved by firstly enriching a random oligonucleotide library to recombinant Clec9A immobilized on magnetic beads and then to its natural state as cell receptors on $CD8^+$ cDCs. A bioinformatics pipeline was applied to NGS data to identify potential aptamers that bind Clec9A which was based on a range of criteria shown to be indicative of target affinity. These included, reads per million, cluster number, enrichment, and rank. Candidate aptamers were screened for their affinity to Clec9A using two established characterization techniques, a modified gold nanoparticle assay and circular dichroism (CD) spectroscopy. CD spectroscopy results found four candidate aptamers that were suggested to exhibit an affinity to Clec9A, however, further experiments will need to be performed to confirm this. Furthermore, this study highlights the necessity for standardized and robust characterization procedures to obtain reproducible, comparable and reliable results.

In summary, A novel hybrid approach of SELEX technology four potential aptamer candidates that exhibited specific binding interactions towards Clec9a.

ACKNOWLEDGEMENTS

Ehara tōku toa i te toa takitahi. He toa takitini tōku toa.

My strength is not due to me alone, but due to the strength of many.

I feel extremely lucky to have been supported and surrounded by so many smart, inspiring and hardworking scientists in the past two years. I feel especially grateful to have been led by two unbelievably exceptional women in STEM who I look up to so much. Janet and Jen, I am deeply grateful to have been able to grow and learn under your guidance. You challenged me to think about science in a deep and meaningful way and allowed me to see my strengths and had faith in my abilities when I could not. Thank you for all the opportunities you have given me and the hard work, time, patience and care you have put in to helping my produce my thesis.

To my family, thank you for everything. Thank you for providing me with the opportunity to peruse whatever I wanted in life and being equally excited and passionate about it. Thank you for instilling me with the tools to succeed, hard work and commitment and an enthusiastic attitude. Thank you for financially supporting me to allow me to focus purely on my thesis for this last year. I am in an extremely privileged position and hope that I have made just use of these opportunities. I would not be here today if it wasn't for your love, support, homemade lasagna, lunch dates, and late-night phone calls assuring me everything will work out. I needed it more this past year than ever. I am extremely lucky and thankful.

To Will, my number one fan, thank you for your unwavering support. Thank you for sharing my excitements, shouldering my stresses, listening to me. Thank you for providing me with a space to thrive. Thank you for always matching my excitement and energy, extending your hand to help me in whatever way I needed (even when I didn't know what I needed). Whether that be proofreading my work, picking me up at late hours of the night, listening to my 'plans' because you know I need to voice them to do then, and keeping me fed with delicious snacks. Thank you for helping me confront my vulnerabilities and find strength from them. You never stopped believing in me and I could not have done this without you.

To my besties, thank you. Thank you for listening to me excitedly explain complex scientific concepts and enthusiastically listen. Thank you for being a space to complain, brainstorm stress, even cry. Thank you for being there to help me unwind after a stressful day and helping

me see the lighter side of life when I was all rain clouds and thunderstorms. You are my family away from home. Thank you for always lifting me up and encouraging me to keep going. Your friendship is immeasurable.

To Sophia, thank you for undertaking this journey with me. Thank you for learning and growing with me. You helped me reground myself on days where I felt overwhelmed. You helped me find strength and motivation in moments of weakness. We did this and I am so proud of you.

Thank you to the Pitman group. Hamish and Odey, thank you for your patience and willingness to help me learn new techniques. Thank you for providing your insight and knowledge to my work. Sarah, Zara, Mel, Matire, Amey, Niamh, Ellie, Ben, and Stacey. Thank you for all your kind words of encouragement, checking to see how I was getting on, your support and friendship.

Thank you to Ian Hermans' lab group at the Malaghan Institute of Medical Research for donating the DC2114 cell line and helping with flow cytometry experiments. Thank you for providing guidance, expertise, and support to my project.

Finally, thank you to you, the reader. Thank you for taking the time to read this thesis and see the growth of a young scientist behind it. I have loved this project so much.

CONTENTS

List of Figures

List of Tables

List of Abbreviations

2ME:	2-Mercaptoethanol
ADP:	Adenosine diphosphate
AMP:	Adenosine monophosphate
ANOVA:	Analysis of variance
APC:	Antigen-presenting cell
ASF:	Area scaling factor
ATP:	Adenosine triphosphate
AuNP:	Gold nanoparticle
bp:	Base pair
CD:	Circular dichroism (spectroscopy)
cDCs:	Classical dendritic cells
cDNA:	Complementary deoxyribonucleic acid
CHO:	Chinese hamster ovary
CO_2:	Carbon dioxide
Cq:	Quantitation cycle
CSV:	Comma separated values
DAMPs:	Danger associated molecular patterns
DC:	Dendritic cell
ddH_2O:	Double distilled water
ddNTP:	Deoxyribonucleotides
Df:	Dilution factor
DMSO:	Dimethyl sulfoxide
DNA:	Deoxyribonucleic acid
dsDNA:	Double stranded DNA
E:	Reaction efficiency
ELONA:	Enzyme linked oligonucleotide assay
FACS buffer:	Flow cytometry staining buffer
FACS:	Fluorescence activated cell sorting
FBS:	Fetal bovine serum (look up Fetal or Foetal)
FDA:	Food and Drug Administration
FMO:	Fluorescence minus one
FSC- A:	Forward scatter area
FSC:	Forward scatter
FSC-H:	Forward scatter height
g:	g-force
GTG:	Genetic technology grade
HCl:	Hydrochloric acid
HNO_3:	Nitric acid
IDT:	Integrated DNA technologies
IMDM:	Iscove's Modified Dulbecco's Medium
ITC:	Isothermal titration calorimetry
K_a:	Binding affinity
KH_2PO_4:	Potassium phosphate monobasic
M:	Slope
MDB:	Membrane desalting buffer
MEMα:	Minimum essential medium α

MHC:	Major histocompatibility complex (I or II)
mRNA:	Messenger RNA
N_2	Nitrogen gas
Na_2HPO_4-$7H_2O$:	Sodium Phosphate dibasic
NaCl:	Sodium chloride
$NaHCO_3$:	Sodium bicarbonate
NaOH:	Sodium hydroxide
NGS:	Next-generation sequencing
NK cells:	Natural killer cells
PBS:	Phosphate buffered saline
PBS:	Phosphate buffered saline
PCR:	Polymerase chain reaction
PE:	Phycoerythrin
Pen/Strep:	Penicillin/streptomycin
PPE:	Personal protective equipment
PRR:	Pattern recognition receptor
QG:	Solubilisation and binding buffer
qPCR:	Quantitative polymerase chain reaction
R^2:	Coefficient of determination
RBC Buffer:	Red blood cell lysis buffer
RCF:	Relative centrifugal force
RNA:	Ribonucleic acid
RPM:	Reads per million
RPM:	Revolutions per minute
SELEX:	Systematic evolution of ligands by exponential enrichment
SPR:	Surface plasmon resonance
SSC:	Side scatter
SSC-A:	Side scatter area
SSC-H:	Side scatter height
ssDNA:	Single stranded DNA
TBA:	Thrombin binding aptamer
TCEP:	Tris(2-carboxyethyl)phosphine
TLR:	Toll-like receptor
ΔG:	Delta G
ΔH:	Gibbs free energy
ΔS:	Enthalpy change

CHAPTER 1 LITERATURE REVIEW

Section 1.1 The Role of Dendritic Cells in the Immune System

The immune system is a series of intricate pathways. It has the responsibility of clearing pathogenic invasions from the body that cause disease and in response, provides the body with future immunity from subsequent and similar invasions. The two arms of the immune system, innate and adaptive, operate in synergy to perform this enormous and important function. For this to occur effectively, the immune system relies heavily on the support of dendritic cells (DCs). DCs are intelligent antigen-presenting cells (APCs) and their role is at the interface of innate and adaptive immunity. They are the only APCs that induce primary immune responses, leading to immunological memory (Tokoyoda et al., 2010). DCs are aptly described as surveyors of the immune system, where their role in the peripheral tissues is to uptake extracellular fluid through the process of phagocytosis or macropinocytosis (Kenneth Murphy, 2017; Swanson & Watts, 1995) The DC uses phagocytosis to preserve pathogenic material rather than to destroy it. This aids in the generation of an immune response by saving the essential information of the pathogen required for T cell presentation and stimulation (Savina & Amigorena, 2007). The routine uptake and processing of particulate matter and extracellular fluid by immature DCs provide continuous surveillance of the immune system. In this role, DCs display processed particulate matter in two ways. Exogenous material is recognised by major histocompatibility complex (MHC) class II molecules and presented to $CD4^{+ve}$ T cells which secrete cytokines and interferons to aid in B cell antibody development (Zhu & Paul, 2008). Secondly, DCs can also present antigens to MHC class I molecules from endogenous or exogenous origins. The classical MHC I presentation pathway involves the recognition and presentation of endogenous pathogenic material by the DCs to their MHC class I molecules and in doing so, stimulates $CD8^{+ve}$ T cells to respond and carry out cytotoxic function, killing cells that present pathogenic material. Alternatively, the MHC I presentation pathway can be manipulated to present exogenous material through a process known as cross-presentation. This allows the DCs to specifically prime $CD8^{+ve}$ T cells to detect and exhibit cytotoxic function, killing the invading pathogen (Heath et al., 2004; Joffre et al., 2012). The processes in which the DCs capture antigens is sophisticated and performed at high rates, specifically two orders of magnitude faster than any other antigen-presenting cells (Liu & Nussenzweig, 2010). Without the influence of DCs, unity between innate and adaptive immunity would not be possible.

Section 1.2 Current Trends in Immunotherapy

Immunotherapies are treatments that introduce allergens or antigens to a host in a regulated manner, to create an efficient immunological response. Presenting the body with immunostimulants reduces the severity of disease in subsequent exposure (Gordon, 1995). Understanding how immunological responses occur has allowed for medical intervention via vaccines to treat many forms of infectious disease. A greater understanding of the intricacies of our immune system has given rise to tailored therapies such as active and passive immunotherapy. Active immunotherapy has a primary focus to enhance the current role of APCs by sensitising them to disease-specific antigens. Recognition of antigen by APCs causes the recruitment of T cells via co-stimulatory signals produced by the APC. This leads to activation and clearance of infection (Bregy et al., 2013; Pardoll, 2002). Treating disease in this way is preventative if subsequent exposure to the disease is a risk. Activation of T cells from the presentation of antigen on APCs causes the cells to differentiate into effector and memory cells. Memory cells are essential for long term immunity and are readily activated under secondary exposure to the disease, while effector cells are utilised immediately in the immune response to clear infection (Kenneth Murphy, 2017).

Passive immunotherapy generates protective agents in the host towards disease-specific pathogens. The protective agents are collected via the blood and administered to a patient. Originally, the protective agent being used were antibodies, but recent use of T cells has been demonstrated. The T cells, stimulated with interleukins, are cultured and proliferated outside the patient and are then administered to them in their active form (Farran et al., 2019; Graham & Ambrosino, 2015; Murphy, 2010). Passive immunotherapy using antibodies and T cells requires multiple doses of the primed antibody to clear the infection. This can sometimes be circumvented by concurrently administering interleukin 2 (IL-2) or $CD4^+$ T cells (Ho et al., 2002).

1.2.1 Dendritic cell-based immunotherapy

DCs are an attractive candidate for use in immunotherapy because their activation directly influences the immune response. DCs have been used for both passive and active therapies. Passive immunotherapy using DCs is linked to their competency for culture ex-*vivo,* as they can be externally matured to receive antigenic cargo onto MHC molecules for administration as a vaccine (Figdor et al., 2004). Of course, the main challenge for immunotherapy-based treatments involves generating the desired immune response through the appropriate use of

antigen. Early applications used peptides that have in the past been recognised by the MHC class I-specific T cell subsets. These peptides are epitopes of the antigen, ranging from 8-12 amino acids in length. Furthermore, they are specifically designed to be recognised by subsets of T cells presented on MHC class I or II by the DC to give rise to immunological activity (Mayordomo et al., 1995). In this vein, the peptides behave as stimulants to mature and activate the DC. Re-administration of these DCs into a patient stimulates peptide-specific T cell receptors on cytotoxic cells to manage and clear infection (Pardoll, 2002; Porgador & Gilboa, 1995; Schuler et al., 2003; Van Der Burg et al., 1996). Other approaches include the use of gene transfer vectors to produce cells that contain genetic material specific to the antigen of interest (Song et al., 1997). Alternatively, tumour cell-derived messenger RNA (mRNA) has been utilised similarly to amplify the antitumour response when tumour related antigens are inaccessible or only presented in small concentrations. By using mRNA, the DC can be presented with the whole transcriptome of the tumour cell. Thereby, leading to increased concentration of the tumour specific antigen (Boczkowski et al., 1996; Chen et al., 1996; Dyall et al., 2001; Pardoll, 2002).

Cell surface receptors expressed by DCs can be used for active immunotherapy. Receptors such as DEC205, an apoptotic cell recognition receptor, are exploited using antigenic peptides to stimulate a response via receptor-mediated endocytosis. This develops a highly directed approach to treatment and has been shown to provide stronger $CD8^{+ve}$ immune responses over other dendritic cell-based therapies (Bonifaz et al., 2004; Palucka et al., 2009). Other therapies rely on efficient homing (i.e. return to its territory after removal of the threat) of the DCs after administration into the patient. Targeting DCs within the host with specific delivery vehicles carrying antigenic cargo, offer an alternative approach to circumvent issues involved with homing. Overall, this creates a more direct treatment and targeted downstream immune responses. Some receptors of interest include pattern recognition receptors (PRR), C-type lectins or toll-like receptors (TLR) which either facilitate presentation to MHC class I or class II molecules, activating different T cell subsets (Kreutz et al., 2013). Antibodies are currently the main vehicle for antigenic delivery and have been used to target a range of dendritic cell receptors. For example, humoral immunity has been influenced when targeting lectins such as the mannose receptor (MR^4CD206) with an antibody loaded with antigenic peptide. Targeting

receptors that directly influence APC processing and presentation encourages the uptake of the antigen and promotes the relevant response (He et al., 2007).

1.2.2 Clec9A a C-Type Lectin Receptor as a Candidate for Targeted Immunotherapy

Clec9A is a receptor that belongs to the C-type lectin family. C-type lectins are attractive candidates for targeted DC-based immunotherapy as they are pattern recognition receptors that are programmed to detect danger associated molecular patterns (DAMPs). Detection of these patterns triggers a range of distinct functions such as producing inflammatory mediators, phagocytosing pathogens, or intracellular signalling (Mayer et al., 2018). Clec9A is a Class V C-type lectin, which as a group of lectin were thought to be exclusively expressed by natural killer cells (NK cells). However, Clec9A is unique in that it is primarily expressed on human BDCA3^{+ve} DCs, which are an extremely small subgroup of peripheral blood mononuclear cells (PBMC), incorporating only ~0.05% of all PBMC (Brown et al., 1997; Huysamen et al., 2008). The BDCA3^{+ve} classical DCs (cDC) are analogous to CD8^{+ve} cDCs in the mouse, which are specialized in antigenic cross-presentation in complex with MHC class I molecules. The differential expression of Clec9A on DCs, rather than NK cells, may be observed as an evolutionary trait. Furthermore, the highly restricted expression of Clec9A on DC subsets is an attractive target for biomedical purposes. Clec9A plays a role in immunity by recognising particulate matter of cells undergoing necrotic death from infection or trauma (Zhang et al., 2012). While these subsets are typically recognised and phagocytosed by macrophages, Clec9A can act as a backup in those cases where macrophages fail to do the job.

The binding of Clec9A is achieved through the affinity for exposed actin filaments in the damaged cells, which is the main ligand of Clec9A (Cueto et al., 2020). These filaments are more exposed on necrotic cells due to their damage (Zhang et al., 2012). Recognition of F actin by Clec9A leads to cross-presentation of this material to MHC class I molecules. Studies that used antibodies conjugated with ovalbumin antigen to target the Clec9A receptor investigated how Clec9A contributed to an immune response. It was found that Clec9A behaved as an endocytic receptor, and efficiently provided cross-presentation to MHC class I molecules (Caminschi et al., 2008). Furthermore, the omission of cross-presentation in *Clec9A*-deficient mice confirmed its role in an immune response (Sancho et al., 2009; Sancho et al., 2008). The cross-presentation abilities of Clec9A specifically, for danger associated molecular pattern recognition and the processing of antigens for presentation is regulated by the E3 ubiquitin

ligase, RNF41. It performs this role by ubiquitinating Clec9A for destruction to maintain steady levels of cell surface receptors (Tullett et al., 2020).

Even within its class V C-type lectin family, Clec9A is a unique receptor. It shares its closest structural homology to Clec8A (also referred to as OLR1) and phylogeny to Clec7A (Sancho et al., 2008; Zhang et al., 2012) (Figure 1.1), and while Clec9A forms a homodimer similarly to Clec8A, it is predicted to express only a single C-type lectin domain (Sancho et al., 2008). Harnessing the native endocytic features of Clec9A would be beneficial to progress in the field of immunotherapy. Caminschi *et al.* demonstrated that targeting to Clec9A, using anti-Clec9A antibody with antigenic peptide ovalbumin, resulted in a response that was much more sensitive than that observed with the antigenic peptide alone. Administration of the antigen alone required a 1000-fold greater dose to elicit a similar response (Caminschi et al., 2008).

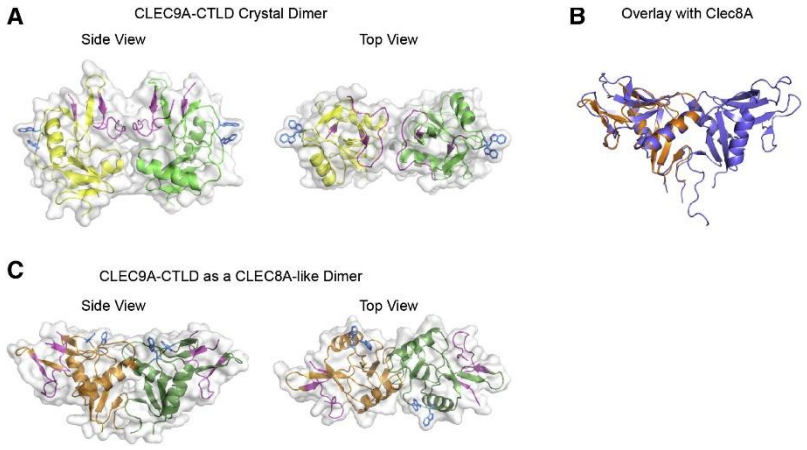

Figure 1.1: Crystal structure of Clec9A compared to Clec8A.
A) is shown as a dimer and is most unique for C-type lectin like domains. Areas in pink suggest binding areas for antibodies to target with antigen, furthermore, suggesting the presence of this area on the surface. B) Overlay with Cle8A to illustrate the homology of Clec9A to other C-type lectin members. Orange is Clec9A represented as a monomer compared with the Clec8A dimer shown in purple. C) Clec9A represented the way it would look if it was expressed as a Clec8A dimer. Slightly different in orientation to image A. Reprinted with permissions from (Zhang et al., 2012) and RightsLink

1.2.3 Limitations of Antibodies

Whilst antibodies have been established as a valuable tool in immunotherapy, they have their limitations. Therapeutic monoclonal antibodies are routinely used in immunotherapy and cancer therapy as stand-alone treatments.

Rituxan or Rituximab is the first therapeutic monoclonal antibody to be approved for cancer therapy and was used to treat non-Hodgkin's B-cell lymphoma (Firer & Gellerman, 2012; Yamada, 2011). Since Rituximab, many other antibodies for immunotherapy and cancer therapy have been established. As of May 2021, the US Food and Drug Administration (FDA)

has approved over 100 therapeutic monoclonal antibody products (Mullard, 2021). Whilst this illustrates the importance of antibody use in medicine, science is constantly seeking ways to improve the current landscape.

Antibodies are created by immunising a host animal such as a mouse with toxin or antigen. The spleen cells that contain B cells specific to the antigen are harvested to create antibodies. The materials used in the production of antibodies are required to be free of any pathogens, bacteria, fungus that would compromise production, and all animals used are required to meet specific pathogen free conditions (Morton et al., 2008). However, batch to batch variation is still prevalent, which affects purity, potency, and contamination. Moreover, antibody production is highly sensitive to alterations in purification protocols or variations in culture conditions, leading to changes in the antibody's functionality (Maiorella et al., 1993; Werner, 2004).

Following antibody generation, further methods are required to 'humanise' the antibodies borne from animal origin. Humanisation is achieved by substituting engineered amino acids to make the resultant antibody more like the human-derived form. It is difficult to determine the level of modification required for the antibody to pass as 'humanised'. While, incorrect humanisation may lead to adverse immune responses generated against mouse antibody sequence such as human anti-mouse antibodies. This results in the ultimate clearance of the antibody, which reduces its efficacy, and increases the chances of hypersensitivity. Cetuximab, a chimeric mouse-human monoclonal antibody, used to treat colorectal cancer and squamous cell carcinoma by binding to the epidermal growth factor receptor has been shown to induce hypersensitivity in 25 out of 76 patients (Chung et al., 2008). Even antibodies deemed 'fully human', such as two checkpoint blockade antibodies that target CTLA4 and PD-1, have been found to elicit adverse responses in the form of anaphylaxis and cardiac dysfunction, colitis, dermatitis, pneumonitis, and hepatitis (Demlová et al., 2016; Doessegger & Banholzer, 2015; Mall et al., 2016). Under these circumstances, repeated doses to maintain its efficacy, are not possible for these patients (Catapano & Papadopoulos, 2013; Reichert et al., 2005; Samaranayake et al., 2009). Dosage creates a twofold problem; single doses limits the efficacy of the treatment while repeated dosage can lead to unwanted immunogenicity. A typical administration of monoclonal antibodies for treatment ranges from 5-20 milligrams per

kilogram of patient body weight. This is required to maintain high antibody concentrations in plasma (Samaranayake et al., 2009).

The demand for safe and effective antibody production increases in parallel with the use of antibodies for therapeutics. These demands create a bottleneck in manufacturing and production. Antibody manufacturing is large scale, so companies tend to outsource manufacturing to achieve high volume returns. However, this is only available when resources are abundant. Antibodies for therapeutic purposes make up a considerable proportion of all FDA approved filings, creating a bottleneck in the current climate. Factors contributing to this bottleneck include the ongoing COVID-19 pandemic, and secondly, the need for repeated doses of antibody to create a viable treatment in antibody-based therapy. These factors together, create a strain on the availability of antibodies (Langer, 2009; Werner, 2004). Furthermore, the more complex and laborious the manufacturing and clinical trial processes, the greater the cost. Since 2007, the cost of bringing a new pharmaceutical antibody to market averaged around USD 1.6 billion, with a success rate of 30%. Over time, the success rate has decreased while the cost continues to rise. In 2016, the success rate had dropped to 12% and the cost of development increased to USD 3.1 billion (2021 Q4 dollars) (Elvin et al., 2013; Farid et al., 2020). It is expected that the global monoclonal antibody market will exceed USD 380 billion by 2027 (Inc., 2021) and unfortunately, these costs are shouldered by the consumer who desperately requires the treatment and has no choice. The average cost for monoclonal antibody therapy for a patient over a year in 2018 was USD 96,731 but can reach up to USD 200,000 per year (Hernandez et al., 2018; Shaughnessy, 2012).

Relating to their performance, immunotherapies such as targeted drug or peptide delivery require internalisation via binding of endocytic receptors to deliver cargo directly into the cell. The ability of antibodies to internalise into a cell during production is often not considered (Firer & Gellerman, 2012) and can vary in internalisation efficiencies, thus reducing their efficacy. Additionally, antibody size limits the antibody's capability as a therapeutic tool. Due to their size, tissue penetration is limited in antibodies used to treat cancer. The antibodies rely on the penetrability of the cell itself rather than the ability of the antibody being able to penetrate. Other factors that complicate antibody penetration are antibody affinity, internalisation of the antigen, and antibody metabolism within the cell (Tabrizi et al., 2010; Zarganes-Tzitzikas et al., 2016). Internalisation analyses can be carried out using radiolabelled

antibodies or the high content imaging methodology with pH-sensitive dyes such as pHAb (Zwaagstra et al., 2019). However, performing screening in this way is extremely costly when many libraries are required for screening (Mehrling & Soltis, 2018; Riedl et al., 2016). Manipulating the immune response through immunotherapy requires the consideration of checks and balances to these treatments. For example, Rituximab was found to activate the complement cascade; but its therapeutic effect was limited by the interaction of regulatory molecules for complement, CD55 and CD59. To prevent this, additional antibodies could be used to inhibit the function of regulatory molecules. However, it is not known what effect this will have on the host and if there would be any toxic consequences (Borrebaeck & Carlsson, 2001). Moreover, when used *in-vivo*, antibodies may incorrectly bind or have an undetected affinity for inhibitory receptors on B cells or APCs. In cells responsible for the mediation of the immune response, there is a co-expression of activating and inhibitory receptors. Under regular conditions, when there is no concern for an immune response, more inhibitory receptors are expressed on the surface. Receptors designed for activating receptors may incorrectly bind inhibitory receptors under these conditions, resulting in a muted immune response (Chames et al., 2009; Nimmerjahn & Ravetch, 2007).

There is a reason for the routine use of antibodies in immunotherapy. They produce effective results for many debilitating diseases. Headway has been made to improve their efficacy and immunogenicity. Furthermore, they can be used to investigate the way proteins function and their expression in cells. They can be developed to bind with high affinity and inhibit or expedite cellular processes. However, the ability to create an immunologically silent antibody, one where there are no levels of adverse immune stimulation, is not guaranteed. More ways need to be investigated to improve the health wellbeing of people through therapeutic development.

Section 1.3 Aptamers

Immunotherapies need to investigate different avenues to overcome limitations associated with antibody-based therapy and one such avenue is aptamers. Borrowed from the Latin word '*aptus'* meaning 'to fit', aptamers are ligands consisting of short oligonucleotide sequences, spanning from 12-80 nucleotides in length, that are created to have affinity and specificity to their target. They achieve this by forming unique tertiary structures that facilitate binding interactions with the target (Khedri et al., 2015). Improving the function of aptamers by

introducing RNA sequence mutations has defined a creative space for aptamer technology. Tuerk *et al.* investigated the effect of introducing mutations within the hairpin loop associated with translational regulatory mechanisms involved in the bacteriophage T4 gene. Its mutation affected the synthesis of the polymerase during replication (Gold et al., 2012) and the systematic evolution of ligands by exponential enrichment (SELEX) was born. Following this success, Ellington and Szostak (1990) demonstrated the ability to create copious quantities of RNA using the SELEX methodology. From this, ligands that have the potential to bind molecules of interest by forming complex structures that provide binding and catalytic function were isolated (Ellington & Szostak, 1990). From here, the applicability of aptamers was realised in a range of scientific areas. Aptamers can be evolved to bind a range of targets such as whole cells, bacteria, proteins, and small molecules. NeXstar, a company previously known as NeXagen and now taken over by Gilead Sciences, exhibited an interest in developing aptamers for therapeutic use as antibody analogues. Macugen, also known as Pegaptanib, is an RNA aptamer developed by NeXagen which is used to treat age-related macular degeneration by binding to vascular endothelial growth factor-165 (VEGF-165). It is an FDA approved aptamer and has been utilised as a treatment for many other conditions (Bunka et al., 2010; Gold et al., 2012). The success of Macugen has solidified aptamers for use as therapeutics. Furthermore, aptamers exhibit little to no adverse immune responses with treatment, and as such, have a great advantage over current therapeutics.

1.3.1 How Aptamers Bind

The interaction between aptamer and target is achieved via a range of different bonding mechanisms. These interactions facilitate the different secondary structures required to reach a state of stability. Furthermore, aptamer and target interactions hinge on the flexibility to form a range of different structures. Hairpins, bulges, pseudoknots, and G-quadruplexes are all structures that create stability in the aptamer-target complex (Cai et al., 2018). The aptamer itself consists of a negatively charged phosphate backbone and interactions with positively charged targets stabilises the aptamer. Hydrogen bonding is the most prevalent interaction involved in target binding. Some aptamers that have been identified to rely on hydrogen bonding for efficient aptamer-target interactions include the thrombin binding aptamer (TBA), and an RNA aptamer R23 (specific to the aminoglycoside neomycin B). Dissimilarly, both aptamers interact with hydrogen bonds to form different structures to reach a state of stability.

TBA was found to develop a G quadruplex structure, which is the association of four guanines forming a ring confirmation due to the high guanine content, while R23 formed a stem-loop structure (Cai et al., 2018; Cowan et al., 2000; Nagatoishi et al., 2011).

Aromatic ligands i.e. closed-looped electron structures create highly specific interactions with aptamers through hydrogen bonding and π–π stacking (Hermann & Patel, 2000). For example, the theophylline binding RNA aptamer can discriminate between theophylline and caffeine which are both aromatic ligands with one difference in a methyl group at the seventh nitrogen position in caffeine. The theophylline aptamer can bind theophylline with 100-fold greater affinity (Zimmermann et al., 2000).

Finally, non-covalent bonds contribute to the binding specificity of aptamers that can decipher between structurally similar targets. For example, L-citrulline and L-arginine binding aptamers bind targets that have prominent levels of structural similarity. L-citrulline has a C=O instead of the C=N-H on L-arginine. The aptamers are highly specific towards their allied amino acid (approximately K_d=10 μM) without expressing affinity to the alternate amino acid (Famulok, 1994; Patel & Suri, 2000). The intricacies of aptamer binding mechanisms result in a tool that can sensitively discriminate between molecules of similar structure, providing significant use in many areas of science.

1.3.2 Aptamers as Potential Tools in Immunotherapy

Aptamers are applicable in many areas of science. One area of interest is immunotherapy. Aptamers can be developed to bind targets such as surface receptors that aid in the inhibition or activation of that molecules' function (Santulli-Marotto et al., 2003). The ability to modulate cellular functions is essential for understanding and developing immune responses. Aptamers may also be recruited to act as delivery vehicles for the transfer of therapeutic or antigenic material to specific cell types (McNamara et al., 2006). Antibodies are routinely used in therapeutics as immune checkpoint inhibitors, to block the activity of molecules such as CTLA-4 (Huang et al., 2017). Aptamers for CTLA-4 are being developed to challenge this current trend. Huang et al. created an aptamer to CTLA-4 with a binding affinity of K_D= 11.84nM. Compared to the dissociation constant (K_D) of ipilimumab (K_D= 18.82nM), the CTLA-4 aptamer has a stronger binding affinity towards CTLA-4 since binding affinity and K_D are inversely related (He et al., 2017; Huang et al., 2017). This aptamer could elicit relative anti-tumour responses

to the equivalent antibody (Ipilimumab). This is exciting as the same result was achieved in the absence of any adverse immune responses.

Furthermore, manipulating the structure of an aptamer can influence its performance. In 2020, a multivalent aptamer was developed to have chimeric antigen receptor-like (CAR-like) capabilities. The overall goal was to induce targeted killing of B16 melanoma tumour cells via the activation of T cells. This aptamer was comprised of a dimer of a CD28 aptamer and a tetramer of CTLA-4 RNA aptamer, Figure 1.2. This provided a dual functionality; affinity to CD28 for co-stimulatory signals to activate T cells, in synchronisation with CTLA-4 immune checkpoint inhibition by binding to CTLA-4 (Bai et al., 2020). This multivalent aptamer complex stunted the progression of B16 melanoma cells. Research in these ways, convey the suitability of aptamers in areas of science where creativity and duality are essential.

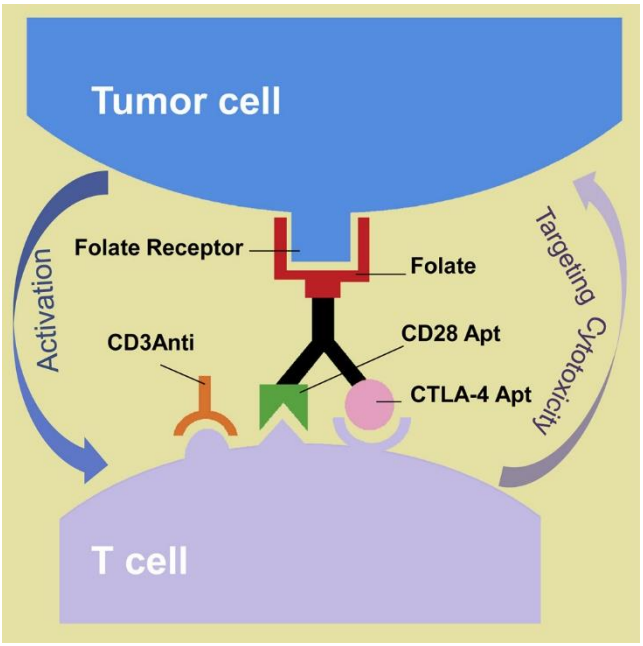

Figure 1.2 Graphical depiction of a multivalent aptamer that binds CTLA4 and CD28 to provide stimulatory signals for the activation of T cells while suppressing CTLA4 checkpoint blockade features. Figure reprinted from (Bai et al., 2020) and RightsLink with permissions.

As the field of immunology investigates new avenues of therapy, aptamers are amongst the contenders. Aptamers that elicit immunomodulatory effects are coined antagonistic aptamers. The opposite is known as agonistic aptamers and these are aptamers that provide an activating signal through the binding of co-stimulatory receptors such as 4-1BB, OX-40 or CD28 (Soldevilla et al., 2016). Recently, aptamer versatility is demonstrated through techniques such as targeting cell surface biomarkers, specific delivery of therapeutic drugs, or immunostimulatory

components by targeting isolated receptors on cell types. Aptamers that target and allow for the discovery of specific biomarkers provide a twofold benefit to immunotherapy. Firstly, aptamers that are identified to bind with high affinity and specificity can be employed for theragnostic purposes or molecular imaging. For example, an RNA aptamer that binds CD133 on cancer stem cells could efficiently permeate through the cancer cell layer and persist in the cellular environment for at least 24 hours (Shigdar et al., 2013). These properties are invaluable for molecular imaging as it provides a way of understanding cellular processes and has for example contributed to a greater understanding of tenascin-C. It is now understood that it is a receptor that is highly expressed when tumour cells undergo tissue reconstruction and growth (Wang & Farokhzad, 2014; Winnard et al., 2008).

Secondly, targeting cell surface receptors allows for the discovery of new receptors via aptamer facilitated biomarker discovery. These are essential tools that allow diseases to be screened and a way to inform relevant medical treatments. Furthermore, they widen the body of knowledge around cell types and how receptors relate to cellular function. Aptamer facilitated biomarker discovery was applied to identify markers present on mature and immature dendritic cells. A thorough understanding of receptors on these cells could provide direction for targeted immunotherapies. Furthermore, while identifying biomarkers present on cells via aptamer facilitated biomarker discovery, a range of aptamers with affinity to the biomarkers in their native conformations have been simultaneously created (Berezovski et al., 2008).

Discovering aptamers to different receptors on cell types provides a way to achieve targeted delivery for therapeutic purposes. The aptamers, although sometimes possessing innate functionality, can also be directly conjugated with therapeutic drugs such as doxorubicin, a chemotherapy medication, to target specific cells and thus limit the toxicity of the drug throughout the body but concentrate it in areas where it is required (Huang et al., 2009). Furthermore, conjugation of therapeutic agents with aptamers is an uncomplicated process that relies only on the hybridisation of complementary sequences or the addition of linker molecules (Gilboa et al., 2015; Huang et al., 2009). Aptamers can provide improvements to existing treatments in immunotherapy that result in an improved therapeutic outcome. Aptamers provide value when used in combination with other techniques or agents. In a comparable way to conjugation, small interfering RNA (siRNAs) can be conjugated to aptamer

complexes for their delivery into target cells. This provides an alternative avenue to cancer therapy devoid of drugs by using siRNAs to target mRNA expression and act to suppress or inhibit the translation of survival genes (Chu et al., 2006; Shigdar et al., 2011; Zhou & Rossi, 2017).

Antigenic peptides are another molecule of interest for targeted delivery. The role of the peptide is to elicit an immune response. Conjugation of a peptide to the aptamer, targeted to an immune cell receptor, will result in the delivery of the immunostimulant to effect response. Receptors targeted will be present on an immunomodulatory cell such as a dendritic cell or another form of APC to drive the desired response by the presentation of peptide to a subset of T cells. Harnessing specific immune responses relative to cancer hallmarks is essential to control the progression of disease caused by tumours. As cancer evolves and dominates a host, immunosuppressive cells are taken hostage by a highly concentrated tumour environment in a way to persist and avoid immune checkpoints (Lozano et al., 2016). Regulatory T cells (Tregs) that are present within tumour microenvironments suppress adaptive immunity and silence anti-tumour responses (Joshi et al., 2015). One way to mitigate this problem is to suppress the function of Tregs so that immune responses persist in the absence of checkpoints. Foxp3 inhibition obstructs the Tregs' ability to suppress immune responses. The synthetic peptide P60 was developed to carry out this function but it exhibited poor specificity. However, the conjugation of P60 with a chimeric aptamer complex was used to increase the specificity of P60 to Tregs by binding to CD28. In this event, the inhibition of regulatory responses could mount antitumour responses (Lozano et al., 2016).

Antigen delivery to induce an immune response is achieved by targeting surface receptors on cells that mediate immune responses. APCs, such as DCs, are of interest due to their capability to present antigenic fragments to MHC molecules for presentation to T cells. The DEC205 is a C-type lectin receptor expressed on thymic epithelial cells and subgroups of DCs. Akin to Clec9A, it functions as an endocytic receptor and facilitates the cross-presentation of antigens within cells exposed by apoptosis (Shrimpton et al., 2009). Attributing to its applicability in immunotherapy, DEC205 has been the target for antibody-based delivery of the tumour antigen, NY-ESO-1 to augment T cell immunity towards cancers (Dhodapkar et al., 2014).

The DCs sit at the cusp of innate and adaptive immunity. Their ability to potentiate effector function and generate memory is essential to developing immunity against cancer.

Combinatorial approaches to immunotherapy such as targeting receptors on DCs with aptamers provide a unique avenue of therapy for diseases that are harder to treat.

1.3.3 Aptamers vs. Antibodies

Table 1.1 compares the features relating to aptamer and antibody development, functionality, and characteristics.

Table 1.1: Comparison of aptamers and antibodies.

Feature	Aptamers	Antibodies
Production variability	Chemically synthesised, presenting no batch-to-batch variation and cost-effective (Chen & Yang, 2015).	High levels of batch-to-batch variation. Circumvented by the use of recombinant antibodies but currently not cost-effective as they are irreproducible, and unreliable under different handling and storage conditions (Bauer et al., 2019; Chen & Yang, 2015).
Storage	Long shelf life. Does not require laborious storage procedures or other biological components for production. Can be stored at room temperature if lyophilised or -20°C if hydrated (Chen & Yang, 2015).	Cells that are used for antibody preparation are required to be stored and frozen at separate places to prevent loss of cell banks, death, or inappropriate freezing procedures. The antibodies are extremely sensitive to temperature and do not have an extensive shelf life (Chen & Yang, 2015; Jayasena, 1999).
Manipulation	Can be easily modified or truncated to improve performance or kinetic characteristics (Chen & Yang, 2015). Can also be modified with labels for detection or with linkers for conjugation without compromising the specificity and activity of the aptamer	Not as easily modified or manipulated. Cannot be changed on demand. Improvements to find antibodies that work will require antibody generation process to start from the beginning (Chen & Yang, 2015; Jayasena, 1999).

	(Thiviyanathan & Gorenstein, 2012).	
Biological target	As it is chemically made, it does not rely on the survival of the host to generate aptamer. Thus, can be made towards toxins and diseases or other targets that would kill a host (Jayasena, 1999).	Are created by raising antibodies in a host and therefore, survival of the host is essential. Limited window of targets antibodies can be made against (Jayasena, 1999).
Stability	Is susceptible to denaturation, but this process is reversible within a matter of minutes (Jayasena, 1999).	Is susceptible to irreversible denaturation (Jayasena, 1999).
Performance	Each batch is identical, meaning that the performance (relating to stability, affinity, and specificity) of each batch will be the same (Chen & Yang, 2015).	Variation between batches requires immunoassays to undergo new optimisations with each new batch (Chen & Yang, 2015).
Size	Aptamer size ranges from 6-30kDa. Being smaller provides advantages as they are less immunogenic; highly bioavailable and tissue penetration is more efficient (Bauer et al., 2019).	Antibody size ranges from 150-180kDa. Much larger. Creates issues with immunogenicity and bioavailability (Bauer et al., 2019)
Figure 1.3 presents a comparison of size between aptamers and antibodies		
Flexibility of application	Can be used in sensing formats in unique ways. Can be designed to undergo conformational changes to bind targets making them more versatile (Bauer et al., 2019).	Unable to undergo conformational change so limited use with biosensing assays (Bauer et al., 2019).
Production	It is an iterative in-vitro process that can be designed to be fully automated thus producing copious quantities at an affordable price (Thiviyanathan & Gorenstein, 2012).	Requires in-vivo modification and generation thus relying on many components and large amounts of lab space increasing costs and removing the ability for automation (Thiviyanathan & Gorenstein, 2012).

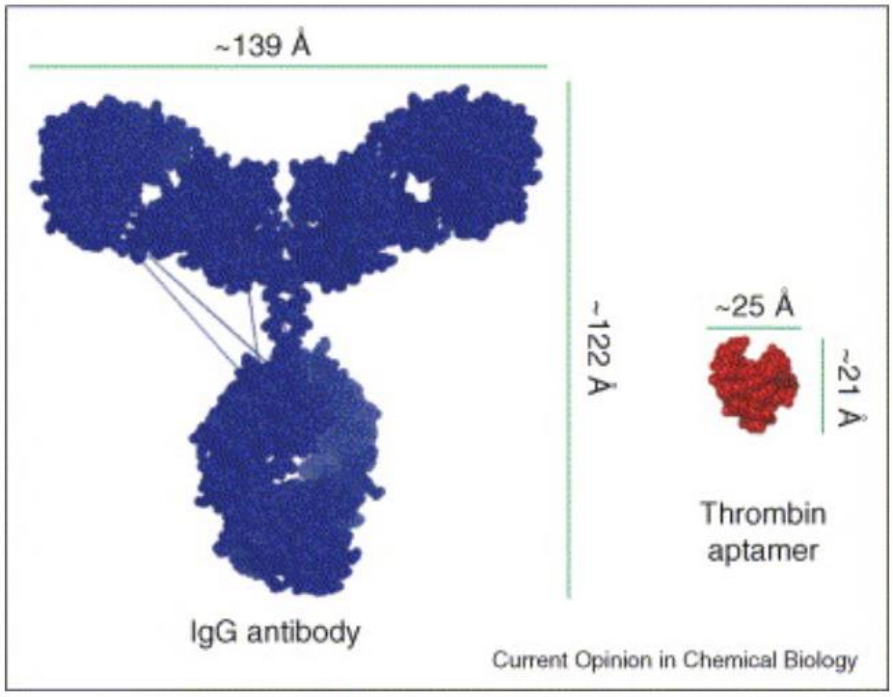

Figure 1.3: Comparison of size of antibodies compared to aptamers.
The smaller aptamer size, approximately 10 times smaller than the antibody, is advantageous for tissue penetration and prevention of immunogenicity within the body. Figure reprinted with permissions from (Lee et al., 2006) and RightsLink with permissions .

1.3.4 Systematic Evolution of Ligands by Exponential Enrichment (SELEX)

Aptamers are created through an iterative process termed; the Systematic Evolution of Ligands by Exponential Enrichment (SELEX). This is an evolutionary approach that evolves an oligonucleotide library to have sequence specificity and affinity to a defined target. This is achieved by introducing selection pressures that allow for only highly binding sequences to persist in this environment. The SELEX process begins with a starting library of single-stranded oligonucleotide sequences with a high level of complexity. Incubation of these sequences with the defined target is performed to separate those that bind and have specificity towards the target and those that do not. Isolation and amplification of bound sequences, after manipulation back to ssDNA, becomes the starting library for the following round. This is defined as one round of SELEX and is illustrated in Figure 1.4. Multiple rounds of SELEX are performed until the oligonucleotide pool is enriched with specificity and affinity towards the target (Gopinath, 2007; Komarova & Kuznetsov, 2019). The steps within the SELEX process are each discussed in more detail below.

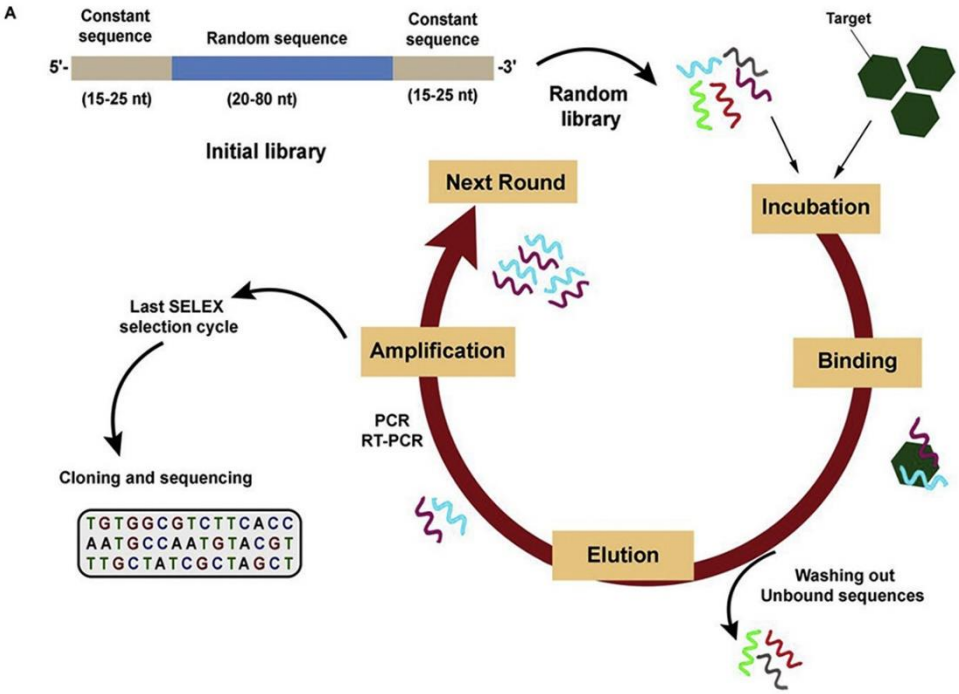

Figure 1.4 Schematic of a classical SELEX process. *The initial single-stranded oligonucleotide library is incubated with the target, unbound sequences are removed. The sequences that are bound and remain on the target are eluted and amplified using PCR. The amplified product is transformed to single-stranded DNA and this becomes the starting library for the following round. Once a sufficient number of selection rounds are reached, the oligonucleotides are sequenced and characterised. Figure reprinted with permissions from (Bayat et al., 2018) and RightsLink with permissions.*

1.3.4.1 Starting library and library design.

The starting library is an essential component of SELEX that attributes to its success. This starting library must contain the maximum amount of diversity to provide the greatest probability for unique sequences to bind and thus be reintroduced into the following starting pool. A starting library for SELEX is comprised of a random core region of 20-60 nucleotides in length, flanked by specific primer sequences. The primer regions are required for PCR amplification (Hall et al., 2009). In the SELEX process, the design of both the randomised library and the primers are essential to limit any uncontrollable bias within the procedure (Hall et al., 2009; Komarova & Kuznetsov, 2019). Selection bias is minimised when the starting library is completely random and unknown. However, bias within the starting library can sometimes be exploited in selections when information is understood regarding pre-defined binding sites on an identified target. For example, sequences that are known to bind to a target can be 'doped' into the starting library with a proportion of random sequences in a way to drive the library bias towards selection and thus mutation of previously identified specific sequences so the product is better performing than the original aptamer (Baskerville et al., 1995; Hall et al., 2009). The use of a completely random starting library creates an opportunity for a more diverse range of sequences to be generated towards the target.

The length of the oligonucleotide starting library is a feature of the SELEX design that must be considered. The length of the oligonucleotides within the pool influences the ability to perform end-point analyses. For example, it is more difficult to identify conserved motifs relating to structural integrity in longer sequences (e.g. 90 compared to 40 nucleotides in length) (Komarova & Kuznetsov, 2019; Lozupone et al., 2003). Furthermore, longer oligonucleotides have an increased risk to interact with themselves to form homo- or heterodimer structures rather than to the intended target molecule (Hall et al., 2009). The length of the oligonucleotides can also compromise library randomness. Random oligonucleotide synthesis is a technique that uses nucleoside phosphoramidites which are modified nucleosides that add DNA bases onto a growing oligonucleotide chain in sequential order. When the oligonucleotide sequences to be synthesised are short, this process of randomising the subsequent base to be added is performed randomly. However, as the chain grows, the subsequent phosphoramidite is preferentially skewed towards the first one added due to the exposed and active 5' hydroxyl sites (Pollard et al., 2000). This is prevented by mixing the nucleotides at defined ratios to

create equal nucleotide representation. An A:C:T:G ratio of 3:3:2:2.4 compensates for the faster coupling times of T and G (Hall et al., 2009). Good primer design contributes to the resultant aptamer structure and its ability to bind during the selection processes (Komarova & Kuznetsov, 2019). Inefficient primer design incorporated into the SELEX process will result in by-products during the PCR process that is not indicative of the oligonucleotide binding to the target molecules but could instead result in primer dimers. This is an event where the primers either anneal with complementary sequences within the primer or the alternate primer. During SYBR green PCR, the presence of primer dimers will result in an increase in fluorescence which is indicative of the intercalation of SYBR with dsDNA, implying the sequences are being amplified, but they are not.

To mitigate unwanted by-products during the selection procedure, some guidelines can be followed. For example, primers should be 18-24 base pairs (bp) long. Longer primers require more time to hybridise and create larger regions for incorrect binding. Melting temperatures of both primers should be between 54-68 °C and should be within one degree of one another. Primer repeats that promote mispriming should be avoided such as sequences with repeating base pairs, e.g. CTCTCT. This is the same for palindromic sequences CTAAAAATC. Thermodynamics is also an essential consideration. The more spontaneous the free energy of the primer, the more likely it will form undesirable structures. Therefore, a delta G (ΔG) of greater than –4 is desirable. Finally, a G/C content of 40-60% is favourable. These criteria can be stipulated before synthesis via online analysis platforms.

1.3.4.2 Oligonucleotide Incubation

Three incubations can be performed during the SELEX process. These are incubations of the oligonucleotide library with either the target of interest, a molecule that is structurally similar to the target of interest (counter section) and the omission of any molecule (negative selection). Counter selection steps are designed to remove those sequences that bind similar molecules to the target molecule by introducing a molecule that may be similar in structure or characteristics to the target molecule. Alternatively, negative selection can be performed against agents that are present within the selection process. For example, bare magnetic beads are required for target immobilisation (Komarova & Kuznetsov, 2019). By doing this, the resultant oligonucleotide sequences gain greater specificity towards the target molecule.

To allow for ease of manipulation and separation from the sequences that do not bind to the target, the target is immobilised on a solid support. The first reports of SELEX used nitrocellulose filters and agarose affinity columns for immobilising the target molecule (Tuerk & Gold, 1990). Since then, the SELEX procedure has become more sophisticated, where targets can be immobilised through magnetic beads, affinity tags, and UV cross-linking (Dobbelstein & Shenk, 1995; Pelle & Murphy, 1993). The expansion of the SELEX methodology to create aptamers to a range of different targets have allowed for the evolution of methods tailored for these targets. Cell-SELEX is the process where the oligonucleotide sequences are selected against a whole cell, either immobilised (adherent cells) or free in solution (suspension cells) (Kaur, 2018; Komarova & Kuznetsov, 2019). In the cell-SELEX process, negative selection can be employed using cells that express many of the same surface receptors, apart from the target receptor. For example, one group used CRISPR-mediated isogenic cell-SELEX as a knock-out approach to remove the SLC2A1 gene that encodes for the glucose transporter 1 (GLUT1). These cells behaved as the negative control to isolate aptamers that had specificity towards GLUT1 (Rosch et al., 2020). Based on this design, the only point of difference between cells was the presence or absence of GLUT1 transporter. Thus, aptamers created from this should be highly specific to the target molecule.

Counter selection improves the specificity of the aptamer by introducing candidate sequences to molecules that are similar in structure to the target molecule. An adenosine diphosphate (ADP) binding aptamer was developed that possessed the ability to sensitively discriminate between ADP, adenosine triphosphate (ATP) and adenosine monophosphate (AMP). This was achieved by introducing counter selection steps using ATP and AMP bound in agarose resins. This was an exciting development as an ADP aptamer developed almost 30 years previously could not discriminate between such molecules. Yet, identification and specificity towards ADP in an abundance of APT is essential for developing ADP specific biosensors (Sassanfar & Szostak, 1993; Srinivasan et al., 2004).

As SELEX technology became more prominent in the science community, proving its utility in many areas of science has caused the technology itself to evolve. SELEX can create aptamers to several different targets based on the type of SELEX methodology employed. SELEX towards protein targets has been performed using nitrocellulose filters and bead-based SELEX, where the target is immobilised and incubated with oligonucleotides. Nitrocellulose filters can be

used to immobilise protein targets and thus perform the selection. Bead-based SELEX has also been utilised to select for targets such as small molecules and tumour biomarkers. While other successful methods used to generate aptamers include Capillary Electrophoresis SELEX, Microfluidic-SELEX, Capture-SELEX and Cell-SELEX (Bruno & Kiel, 2002) (Bayat et al., 2018; Yazdian-Robati et al., 2017).

1.3.4.3 Comparison of SELEX Methods

Few investigations have been made to compare different SELEX methods to isolate aptamers to the same target. One paper investigated the differences between using Cell-SELEX and Protein-SELEX to Tenascin-C, an extracellular matrix protein. The researchers identified that both procedures resulted in aptamers towards Tenascin-C with conserved sequences across both conditions (Hicke et al., 2001). However, a combinatorial approach termed hybrid SELEX, was found to provide the best outcome where the limitations in one method were mitigated by the advantages of the other, and vice versa (Hicke et al., 2001; Komarova & Kuznetsov, 2019). It is common for hybrid SELEX to combine techniques such as Protein-SELEX and Cell-SELEX to create aptamers that can identify the target molecule in a more complex physiological environment (Uemachi et al., 2021). Variations of the approach use Cell-SELEX to firstly select for oligonucleotides that bind receptors in their native state. After enrichment of library, Cell-SELEX is replaced with Protein-SELEX to drive high specificity towards the receptor. In immunotherapy, the hybrid SELEX methodology has been utilised towards CD4 (Zhao et al., 2014) and CD30 (Parekh et al., 2013). Where akin to Tenascin C, the protocol involved cell selection in the first instance and refined selections in the second. The reverse order was considered for the development of aptamers towards DEC205 (Wengerter et al., 2014) and PD1 (Khedri et al., 2020).

1.3.4.4 Monitoring Oligonucleotide Pool Enrichment

The progression of the SELEX procedure can be monitored during the selection rounds. It is common for one SELEX round to take up to a week due to the techniques required to prepare the oligonucleotides for the following round. Monitoring the evolution of the oligonucleotide library towards binding the target molecule means that the procedure can be stopped at the optimal time to create a library that is highly enriched towards the target (Komarova & Kuznetsov, 2019). Excessive rounds of selection can shift the evolving pool to develop a bias towards sequences to have a greater amplification efficiency but do not have a strong affinity

and specificity towards the target molecule (Avci-Adali et al., 2013). A common way to monitor the progression of SELEX is via real-time PCR. Since real-time PCR is employed for preparative purposes, i.e. amplification of dsDNA for the next selection round, it can easily be adapted for analytical use (Avci-Adali et al., 2013; Kolm et al., 2020; Savory et al., 2014). Real-time PCR can be used to determine the proportion of ssDNA which has an affinity to the target molecule per selection round. Enrichment towards the target is achieved when the SELEX rounds maintain a constant concentration. A standard curve made from standards of the oligonucleotide sample is used to determine the amount of unknown oligonucleotide present at each SELEX round (Kolm et al., 2020). A preliminary understanding of the progression of SELEX can be made by visualising quantification cycle (Cq) values that indicate the amount of product that has been amplified within a reaction. The Cq value is inversely related to the amount of product. Thus, the lower the Cq value, the more product present. Real-time PCR for amplification of the oligonucleotide library enables the SELEX process to be stopped within the exponential phase, to limit the accumulation of spurious products that form during reagent deficiencies.

Other methods worth noting to monitor the progression of SELEX include surface plasmon resonance (SPR) (Di Primo & Lebars, 2007), enzyme-linked oligonucleotide assay (ELONA) and fluorescence-activated cell sorting (FACS) (Haghighi et al., 2018; Mohammadinezhad et al., 2020). These methods enable SELEX progression to be monitored based on affinity and binding.

1.3.4.5 PCR Amplification and Strand Purification

The oligonucleotides that have bound to the target from a cycle of SELEX are used as the starting oligonucleotide library for the subsequent round. This is theorised to systematically enrich a population with sequences that exhibit specificity to the target of interest as prior steps have been efficient at removing the non-binders from the pool (Gopinath, 2007). Before the introduction of oligonucleotides to the following incubation, amplification and separation steps are required. The sequences are amplified to create multiple copies of the resultant oligonucleotides using polymerase chain reaction (PCR). This amplifies the region of DNA within the primer regions and ensures there is an adequate number of oligonucleotides to be introduced to the following round. (Tolle et al., 2014). Following amplification, the DNA strands must be separated and purified to return the sequences to single-stranded form. A robust

SELEX experiment understands the importance of DNA quality for the success of SELEX. Techniques such as strand separation using streptavidin-coated magnetic beads with a biotin labelled antisense strand are effective and routinely used to produce pure ssDNA. During the amplification process, a 5' biotin labelled reverse primer is incorporated. This amplifies the antisense strand of the double-stranded DNA to be biotin labelled at the 5' end. Labelling the unwanted strand with biotin is an efficient way to separate the strands. Streptavidin labelled magnetic beads are employed to isolate and immobilise the biotin labelled strand through biotin and streptavidin non-covalent chemistry. The biotin-streptavidin bond is one of the strongest bonds in nature, meaning that intense manipulation and denaturation can be performed without damaging this bond (Chivers et al., 2011). The amplified DNA is incubated with the beads for conjugation. Following biotin and streptavidin binding, the DNA is denatured using alkaline substances such as sodium hydroxide (NaOH) to disrupt the hydrogen bonds between nucleotides and liberate the non-biotin labelled strand in solution (Kilili et al., 2016). Further steps can be taken to develop extremely pure ssDNA before or after the strand separation step. Gel electrophoresis can be employed to isolate DNA based on size by applying an electrical current through an agarose matrix, where the negatively charged DNA travel to the positive cathode. This allows for the efficient removal of spurious contaminating products from the amplification process. Smaller molecules will travel faster through the matrix while larger ones slower. This ensures the product can be removed of the desired length, leaving behind contaminants (Gopinath, 2007). It has been found that incubation of streptavidin with NaOH for long periods can disrupt bonds and cause the contamination of biotin labelled antisense strands into the cleaved sense strands. Incubation times are typically reduced only to a couple of minutes. However, in the case where this may be an issue, gel electrophoresis can be used at this point (Kilili et al., 2016). Additional use of purification kits can improve the quality of the ssDNA post-separation. Kits such as Qiagen QIAEX® II are effective at purifying ssDNA from agarose and salts. Since this separation and purification step is essential to the success of SELEX, other separation methods that have been used are asymmetric PCR, lambda exonuclease digestion, and chemical or structural modification using urea-polyacrylamide gel (Liang et al., 2015; Svobodová et al., 2012).

Section 1.4 Aptamer Candidate Characterisation

After SELEX, identification of the sequences evolved to bind to the target molecule must be made. Presuming the correct number of selection rounds were followed based on enrichment assessment from round to round, the final pool of oligonucleotides should be highly enriched towards the target. Sanger sequencing and next-generation sequencing are two methods that can be employed for aptamer identification. Sanger Sequencing is a form of DNA sequencing developed by Frederick Sanger and relies on chain-terminating deoxyribonucleotides (ddNTPs) in a unique type of PCR (Valencia et al., 2013).

1.4.1 Illumina Next-Generation Sequencing

Sanger sequencing laid the groundwork for future adaptations and improvements. Next-generation sequencing (NGS) has elevated the possibilities of traditional sequencing methods and provides a massively parallel analysis of millions to billions of oligonucleotide sequences at an attractively low cost due to their high throughput application. NGS is an umbrella term for a range of DNA sequencing systems. Although different in application, they share advantages over the traditional Sanger sequencing method including their ability to produce such techniques in a highly parallel manner, microscale reactions contributing to their ease of production speed of application and cost (Rizzo & Buck, 2012). As an overview, all NGS systems operate by tracking the addition of nucleotides to a DNA template to understand the exact sequences present. This is no different to Sanger sequencing however, NGS performs this in a highly parallel fashion. A platform that is commonly employed is Illumina sequencing and involves four main stages of library preparation, sequence clustering, sequencing, and data analyses and each are briefly discussed below.

The DNA library of interest is prepared using the mate-pair library method. The library sequences are fragmented, biotinylated oligonucleotides that are added to either end of the fragmented samples for repair. In this repair process, both biotin ends become located adjacent to each other in a circular orientation. This complex is then fragmented again so that the sequences originally tagged with biotin are in the middle of the fragment (Berglund et al., 2011). Adapters are attached to the end of the fragment and this facilitates attachment onto the flow cell. The flow cell is a solid support and consists of eight channels. Fragmentation of DNA libraries are performed so that they are more manageable, and thus more preparations

can be made at once. The fragment lengths are usually 200-600 base pairs (Raghavendra & Pullaiah, 2018).

In Illumina sequencing, sequencing is performed directly in the flow cell. Therefore, the oligonucleotides connected to adapter complexes become amplified and linearised to create clusters of specific sequences. The amplification of sequences results in clusters that can be visualised by a camera (Raghavendra & Pullaiah, 2018) and linearised using an enzyme for sequencing.

For sequencing, nucleotides designed for chain termination and can be detected by fluorescence emission are added to the flow cell. NGS follows the same chain termination technique used in Sanger sequencing methodology whereby an extension of the DNA sequence by DNA polymerase is halted when in contact with terminator molecules on the sequence. The fluorescence of the chain terminator nucleotides is detected by a camera and recorded. This is performed base by base. Therefore, after recording the first base with a fluorescent reporter, it is cleaved, and the second base is recorded when a new set of oligonucleotides is added. This meticulous framework makes Illumina a highly accurate method of sequencing (Berglund et al., 2011; Raghavendra & Pullaiah, 2018).

1.4.2 Bioinformatics Analyses of NGS Data

Once the data is generated, cluster analysis can be performed to identify pools of similar sequences within the library for further analysis with characterisation experiments. The resultant sequences identified from a sizeable number of SELEX rounds are enormous. Bioinformatic approaches to make this information more manageable are essential. Oligonucleotide analysis can be segmented into a range of different analyses, data processing, primary enrichment analysis, library clustering and binding motifs identification (Komarova et al., 2020). FASTAptamer is an aptamer-specific bioinformatics tool kit that allows for a range of initial analyses to be made. FASTAptamer utilises the FASTA format, which is a display format that represents oligonucleotide or amino acid sequences. The software provides information on the sequence and count while carrying out commands to compare between sequences, clusters, identify enrichments within the library, and the ability to search conserved sequences (Kinghorn et al., 2017; Komarova et al., 2020).

1.4.3 Characterisation Techniques

Candidate aptamer sequences that have been selected using bioinformatic tools can be characterised through a range of different techniques to understand information around aptamer affinity and specificity towards the target. Robust characterisation methods must be taken to develop a detailed understanding of the aptamer.

Interestingly, within the literature, many previously established aptamers, thought to have bound well to their target, have been proven to not bind when thorough characterisation methods were applied (Tao et al., 2020; Zong & Liu, 2019). Documentation of the arsenic binding aptamer and many others presenting no binding to their target highlight the value of effective aptamer characterisation methods (Bottari et al., 2020; Zong & Liu, 2019).

Robust aptamer characterisation methods measure the affinity and specificity to which the aptamer binds its target molecule, and what secondary structures are formed relating to the stability of the aptamer/target interaction. Isothermal titration calorimetry (ITC) is the gold standard for aptamer characterisation by quantifying the amount of energy associated with a biochemical reaction in the form of heat exchange. Molecular interactions between a ligand and its cognate target result in the release or absorption of heat (Velázquez-Campoy et al., 2004). Performing ITC involves the titration of the target molecule into the sample within the cell creating interactions that lead to a difference in temperature. To understand the amount of heat created through a binding event, the ITC method is based on the dynamic power compensation principle, where the power required to maintain a constant temperature difference is measured. Thus, the reaction cell is constantly working to compensate for the imbalance generated by the addition of titrant and the energy required to do so can be enumerated (Ruso & Piñeiro, 2013). This provides a detailed profile of the binding interaction occurring relating to the binding affinity (K_A), reaction stoichiometry, how much of one substance binds the other, entropy change (ΔS) enthalpy change (ΔH) and Gibbs free energy (ΔG) (Ruso & Piñeiro, 2013). ITC has been used to determine the binding characteristics of many aptamers and is a preferred characterisation method as it is label-free, and a wealth of information can be obtained in one experiment

For the characterisation of aptamers that bind to cell surface receptors, several techniques can be used. As an indication that the candidate aptamers have specificity to an isolated cell type, fluorescence microscopy can be employed. Aptamers can be stained with fluorescent dyes or

chemically labelled with a fluorescent tag for detection under a fluorescence microscope (Civit et al., 2018; Shangguan et al., 2006; Zhao et al., 2015). Like immunohistological staining, the biotin/streptavidin interaction can be used to assess aptamer binding. The aptamer sequence can be modified with a biotin probe and incubated with the target molecule. The biotin-streptavidin interaction is one of the strongest non-covalent bonds, therefore, washing with Phycoerythrin (PE) conjugated streptavidin will induce binding of biotin on the aptamer (bound to the target) to streptavidin on the fluorescent probe resulting in the detection of fluorescence. Measured fluorescence can then be attributed to aptamer target binding (Sefah et al., 2010). characterising aptamers in this way provides a good overview of the specificity of the aptamer to the cell type. Furthermore, fluorescence microscopy provides information around aptamer localisation on the cell and possible internalisation features (Li et al., 2008).

Other techniques such as flow cytometry can be used to inform binding characteristics to the target of interest on the cell (López-Colón et al., 2011). Flow cytometry is a technique that uses a laser to identify cells one by one within a population of cells. Components of cells are labelled with different fluorescent probes and exposed to lasers which cause the probes to excite at different wavelengths creating different patterns of light scattering allowing for the segregation of cells within a population. Flow cytometry can be manipulated for aptamer characterisation by labelling each candidate aptamer with a fluorophore. Candidates will be incubated with the target or control cells and binding profiles of the aptamers can be assessed via flow cytometry. An aptamer sequence that is specific to the target cell will show a histogram with the fluorescence intensity of the aptamer being greater than what is observed with control cells and incubation of the starting (N40) library with the target cells (Meyer et al., 2013; Shangguan et al., 2006).

1.4.3.1 Gold Nanoparticle (AuNP) Assay

The gold nanoparticle (AuNP) assay is an efficient technique that provides a colourimetric response to the aptamer/target interaction. The principle of the AuNP is simple but provides valuable information around the detection limits of aptamers when a concentration range is tested. The assay takes advantage of the nanoparticles' sensitivity to salt. Increasing concentrations of salt cause aggregation of the nanoparticles and a concomitant colour change of the nanoparticles is observed from deep wine red to dark blue/grey. The electrostatic interactions of aptamers, when applied to the surface of the nanoparticles, create a protective layer, preventing salt induce aggregation. When target is added to the solution, aptamer specific to the target should undergo a conformational change to bind the target and thus leave the nanoparticles bare and susceptible to aggregation by NaCl. The colour change from red to blue/grey will indicate the aptamer target interaction (Figure 1.5). The level to which aggregation occurs and thus target binds can be determined using UV-Vis spectrophotometry. The AuNP assay is an effective, fast, and label-free method to detect aptamer and target interactions in low concentration ranges (Bottari et al., 2020; McKeague et al., 2015).

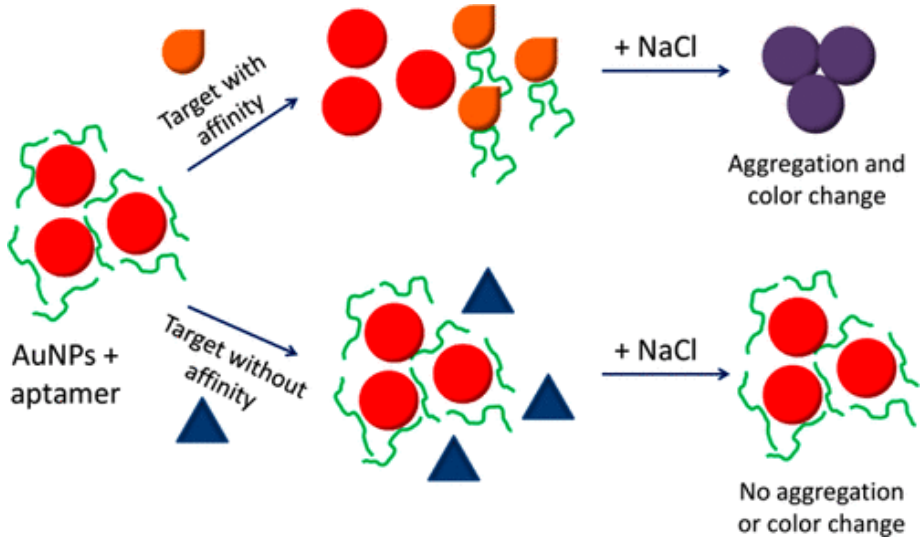

Figure 1.5: Schematic representation of colourimetric detection of aptamer/target binding using the gold nanoparticle (AuNP) assay. *Figure adapted with permissions from RightsLink.*

1.4.3.2 Circular Dichroism (CD) Spectroscopy

Circular dichroism (CD) spectroscopy is a technique that can be used to understand the binding characteristics of aptamers and their cognate target relating to the formation or change in secondary structure upon binding. It is a method that measures the absorption of left and right circular polarised light, the difference in absorption is quantified, creating a linearly polarised wave. Interaction of the aptamer with its target molecule changes the absorption of polarised light and thus, binding interactions can be observed (Daems et al., 2021). Figure 1.6 shows circular dichroism spectra for the assessment of the molecular structure and changes in this structure of aptamer VDBA14 for the detection of 25-hydroxyvitamin D. Changes in the secondary structure of the aptamer upon target binding are identified by a shift or attenuation of the spectrum (Prante et al., 2019). Distinctive peaks in the wavelength pattern will indicate the type of secondary structure the aptamer is conforming to. For example, a broad positive peak at 280 nm with a negative peak at 245 is typical of Watson and Crick B form DNA, while G-quadruplex structures tend to exhibit a positive band at 260 (Kypr et al., 2009). CD spectroscopy is an attractive technique to study binding interactions of aptamers as it is largely inexpensive, label-free, fast, and highly sensitive.

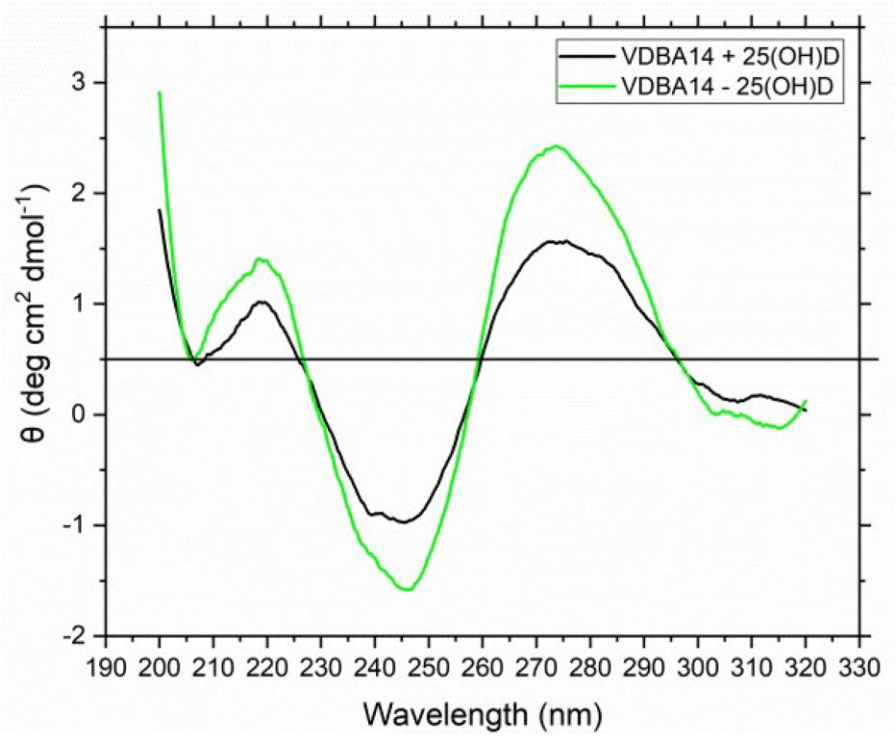

Figure 1.6: Representation of a circular dichroism differential absorbance spectra*CD Spectroscopy detects changes in an aptamers secondary structure upon interaction of a target, indicative of a binding event. The black line indicates the spectra of the aptamer with the target molecule while green is without the target molecule. Figure adapted with permissions from Prante et al., 2019.*

Section 1.5 Research Aims

The overall objective for my Masters' research was to generate aptamers that had affinity and specificity to the DC surface receptor, Clec9A.

In generating an aptamer that binds Clec9A, I hypothesise that using a hybrid SELEX method which uses both Protein-SELEX and Cell-SELEX methodologies to aid in enriching the SELEX library with oligonucleotides will be highly specific to Clec9A under complex, physiologically representative conditions.

To enable the generation of a Clec9A aptamer using Cell SELEX, the DC2114 cell line will be investigated as an appropriate positive target cell. The stable expression of the surface receptor Clec9A will be required to aid in isolating Clec9A specific candidates during cell SELEX experiments.

These objectives will be achieved by the following aims:

1. Characterise the expression of Clec9A mRNA within and the presence of Clec9A on the surface of DC2114 cells.
2. Generate aptamers using hybrid SELEX.
3. Identify and characterise candidate Clec9A-binding aptamers using two aptamer characterisation techniques: namely gold nanoparticle (AuNP) assay, and circular dichroism (CD) spectroscopy.

Successfully isolating aptamer candidates that can bind Clec9A under *in-vivo* conditions could have use in downstream applications such as immunotherapy. An aptamer that binds Clec9A could be engineered to carry antigenic or therapeutic cargo such as a peptide or chemotherapy drug, enhancing the immune response by facilitating cross-presentation. This would be advantageous in the field of immunotherapy as progression in this field is limited by antibodies.

CHAPTER 2: MATERIALS AND METHODS

Section 2.1 Experimental Design for Objective 1

The experiments to address Objective 1 were designed to investigate the effect of passage number on the expression of *Clec9A* mRNA in DC2114 cells in cell culture. Moreover, the proportion of DC2114 cells that expressed Clec9A protein on their cell surface was examined by using flow cytometry.

2.1.1 Maintaining the DC2114 Cell Line

The DC2114 cell line, formerly known as mutuDC2114, is an adherent mouse dendritic cell (DC) line named after 'murine tumour'. This cell line has the morphology and functional characteristics of *in vivo* splenic CD8α$^+$ classical DCs (cDCs) (Fuertes Marraco et al., 2012). The CD8α$^+$ cDCs are known within the cDCs subset as cDC1. These cells are characterised by their ability to prime the CD8 T cell subset through cross-presentation of antigen (Backer et al., 2019; Theisen & Murphy, 2017). The DC2114 cells express the characteristic surface markers of DEC205, CD24 and Clec9A and were kindly donated project by Professor Ian Hermans at the Malaghan Institute of Medical Research (Wellington New Zealand).

2.1.1.1 Culture Medium

The DC2114 cells were cultured in Iscove's Modified Dulbecco's Medium (IMDM + GlutaMAX Gibco™, ThermoFisher Scientific, New Zealand). The medium was supplemented with 5% (v/v) of foetal bovine serum (FBS), 5000 U/mL of penicillin with 5000 µg/mL of streptomycin (Pen/Strep) and 55 µM of 2-Mercaptoethanol (2ME; Gibco™, ThermoFisher Scientific, New Zealand). Following the addition of all reagents, the medium was referred to as supplemented IMDM.

2.1.1.2 Adherent Cell Culture Vessels

A variety of culture flasks sizes were used for the culturing of DC2114 cells. The size of flask was influenced by the use required. The T25 flask (25cm^2) was used for small scale experiments while the larger T175 flasks (155cm^2) were used when resurrecting cells from cryopreservation

due to large cell numbers within the frozen stocks. Finally, after passaging the cells, the concentration of total cells counted determined the size of the flask (T25 to T225) required for re-plating (see Table 2.1).

Table 2.1: Culture vessel size guide

Flask	Seeding density	Cells at confluency	Volume of	
			TrypLE (mL)	Medium (mL)
T25	$0.7x10^6$	$2.8x10^6$	3	3-5
T75	$2.1x10^6$	$8.4x10^6$	5	8-15
T175	$4.9x10^6$	$23.3x10^6$	17	35-53
T225	$6.3x10^6$	30.10^6	22	45-68

2.1.1.3 Thawing of DC2114 Cells from Cryopreservation

The cryovials containing the DC2114 cells were removed from liquid nitrogen storage and immediately placed into a 37°C water bath. The cells were thawed for approximately 1 minute, until only a small portion of ice remained. The outside of the cryovial was sprayed with 70% ethanol, wiped dry with a Kimwipe (Kimtech Science™, Kimberly Clark, New Zealand) and placed in a sterile biohazard cabinet. The ~1 mL contents of the cryovial were transferred into a 15 mL falcon tube and 10 mL of supplemented IMDM at room temperature (20-22°C) and added to the falcon tube in a dropwise fashion to prevent shock to the cells. The cell suspension was centrifuged at 500 x *g* for 4 minutes and the clarity of the supernatant was observed before being removed, thus retaining the cell pellet. The pellet was re-suspended in another 10 mL of supplemented IMDM at room temperature and transferred to a T175 flask (Nunc™ EasYFlask™, ThermoFisher Scientific). Additional medium was added to the T175 flask to a total volume of 35-50mL.

2.1.1.4 Cell Culture and Maintenance of the Adherent DC2114 Cell Line

The DC2114 cell line was cultured in a humidified 37°C incubator with 5% carbon dioxide (CO_2). The cells were passaged every 2-3 days or when they were estimated to reach 80% confluency. For passage, the media used to incubate the cells (spent media) was removed via serological

pipette and discarded. The DC2114 cells were then washed with 10 mL of 1X PBS (1.06 mM potassium phosphate monobasic (KH_2PO_4), 155.17 mM sodium chloride (NaCl), 2.97 mM sodium phosphate dibasic (Na_2HPO_4-$7H_2O$)) (ThermoFisher Scientific, New Zealand) by passing the PBS across the tilted flask bottom with a pipette several times. The PBS was removed and 17 mL of TrypLE (Gibco™, ThermoFisher Scientific, New Zealand) was added (Table 2.1). The flask was placed in the CO_2 incubator for 10 minutes to allow for enzymatic dissociation of the cells from the bottom of the flask. After incubation, the flask was held firmly in a horizontal position and the side of the flask was struck sharply three times with the palm of a hand. This displaced most cells from the bottom of the flask which the presence of a cloudy solution confirmed.

The flask was examined under an inverted microscope (Olympus IX51, Olympus, New Zealand) to see if any cells remained on the bottom of the flask. If many cells remained, the solution containing the cells was removed and placed into a fresh 50mL falcon tube, whilst new TrypLE was added to the flask and the process was repeated with a reduced incubation time of 5 minutes. The supplemented IMDM was added to the falcon tube containing the dissociated DC2114 cells at approximately three times the volume of TrypLE present to inactivate the enzymatic reaction. The falcon tube containing the cells was centrifuged at 500 x *g* for 4 minutes, the supernatant was removed and discarded, and the pellet was re-suspended in 1 mL of supplemented IMDM. A 10 µL aliquot of re-suspended cells was taken for enumeration of viable cell concentration by hemocytometer. Once the cell concentration was determined, the cells were seeded into either T175 or T75 flasks at the appropriate seeding density for the final volume of supplemented IMDM (see Table 2.1). Cells were placed in a 37°C incubator under 5% CO_2 conditions for 2-3 days. The flask was checked every day to ensure normal growth and the media was replaced with fresh supplemented IMDM on the second day to enable adequate growth.

2.1.1.5 Cell Counting of DC2114 Cells via Hemocytometer and Trypan Blue Staining

Trypan blue staining is a rapid way to measure the number of viable cells in a dish by assessing the proportion of cells that remained colourless. The trypan blue stain is impermeable to intact, live cells and the cell remains clear in appearance. Conversely, dead cells with damaged membranes become stained with trypan blue.

This test was performed by adding 10 µL of 0.4% (w/v) trypan blue (Gibco™, ThermoFisher Scientific, New Zealand) to a 10 µL aliquot of re-suspended cells and mixed by pipetting. The Neubauer improved hemocytometer (Boeco, Germany) was wiped clean with a Kimwipe along with a glass coverslip. An aliquot of 10 µL of the trypan blue/cell mix was added underneath the coverslip onto the hemocytometer grid.

Cell viability was estimated by counting the number of clear cells in each square at the corners of the grid (top equation). The total number of cells counted in each square was averaged and substituted into the following equation to determine total cell number.

Total cells per mL = Total cell count X df X volume X 10,000.

% viability = # live cells / (# live cells + # dead cells)

[Where df stands for dilution factor]

2.1.1.6 Maintaining Frozen Cell Banks of DC2114 Cells

Cells were stored in liquid nitrogen to maintain adequate stocks for on-going experiments. Excess cells were prepared for storage when the T175 culture flasks reached 80% confluency. The cells were passaged, and a small aliquot was counted using the trypan blue method as described above (Sections 2.1.1.4 and 2.1.1.5, respectively).

The remaining cells were centrifuged at 500 x *g* for 4 minutes and re-suspended in supplemented IMDM culture containing 10% (v/v) dimethyl sulfoxide (DMSO). Depending on total cell number, several cryovials were prepared by transferring 1mL of the IMDM (10% DMSO) media containing $5x10^6$ cells. The cryovials were placed in a CoolCell™ LX Freezing Container, (Merck, Sigma Aldrich, New Zealand) and the container was placed at -80°C freezer. This container ensured the temperature was gradually decreased to prevent cell shock. After 24 hours, the cells were transferred into a liquid nitrogen Dewar for longer term storage. See Figure 2.1 for a graphical depiction.

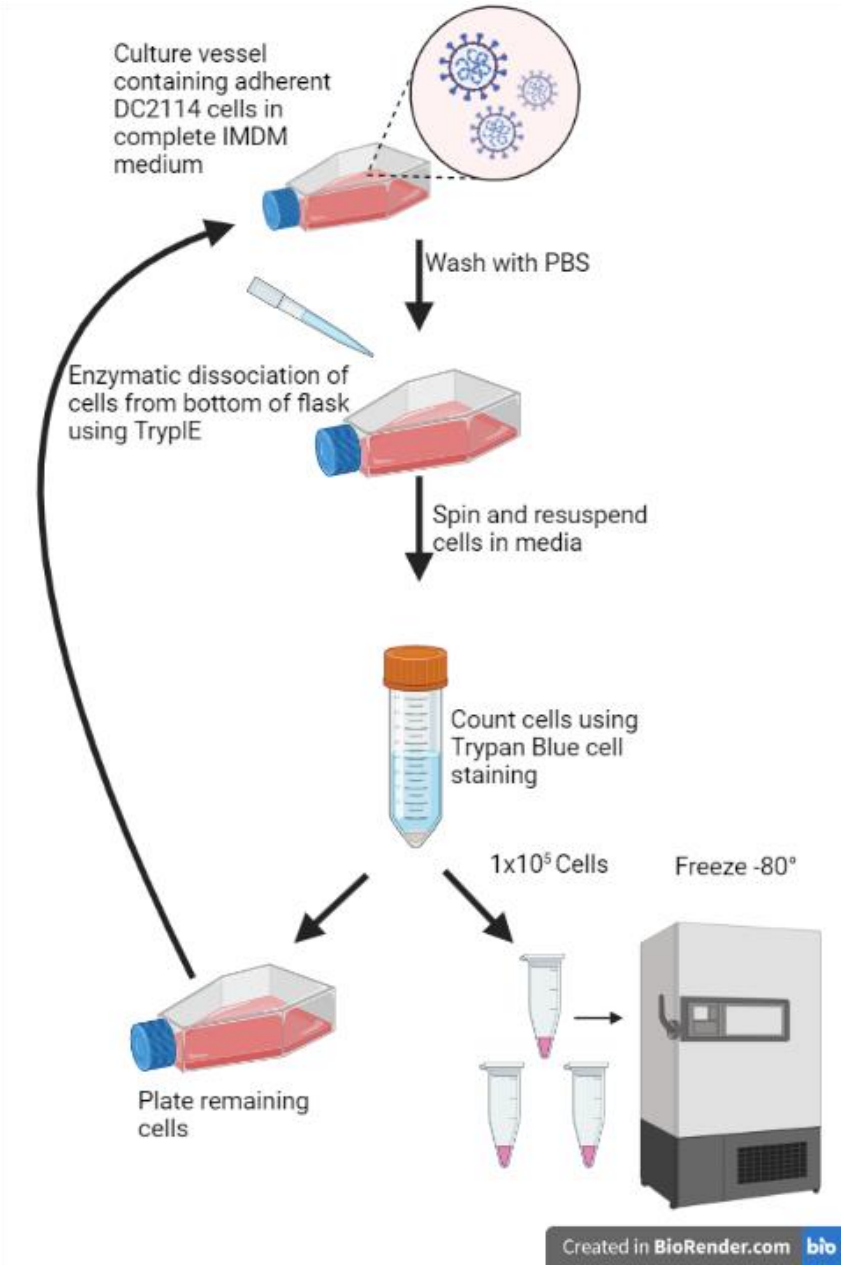

Figure 2.1: Schematic experimental overview of cell passage and collection for later analysis. *Cells were maintained in a culture flask containing supplemented IMDM. When cells reached 80% confluency, they were washed with PBS, dissociated using TryplE, washed and counted to determine total cell number. A portion of cells were transferred into three tubes, each containing 1x105 cells. The cells were washed, pelleted, and stored at -80°C until qCPR processing. The remaining cells were replated in supplemented IMDM for continuation of the experiments. Image created in BioRender.com*

Section 2.1.2 Characterising Clec9a Gene Expression in DC2114 Cells

2.1.2.1 Preparation of Cells for qPCR Analyses

To determine if Clec9A mRNA levels change with passage number, some cells were removed from the culture at each passage and prepared for analyses as shown in Figure 2.1. After passaging, 100,000 cells in supplemented IMDM were transferred into 1.5 mL tubes in triplicate and centrifuged at 500 x *g* for 4 minutes and the supernatant was removed. The pellet was re-suspended in 200 µL of PBS and centrifuged again at 500 x *g* for 4 minutes. This wash step was repeated two more times. The tubes containing the washed cell pellet were snap frozen on dry ice and transferred to the -80°C freezer for storage until qPCR processing.

2.1.2.2 RNA Extraction of DC2114 Cells

To investigate the effect of passage number on the expression levels of *Clec9A* messenger ribonucleic acid (mRNA), total RNA was extracted from the stored frozen pellets and assessed using quantitative PCR (qPCR). The total RNA was extracted from DC2114 cells using the Nucleospin RNA XS RNA isolation kit (Takara Bio, New Zealand) following manufacturer's instructions.

All preparations were performed in a biohazard cabinet. In brief, 100 µL of buffer RA1 and 2 µL of 570 mM Tris(2-carboxyethyl)phosphine (TCEP) was added to each cell sample to lyse the cells and tubes were vortexed twice for 5 seconds. An aliquot of 5µL of 4 ng/µL carrier RNA working solution was added and the tubes were vortexed twice for five seconds.

A NucleoSpin® filter was placed in a collection tube. The contents of the tubes containing the lysed cells (approximately 110 µL) was transferred to the filter and centrifuged for 30 seconds at 11,000 x *g*. The Nucleospin filter was removed and 100 µL of 70% ethanol was added to the tube containing the filtrate and mixed by pipetting up and down. Ethanol is added to precipitate the RNA and wash away the salts in the solution. The filtrate was then added to a NucleoSpin® RNA XS Column in a collection tube and centrifuged for 30 seconds at 11,000 x *g* to bind the RNA to the column. The filtrate from the column was discarded and the filter was placed into a fresh collection tube.

To desalt the silica membrane, 100 µL of membrane desalting buffer (MDB) was added to the column and centrifuged at 11,000 x *g* for 30 seconds. Any contaminating genomic DNA inside the column was digested by adding 25 µL of 8-9 % rDNAse onto the centre of the silica

membrane on the RNA XS column and incubated at room temperature for 15 minutes. The silica membrane in the RNA XS column was washed by adding 100 µL of buffer RA2 to the column and incubating at room temperature for 2 minutes. After incubation, the column was centrifuged at 11,000 x *g* for 30 seconds. The column was transferred to a new collection tube.

An aliquot of 400 µL of buffer RA3 was added to the column and centrifuged at 11,000 x *g* for 30 seconds. The eluant in the collection tube was removed and the column was replaced back into the collection tube. An aliquot of 200 µL of buffer RA3 was added to the column and centrifuged at 11,000 x *g* for 2 minutes.

The column was transferred into a new collection tube and 15 µL of RNase free Ultra-Pure H_2O was added to the column and centrifuged at 11,000 x *g* for 30 seconds. The collection tube containing the extracted RNA was retained and stored in a -80°C freezer for further processing.

2.1.2.3 cDNA Synthesis of Total RNA

The concentration of total RNA in each sample was determined using NanoDrop 2000 UV Visible Spectrophotometer (ThermoFisher Scientific, New Zealand). The surface of the NanoDrop was cleaned using a Kimwipe, initialised using Ultra-Pure H_2O and normalised against Ultra-Pure H_2O. An aliquot of 2 µL from each total RNA sample was added to the nanodrop surface and the total RNA concentration in ng/µL was recorded.

To synthesise complementary DNA (cDNA) from total RNA, the SuperScript™ VILO™ cDNA Synthesis Kit (ThermoFisher, New Zealand) was used. All solutions were thawed on ice, vortexed for several seconds and centrifuged briefly. A mastermix was prepared considering the number of samples being processed, with the addition of two reactions to account for pipetting error. A single reaction contained 4 µL of 5X VILO reaction mix, 4 µL of Ultra-Pure H_2O and 2 µL of 10X superscript enzyme mix.

An aliquot of 10 µL of each total RNA sample was transferred to a labelled 200 µL qPCR reaction tube containing 10 µL of the reaction mastermix. The cDNA synthesis was performed on the Rotorgene Thermocycler (Qiagen, New Zealand) by incubating the tubes at 25°C for 10 minutes, 42°C for 120 minutes and a final incubation at 85°C for 5 minutes. The cDNA samples were stored at -20°C until further processing.

2.1.2.4 SYBR Green qPCR

For qPCR, the Brilliant II SYBR Green qPCR Master Mix (Agilent, New Zealand) was used. Before use, the cDNA samples were thawed on ice, vortexed for 10 seconds and centrifuged to collect the contents at the bottom of the tube.

Primer sets for three mouse genes were synthesised and their sequence information is listed in Table 2.2. The genes included the two reference genes *Rpl19* and *Ppia,* and the gene of interest, *Clec9a*. Reference genes are genes within an organism that are expressed at consistent levels relative to RNA input and should not change under experimental treatments and conditions. The reference genes are used to normalise the expression of *Clec9a*. The *Rpl19* gene encodes a ribosomal protein, part of the 60S subunit (Davies & Fried, 1995) and the *Ppia* encodes a member of the peptidyl-prolyl cis-trans isomerase family (Feroze-Merzoug et al., 2002). To determine the optimal working concentrations of the primers, different concentrations of forward and reverse primers were assessed for each gene, ranging from 50 to 300 nM. The concentrations of the primer pair (forward and reverse) for each gene that gave the lowest Cq values with the lowest primer concentrations was selected as the optimal concentration and were used for all qPCR reactions. The amplification efficiencies of the reactions for each gene were determined and are discussed in detail in Section 2.1.2.5.

Table 2.2: Primer sequences that were designed using sequence information on NCBI (Accession numbers).
The optimised final concentrations for use in SYBR green qPCR experiments are also listed

Primer	Sequence	Accession #	Final Conc (nM)
Clec9A Forward	GTGGAACATCAGTAAGAAGAG	EU339277	300
Clec9A Reverse	GAGAGGAGAAGAGCCATC	EU339277	300
Rpl19 Forward	GACCGCCATATGTATCAC	NM_001159483	300
Rpl19 Reverse	GTGCTTCCTTGGTCTTAG	NM_001159483	300
Ppia Forward	CAGACAAAGTTCCAAAGAC	NM_008907.2	400
Ppia Reverse	TCCTGGAATAATTCTGTGAA	NM_008907.2	300

A master mix sufficient for duplicate reactions of each sample, plus two additional reactions to account for pipette error, was prepared. The 1X master mix (for each sample) contained 26 µL of 2X SYBR mix, either 1.56, 1.56 or 2.08 µL of 10 µM forward primer for *Clec9, Rpl19 and Ppia*,

respectively, and 1.56 µL of 10 µM reverse primer (for all genes). The reaction was made up to a total volume of 49.92 µL (per reaction) with Ultra-Pure H_2O. Following the transfer of 49.92 µL of the master mix into labelled PCR tubes, an aliquot of 2.08 µL of 7.5ng/µL sample cDNA was added to each tube to make a final volume of 52 µL. A no template control was included by replacing the cDNA sample with 2.08 µL of Ultra-pure H_2O. A no-RT PCR control was not included due to an oversight.

The tubes were mixed by vortexing for 20 seconds and were centrifuged for 5 seconds to collect the liquid at the bottom of the tube. Two 25 µL aliquots of each sample reaction were transferred into two 0.1 mL qPCR strip tubes as duplicates of each sample.

The samples were amplified using the Rotor-Gene™ 6000 Real-Time Analyzer (Corbett Life Science, Qiagen, New Zealand) under the following conditions: denaturation at 95°C for 10 minutes, and then 40 cycles of 95°C for 15 seconds and 60°C for 60 seconds, followed by a final extension step at 72°C for 15 seconds. A melt curve was generated from 60-95°C with an increase in 0.95°C at each step.

To calculate the relative expression of *Clec9A* in DC2114 cells, three independent technical replicates of each cell sample were performed. The two reference genes were compared to each other to ensure both genes were behaving as reference genes. Figure 2.2 presents the relationship between the genes. The Cq values for *Ppia* were plotted on the Y-axis, while the Cq values for *Rpl19* were plotted on the X-axis, resulting in a linear relationship. The data fitted the linear equation with a coefficient of determination (R^2) of 0.934, indicating that the Cq values for both *Rpl19* and *Ppia* were closely related and the data points fit the line of best fit well.

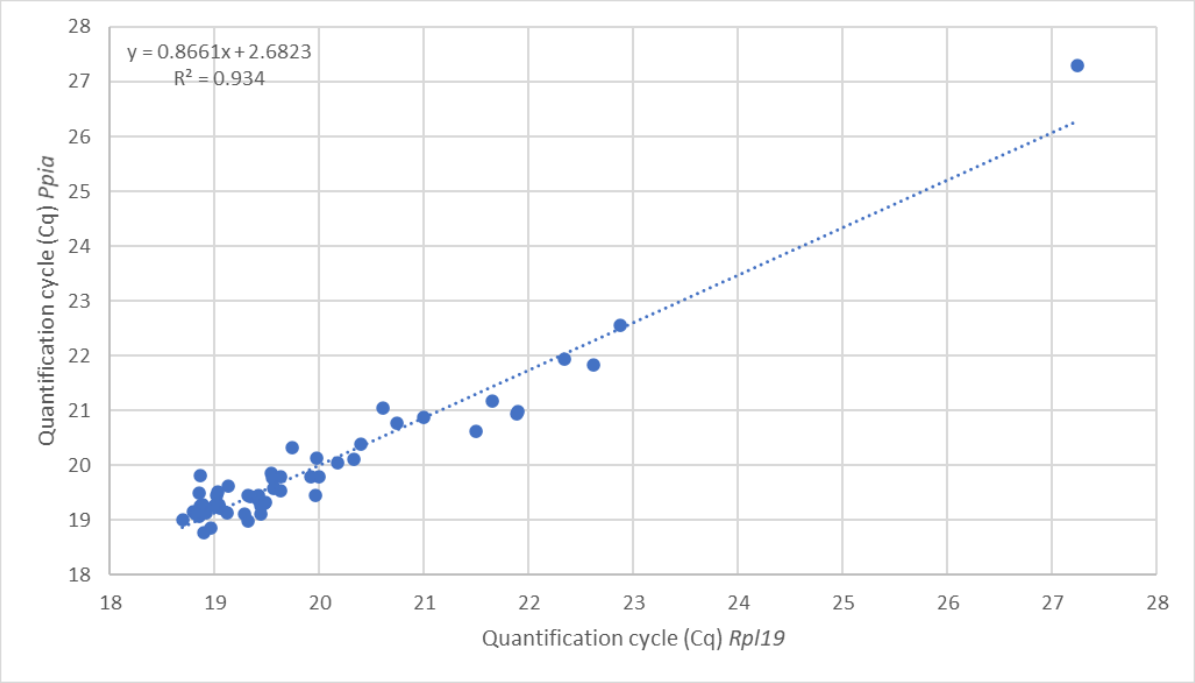

Figure 2.2: Linear regression plot of quantification cycle (Cq) values for genes Ppia and Rpl19.
Ppia (Y axis) and Rpl19 (X axis) for samples 1-54 of DC2114 cDNA. Samples 1-18 are from biological replicate one, passages 1-6 in triplicate. Samples 19-36 are biological replicate two, passage 1-6 in triplicate. Samples 37-54 are biological replicate three, passage 1-6 in triplicate. The R2 value for the linear regression plot is shown on the graph.

The reference gene *Rpl19* was selected to normalise the expression levels of *Clec9a.* This normalisation step accounts for differences in cDNA loading and integrity between samples. The normalisation reference gene selected was *Rpl19* because it exhibited similar Cq values to the gene of interest. Relative *Clec9A* expression levels were calculated using the $2^{(-\Delta\Delta Cq)}$ method and the following equation (Schmittgen & Livak, 2008).

Fold change = $2^{(-\Delta\Delta Cq)}$

Where,

$2^{-\Delta\Delta Cq} = 2^{[-(\Delta Cq)-(\mu\, P1)]}$

ΔCq = GOI – IC

μ P1 = Average of Cq for Passage one (all samples)

GOI = gene of interest

IC = internal control

2.1.2.5 Reaction Efficiency of qPCR

The amplification efficiency for each gene was determined using the optimised forward and reverse primer concentrations. A two-fold serial dilution of cDNA was prepared using 5 ng/µL cDNA at 1, 1:2, 1:4, 1:8, 1:16, 1:32, 1:64, 1:128, 1:256, and 1:512 dilutions. The efficiencies of the qPCR reactions for each gene were determined by the equation below and are illustrated in Figure 2.3.

$$E = -1 + 10^{\left(\frac{-1}{slope}\right)}$$

Where, E is the reaction efficiency, and the closer to one, the more efficient the reaction.
M is slope
And R^2 which illustrates how well the data points fit the calculated line of best fit.

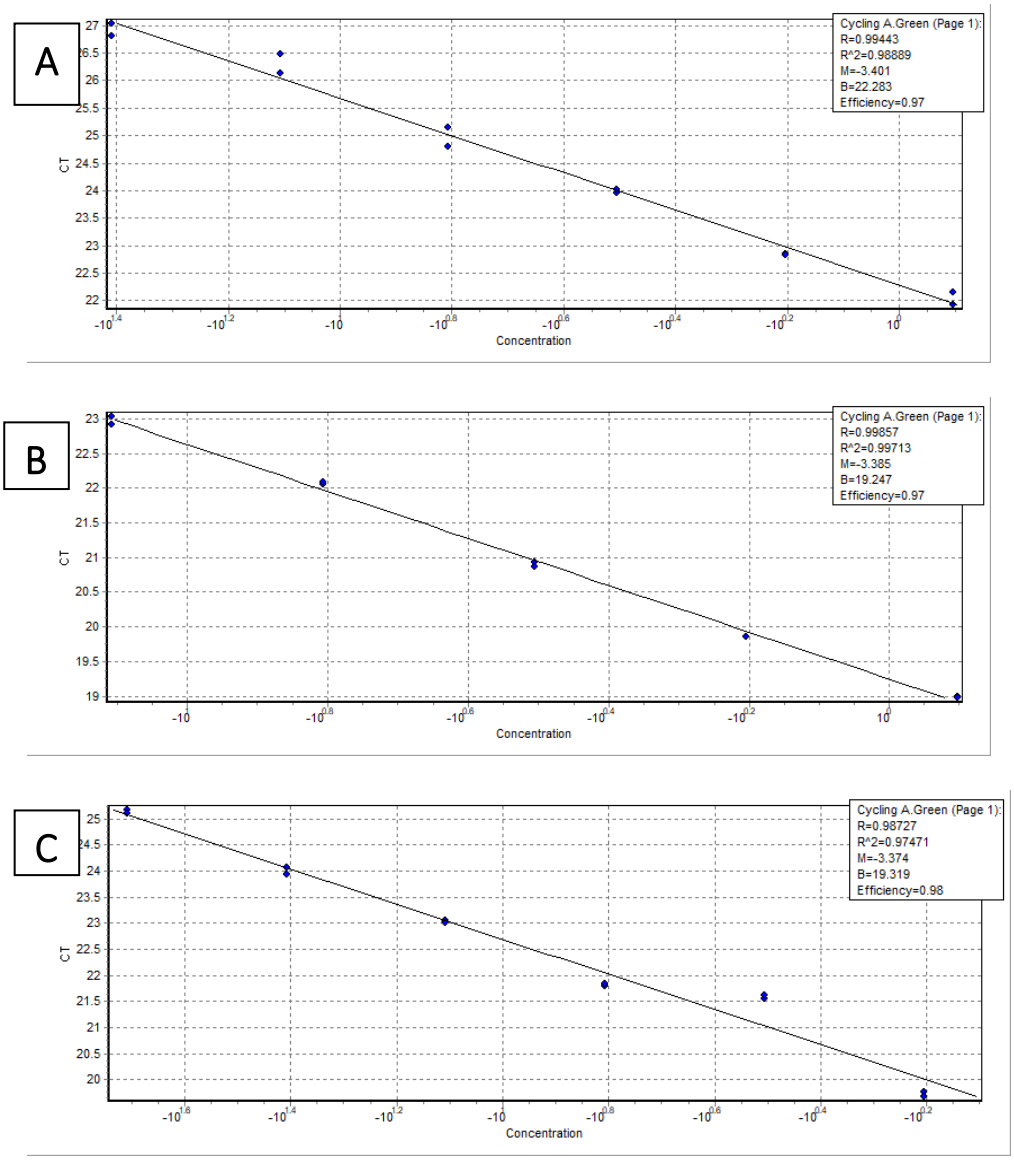

Figure 2.3: Standard curve for Clec9a, Rpl19 and Ppia.
Graphs show 1:1 serial dilutions of 5ng/µL starting cDNA template of DC2114 cells the genes A) Clec9A B) Rpl19 and C) Ppia. The reaction efficiency (E), slope (M), and coefficient of determination (R2) values are indicated on each graph.

2.1.2.6 Statistical Analyses of qPCR Data

All statistical analyses were performed using IBM® SPSS® analytical software. All significant differences were identified at a level of $P<0.05$. Graphs were made using Microsoft Excel.

All data was tested for normality by performing a P-P plot, based on the Levene's test for normality. A one-way ANOVA was performed between vial passage number, and where significant differences were found, were followed by post-hoc Bonferroni tests to determine differences between groups.

Section 2.1.3 Characterising Clec9A Protein on DC2114 Cell Surface

The proportion of DC2114 cells with the Clec9A receptor present on its surface membrane were assessed using flow cytometry. Fresh mouse splenocytes were used as a positive control. The JAWS II cells, a bone marrow derived immortalized immature DC line that harbours characteristics of myeloid derived precursor cells, expressing high levels of CD11b, CD24, CD44 and F4/80 (Jørgensen et al., 2002; Kasahara & Clark, 2012) were used as a negative control. All flow cytometry work was conducted at the Malaghan Institute of Medical Research under the guidance of Prof Ian Herman's research team.

2.1.3.1 Cell Culture and Harvesting of Suspension Cell Line; JAWS II

The JAWS cell line is a suspension DC line, meaning that the cells do not adhere to the bottom of the flask. Following the kind gifting from Prof Ian Herman's group of a culture flask containing JAWS II cells, the cloudy solution in the flask containing the cells was removed and placed into a 50 mL tube. The flask was washed several times with 10 mL of PBS by pipetting up and down with a serological pipette and was also placed in the same tube as the cells. To ensure the removal of all cells, 5 mL of TryplE was added to the flask and incubated in a CO_2 incubator (5%) at 37°C for five to ten minutes. The TryplE was removed from the flask and added to the tube containing the cells. The 50 mL tube containing the cells was centrifuged at 500 x *g* for 4 minutes and the supernatant was removed and discarded. The pellet was re-suspended in 1 mL of Minimum Essential Medium α (MEMα), supplemented with 5% (v/v) FBS and 5000 U/mL of penicillin with 5000 µg/mL of streptomycin (Pen/Strep) (Gibco™, ThermoFisher Scientific, New Zealand). A 10 µL aliquot of re-suspended cells was taken for

enumeration of viable cell concentration by hemocytometer (Section 2.1.1.5). Once the cell concentration was determined, the cells were seeded at the appropriate seeding density and supplemented MEMα was added to the appropriate final volume into either T175 or T75 flasks (see Table 2.1). Cells were placed in a 37°C incubator under 5% CO_2 conditions for 2-3 days. The flask was checked every day to ensure normal growth and the media was replaced with fresh supplemented MEMα on the second day to enable adequate growth.

2.1.3.2 Harvesting Splenocytes from C57BL/6 Mice

Two spleens were obtained from C57BL/6 mice and placed in a 6-well plate containing 1 mL of IMDM per well. Digested and undigested spleens were prepared for analysis using flow cytometry. A digestion mix was prepared by adding 63 µL of 2.5 mg/mL Liberase (Liberase™ Research Grade, Sigma Aldrich, New Zealand) to 5 µL of 20 mg/mL DNase (Sigma Aldrich, New Zealand) and making up to a final volume of 500 µL with supplemented IMDM to final concentrations of 0.313 and 0.2 mg/mL, respectively. The digestion preparation was injected into one spleen and incubated at 37° for 25 minutes. Post incubation, both spleens, digested and undigested, were each pressed through separate 70 µm cell strainers (Fisherbrand™, Fisher Scientific, New Zealand) along with the addition of 10 mL IMDM. The filtrates were placed into separate 15 mL tubes and centrifuged at 500 x *g* for 4 minutes. The supernatants were discarded, and the pellets were resuspended in 1 mL of red blood cell lysis buffer (Roche, Sigma Aldrich, New Zealand). Both sample filtrates were agitated for 1 minute and centrifuged for 1 minute by vortex. The supernatant was discarded and both cell pellets were resuspended in 1 mL of supplemented IMDM. A 10 µL aliquot of re-suspended cells was taken to determine the viable cell concentration by hemocytometer and trypan blue cell staining (Section 2.1.1.5).

A 100 µL aliquot of each cell preparation, containing approximately $1x10^6$ cells, was added to four wells of a 96 well plate and resuspended in the appropriate complete culture medium (Figure 2.4). The appropriate culture media for the JAWS II, DC2114 and spleen cells were supplemented MEMα and supplemented IMDM, respectively. The plates were centrifuged for 2 minutes at 770 x *g*. The supernatant was removed from the plate by turning upside down with a flicking motion into a sink. The cells were resuspended and washed in 200 µL PBS before a final centrifugation step of 770 x *g* for 2 minutes.

	1	2	3	4	5	6	7	8	9	10	11	12
A	JAWS II Unstained	JAWS II + Zombie	JAWS II FMO + Zombie	JAWS II Full Stain + Zombie								
B	DC2114 Unstained	DC2114 + Zombie	DC2114 FMO + Zombie	DC2114 Full Stain + Zombie								
C	Spleen Digested Unstained	Spleen Digested + Zombie	Spleen Digested + Zombie	Spleen Digested Full Stain + Zombie								
D			Spleen Undigested FMO + Zombie	Spleen Undigested Full Stain + Zombie								
E												
F												
G												
H												

Figure 2.4: Format of 96-well plate setup for flow cytometry experiments.
Wells A1-A4 contained the negative control cell line JAWS II. Wells B1-B4 contained the experimental cell line, DC2114. Wells C1-C4 contained the positive control, digested splenocytes, where dig stands for digested splenocyte cell samples. Wells D3-D4 contain further positive controls but undigested condition.

2.1.3.3 Cell Staining

The Zombie NIR™ (BioLegend, USA) fluorescent dye, which is permeable to cells with compromised membranes, was used to determine cell viability within the flow cytometry experiments. A ratio of 1:10000 of Zombie NIR™: PBS was used to determine the viability of both DC2114 and JAWS cells, while a ratio of 1:2000 was used for splenocytes.

A full multicolour stain, containing fluorescent antibodies for MHC II, Clec9A, CD11c, B220 and CD8, in addition to a fluorescence minus one (FMO) stain (cocktail of all antibodies with the omission of the Clec9A antibody), was prepared in flow cytometry staining buffer (FACS buffer) (1xPBS, 5% FBS). See Table 2.3 for details.

Table 2.3: Names and type of fluorescent antibodies used to stain cell conditions for flow cytometry.

A master mix was prepared for a full stain which contained all antibodies at their given volume, and a FMO stain containing all antibodies except for Clec9A PE. The total volume of the master mix was 500 µL in flow cytometry staining (FACS) buffer.

Flow cytometry channel (wavelength)	Antibody	Clone	Dilution	Volume of 10X antibody added to mastermix (µL)
Violet (450)	MHCII BV421	M5/114.15.2	1000	0.5
Yellow Green (1 577)	Clec9A PE	42D2/7H110	100	5
Yellow Green (10 812)	CD11c Pe-Cy7	HL3	100	5
Red (1 660)	B220 APC		200	2.5
Ultra Violet (2 387)	CD8 BUV395	53-6.7	500	1
Total volume in buffer: 500µL				

A 50 µL aliquot of the diluted Zombie NIR™ was added to the respective cell pellets within the 96 well plate as detailed in Figure 2.4, with the exception of the wells containing the unstained cells. The pellets were resuspended in the Zombie NIR™ dilution by pipetting up and down, and the cells were incubated for 15 minutes at room temperature. After incubation, the cells were centrifuged at 770 x *g* for 2 minutes and the supernatant was removed. A PBS wash step was performed three times whereby the cells were resuspended in 200 µL of PBS, centrifuged at 770 x *g* for 2 minutes and the supernatant was discarded.

The washed cells were then resuspended in 50 µL of either the full multicolour antibody mixture or FMO and incubated for 15 minutes at -4°C covered with tinfoil. After incubation,

the cells were centrifuged for 2 minutes at 770 x *g*, the supernatant was removed. Three wash steps were performed as described above After the final wash; the cells were resuspended in 200 µL of FACS buffer.

2.1.3.4 Flow Cytometry

All cell samples were transferred to 5 mL flow cytometry tubes and the experiments were performed on the Cytek Aurora Borealis (Cytek Biosciences) flow cytometer using the scattering conditions detailed in Table 2.4.

Table 2.4: Table of experimental conditions for flow cytometry.
The fluorescence intensities of each antibody were measured via flow cytometry on the Cytek Aurora Borealis flow cytometer for each cell group.

Cell type	Forward Scatter (FSC)	Side Scatter (SSC)	Area Scaling Factor (ASF)
JAWSII	25	40	0.85
DC2114	30	150	1.3
Splenocytes	40	30	1.3
Beads	50	200	

2.1.3.5 Flow Cytometry Data Analysis

Following flow cytometry of cell samples, the proportion of cells from all populations that were expressing Clec9A were determined using the following gating strategy. Single cells were first gated against forward scatter height (FSC-H) and forward scatter area (FSC-A) (Y and X axis respectively). This provided a proportion of cells present diagonally across the dot plot and removed populations of cells that were clumped together. Cells of interest, dendritic cells, were gated using side scatter area (SSC-A) and FSC-A (Y and X axis respectively) to filter cells based on granularity and size, respectively. Live cells were gated using Zombie NIR and FSC-A (Y and X axis respectively). Splenocytes were additionally gated for B220 negative cells, a B cell lineage marker, as splenocytes are not an isolated cell population like the immortalized cells, i.e. DC2114 and JAWS II cells. The B220 signal on the Y-axis was gated against FCS-A on the X-axis. Double positive cells for the cDC1 lineage markers, MHCII and CD11c, were gated with MHCII on the Y-axis and CD11c on the X-axis. For splenocytes, an additional gating step was

required to further isolate cDC1 cells that were both $CD8^+$ (y axis) and $CD11c^+$ (x axis). Finally, cells were gated for $Clec9A^+$ and $CD11c^+$ (or $CD8^+$ for splenocytes) expression. Figure 2.5 is a graphical representation of the gating strategy for splenocytes which included all gating steps for the immortalized cell lines in addition to gating to remove other cell populations such as B cells.

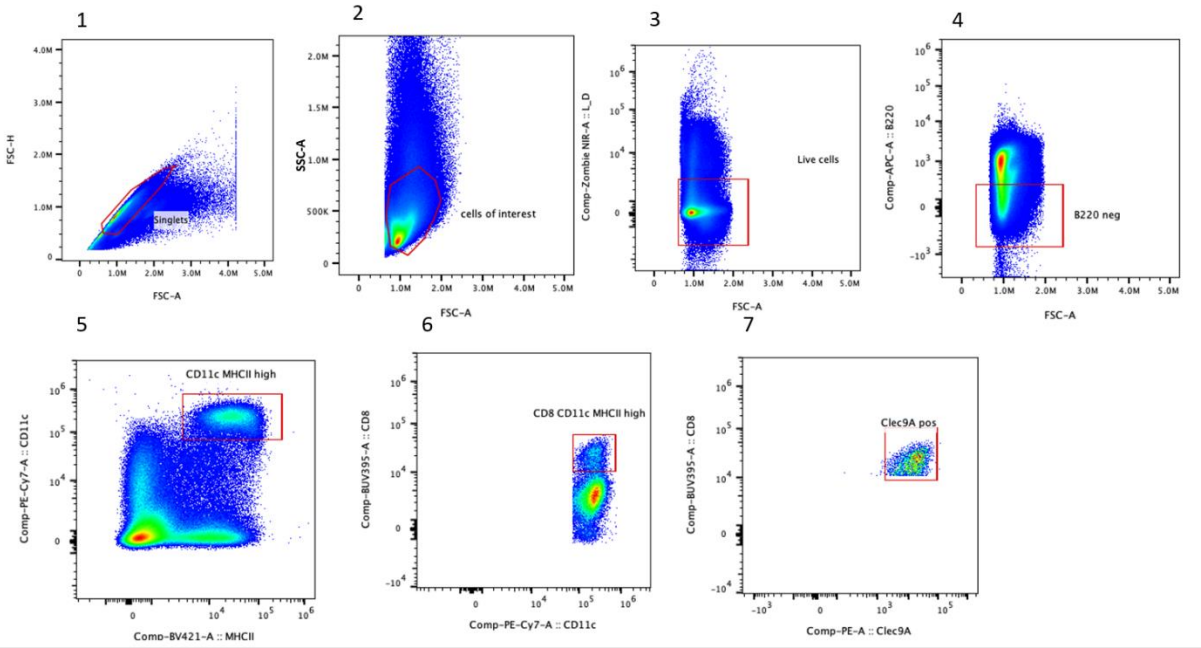

Figure 2.5: Flow cytometry gating strategy.
Strategy used to assess the proportion of specific cells expressing levels of Clec9Ain DC2114, JAWSII and splenocyte cells. The final gate for Clec9A expressing cell populations was compared to the gate for FOM cell populations (without Clec9A specific antibody) to determine the true population of cells expressing Clec9A. Figures 1-7 represent the systematic gating strategies to obtain specific cells 1) Singlet cells, 2) Cells of interest, 3) Live cells, 4) B220 negative cells, 5) Double positive CD11c and MHC II cells, 6) Double positive CD8 and CD11c cells, 7) Clec9A positive cells.

Section 2.2 Experimental Design for Objective 2

2.2.1 SELEX

A hybrid SELEX approach was used that combined Protein-SELEX and Cell-SELEX. Protein-SELEX is the selection method where the oligonucleotide pool is incubated with recombinant or purified protein that is typically immobilised onto beads or a column. Cell-SELEX incorporates oligonucleotide selection against a whole cell to select sequences that bind the cell or receptors expressed upon its cell surface. The first seven rounds of selection were performed using recombinant mouse Clec9A protein (see Protein-SELEX Figure 2.7 for overview). Thereafter, the enriched library was divided into two, and the final two rounds were performed using either recombinant protein or $CD8^{+ve}$ mouse splenocytes expressing the Clec9A receptor (Cell-SELEX, see Figure 2.8 for overview). The $CD8^{+ve}$ mouse splenocytes were selected for Cell-SELEX since the DC2114 cells did not express Clec9a on their surface (see Section 3.1.2).

These experiments were designed with a negative selection step which preceded each round. The negative selection step in these experiments involved either incubation with the magnetic beads alone (for Protein-SELEX) or the $CD8^{-ve}$ splenocytes (for Cell-SELEX). See Figure 2.6 for an overview of the SELEX performed.

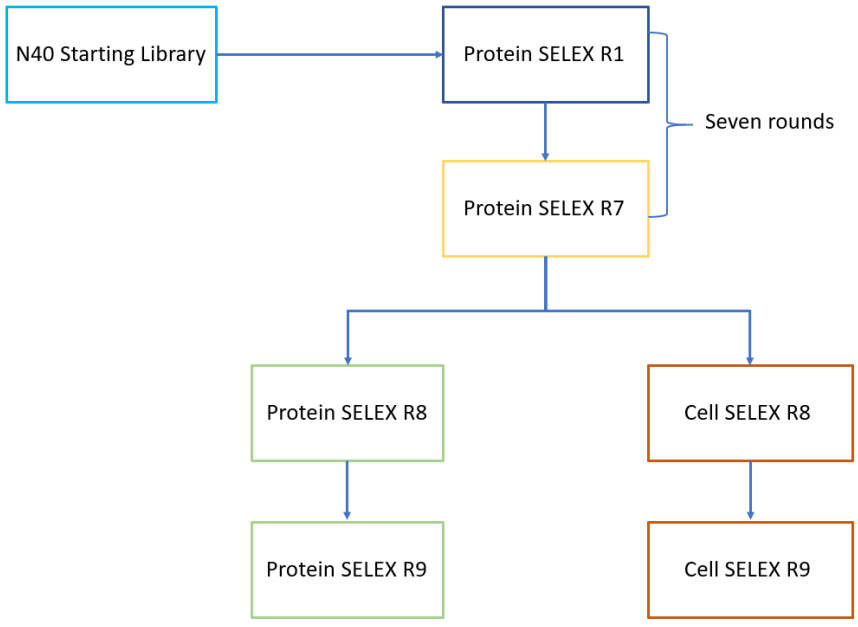

Figure 2.6: Hybrid SELEX experimental schematic.
The N40 oligonucleotide library was used as the starting library for the SELEX experiments. Seven rounds of Protein-SELEX were performed using recombinant Clec9A conjugated to protein G magnetic beads. At Protein SELEX R7, the SELEX library was split and two additional rounds of either Protein-SELEX or Cell-SELEX were continued in parallel.

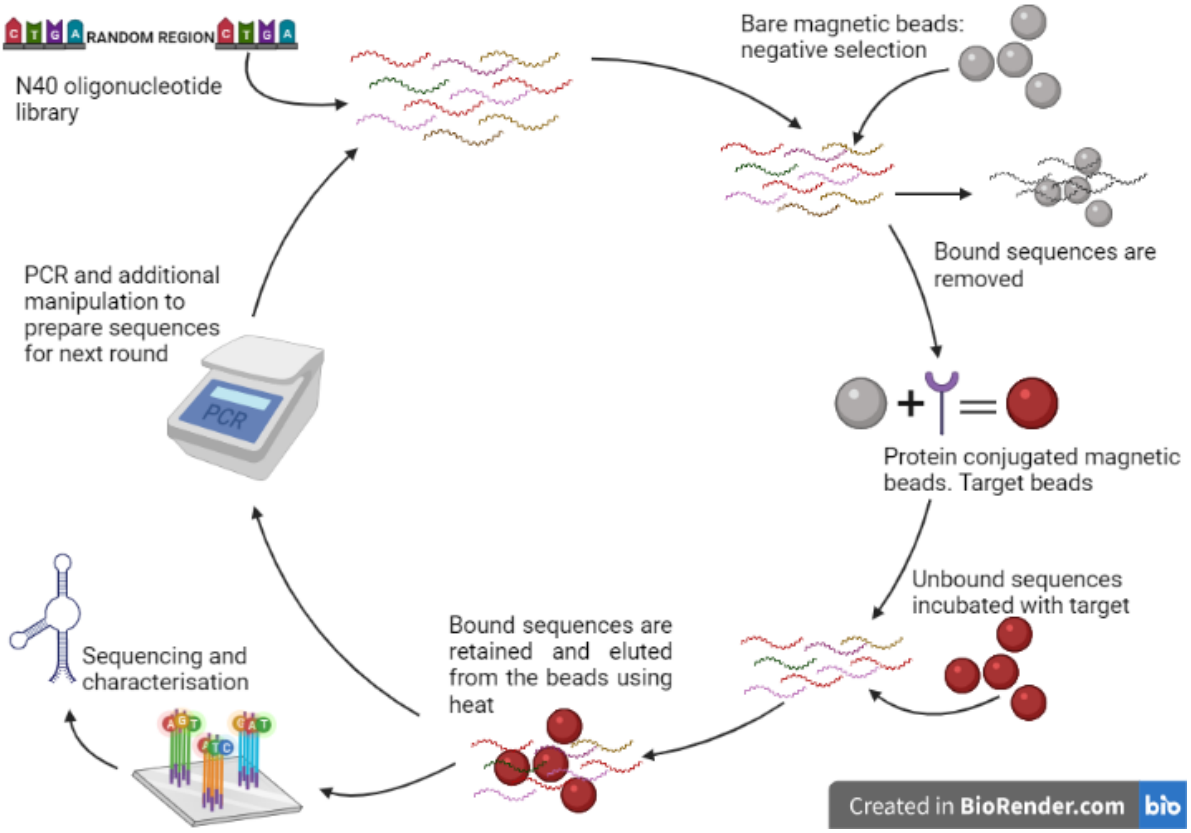

Figure 2.7: Schematic outline of the magnetic bead-based SELEX process.
To begin, a random oligonucleotide library is used for the starting round of SELEX. The library is incubated with bare magnetic beads as a negative selection step to remove non-specific oligonucleotides. The bare magnetic beads with its bound sequences are removed while the sequences that remain in the supernatant are incubated with the target magnetic beads. The target beads are prepared by conjugation through Fc tags on the recombinant Clec9A protein and protein G present on the beads. The sequences that bound to Clec9A present on the beads are removed and amplified using SYBR green PCR. The amplified products are further processed for the following round of selection. After the appropriate rounds of SELEX are met, the library is sequenced, and potential candidates are characterised. Image created in BioRender.com.

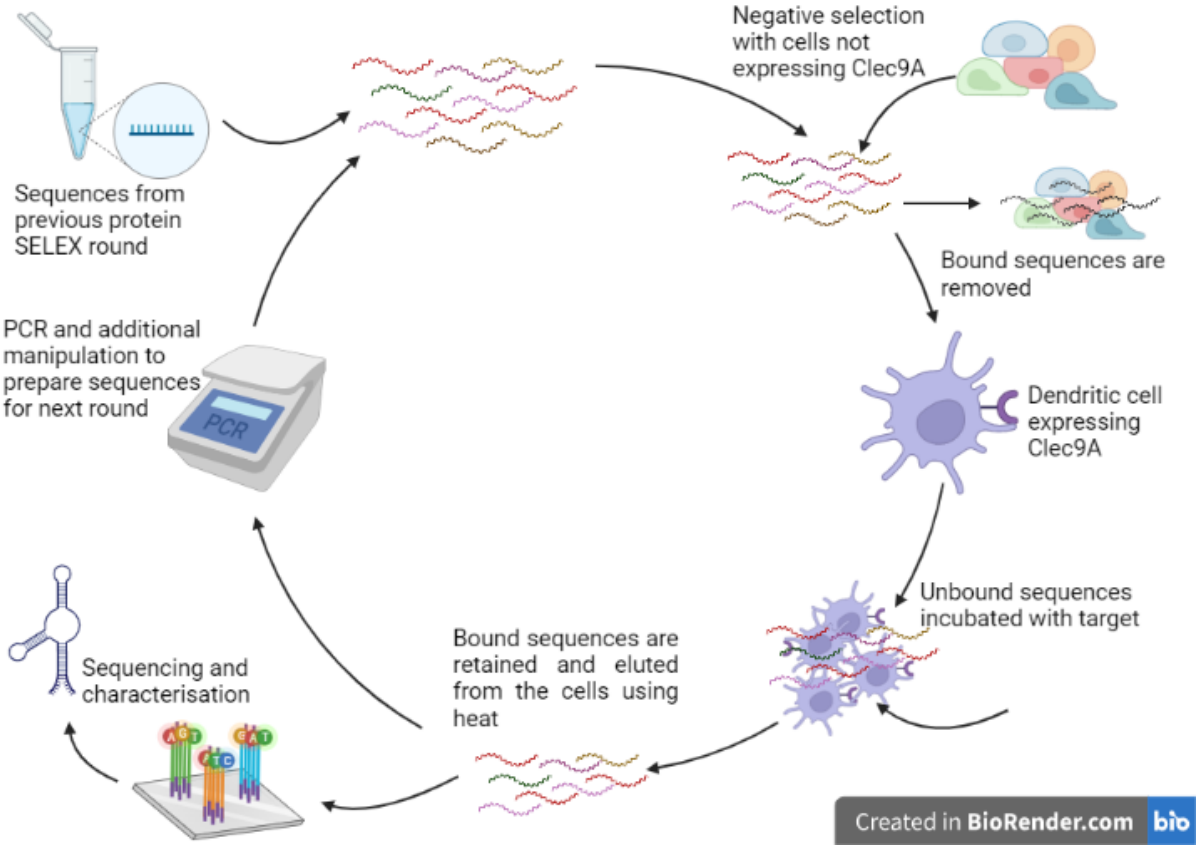

Figure 2.8: Schematic outline of the experimental design for cell-based SELEX using mouse dendritic cells.
The evolved oligonucleotide library from the final round of Protein-SELEX is used for the first round of cell SELEX. The procedure is the same as described above. The oligonucleotides first are incubated with cells negative for Clec9A cell surface expression to remove non-specific sequences. Followed by incubation of non-bound sequences with Clec9A positive dendritic cells. Image created in BioRender.com

2.2.1.1 Primer Region of Starting Library

To enable PCR amplification of random nucleotide sequences, conserved primer regions that flank the random region must be designed. The primer design was generated using Random DNA sequence Generator (Maduro, 2021) to provide rules for the primer creation software. The primers were generated using the Primer 3 software and reaction conditions as previously published (Koressaar & Remm, 2007; Thornton & Basu, 2011) and listed in Table 2.5. Unless otherwise stated, all other conditions remained as the default selection. The primers generated through Primer3 were cross verified using OligoAnalyzer (Owczarzy et al., 2008) which provides information on primer length, melting temperature, GC content (%), ΔG of hairpins formed, self-dimers, and hetero-dimers. Efficient primers pairs have minimal differences between melting temperature and primer length. Furthermore, efficient primers have a ΔG of less than -4 as this minimises mis-priming and spontaneous associations. Efficient primer conditions were achieved by systematically changing bases within the primer sequence and analysing the results.

Table 2.5 Optimal conditions to generate primers using Primer3 online free software.

Condition	Optimal
Primer size	Min: 18, optimal: 20, max: 23
Primer melting temperature (Tm)(°C)	Min: 50, optimal, 57.5, max: 65
Maximum Tm difference (between primers)	1°C
Primer G C content (%)	Min: 40, optimal, 50, max: 60
Numbers to return	10
Max 3' stability	9
Max repeat mispriming	12
Pair max repeat mispriming	24
Max template mispriming	12
Product Tm (°C)	50
Max self-complementarity	4
Max 3' self-complementarity	3
Max-poly X	3

2.2.1.2 Oligonucleotide Library Design for SELEX

The random oligonucleotide library is a library that typically consists of a variable or random region of 40 nucleotides in length, flanked by conserved primer regions. The oligonucleotide library was designed using the optimised primer sequences (Table 2.6). The random oligonucleotide library containing the conserved primer binding sites (Table 2.6) was ordered through Integrated DNA Technologies (IDT, Singapore).

To ensure the random oligonucleotide library consisted of an equal amount of A:C:T:G, the synthesis ratio of 29:29:19:23 was used. The ratios are not equal in order to account for the phenomenon that during oligonucleotide synthesis, G and T bases have faster coupling rates to the available -OH group on the previous deblocked molecule, resulting in a skewed synthesis (Pollard et al., 2000).

Table 2.6: Primers and random oligonucleotide library used for SELEX experiments.
All primers were ordered through IDT Ltd.

Primer	Sequence
Forward primer	GTTAGTTGCTCTGCCTCTGG
Reverse primer	AGGGTCACACTGTCGTCATT
Biotin-reverse primer	Biotin- AGGGTCACACTGTCGTCATT
N40 Library	GTTAGTTGCTCTGCCTCTGG N40AATGACGACAGTGTGACCCT

2.2.1.3 Hybrid SELEX Using Oligonucleotide Starting Library

The random oligonucleotide starting (N40) library was provided in lyophilised form. To ensure the library was located at the bottom of the tube, the tubes were centrifuged at 17, 000 x *g* for 5 minutes. The oligonucleotide library was resuspended to a stock concentration of 100 µM with Ultra-Pure H2O, according to the manufacturer's instructions. To confirm the concentration, an aliquot that was further diluted to 10 µM was quantified by Nanodrop spectrophotometry. Any difference in concentrations were corrected for future use. Aliquots of the library at the corrected concentrations of 10 and 100 µM were prepared to prevent degradation from excessive freeze-thawing. Table 2.7 presents the selection conditions for each SELEX round for hybrid SELEX.

Table 2.7: Hybrid SELEX method outline.

Table identifies the selection steps, type of target and reagents used at each round of SELEX

Rounds	Library added	Negative screening	Positive screening	Incubation volume	Incubation components	Wash conditions
1	2.4 ng/µL	30uL protein G magnetic beads	30uL protein G magnetic beads with rec Clec9A	200 µL	PBS (pH 7.4) only	PBS with 0.001% IGEPAL
2	8.3 ng/µL	30uL protein G magnetic beads	30uL protein G magnetic beads with recClec9A	200 µL	PBS (pH 7.4) only	PBS with 0.001% IGEPAL
3	4.0 ng/µL	30uL protein G magnetic beads	30uL protein G magnetic beads with recClec9A	200 µL	75% PBS and 25% IMDM media	PBS with 0.002% IGEPAL
4	Data not recorded	30uL protein G magnetic beads	30uL protein G magnetic beads with rec Clec9A	200 µL	50% PBS and 50% IMDM media	PBS with 0.002% IGEPAL
5	4.0 ng/µL	30uL protein G magnetic beads	30uL protein G magnetic beads with rec Clec9A	200 µL	25% PBS and 75% IMDM media	PBS with 0.004% IGEPAL
6	12.7 ng/µL	30uL protein G magnetic beads	30uL protein G magnetic beads with recClec9A	200 µL	25% PBS and 75% IMDM media	PBS with 0.004% IGEPAL
7	10.9 ng/µL	30uL protein G magnetic beads	30uL protein G magnetic beads with rec Clec9A	200 µL	25% PBS and 75% IMDM media	PBS with 0.004% IGEPAL
Library is split						
Protein SELEX						
8	2.4 ng/µL	30uL protein G magnetic beads	30uL protein G magnetic beads with rec Clec9A	200 µL	100% IMDM media	PBS with 0.004% IGEPAL
9	3.4 ng/µL	30uL protein G magnetic beads	30uL protein G magnetic beads with rec Clec9A	200 µL	100% IMDM media	PBS with 0.004% IGEPAL
Cell SELEX						
8	2.4 ng/µL	$1x10^5$ Clec9A negative splenocytes	$1x10^5$ Clec9A positive splenocytes	200 µL	100% IMDM media	PBS with 0.004% IGEPAL
9	Data not recorded	$1x10^5$ Clec9A negative splenocytes	$1x10^5$ Clec9A positive splenocytes	200 µL	100% IMDM media	PBS with 0.004% IGEPAL

2.2.1.4 Preparation of Clec9A Target Molecule

Recombinant mouse Clec9A Fc Chimera protein, CF (R&D systems, In Vitro Technologies, New Zealand) is a mouse-derived protein produced in Chinese Hamster Ovary (CHO) cells and has a predicted molecular mass of 50.8 kDa. The Clec9A protein was reconstituted by adding 500 µL of PBS (pH 7.4) to the lyophilized protein in a glass vial to attain a concentration of 100 µg/mL. The solution was gently vortexed on low speed, pipetted into aliquots and stored at -80°C until use.

2.2.1.5 Preparation of Oligonucleotide Library

For the first round of selection, an aliquot of 100 µM of oligonucleotide library was diluted to 1 nM in PBS to a final volume of 220 µL. The tube was incubated on a heat block at 95°C for five minutes to linearise the oligonucleotides and then cooled on ice for 30 minutes.

2.2.1.6 Preparation of Protein G magnetic beads

The protein G magnetic beads were supplied from New England BioLabs and consisted of super-magnetic particles that have recombinant Protein G covalently coupled to their surface. Streptococcal Protein G is an antibody binding protein derived from bacterial origin and has a strong affinity to mouse IgG_{2a} (Akerström et al., 1985) and other immunoglobulins via their Fc fragment (Kato et al., 1995). Protein G magnetic beads were prepared fresh for every round of selection. The tube containing the Protein G beads (New England Biolabs) was gently inverted for 5 minutes to resuspend the beads in solution. Then, 30 µL of beads were transferred into a 1.5 mL tube and a magnetic field was applied to the tube to retain the beads at the side of tube as the liquid was removed. To wash the bead, 500 µL of 0.1 M sodium phosphate (pH 8.0) was added to the tube and the beads were resuspended by pipetting up and down. The beads were then held at the side of the tube with a magnetic field and the supernatant was removed. This wash step was repeated for a total of three washes. After the final wash step, the beads were resuspended in 100 µL of PBS.

2.2.1.7 Conjugation of Clec9A onto Protein G coupled magnetic beads

The recombinant Clec9A protein, conjugated to the Fc region of a mouse IgG_{2a} immunoglobulin, was immobilised onto the Protein G magnetic beads through the binding of Protein G to the Fc fragment.

A magnetic field was applied to the beads from the previous wash steps and the 100 µL supernatant was removed. Aliquots of 100 µL of PBS (pH, 7.4) and 100 µL of reconstituted Clec9A-Fc (100 µg/mL) protein was added to the beads to resuspend the beads. The solution was mixed thoroughly by pipetting several times. Bare Protein G magnetic beads, that were incubated with 200 µL of PBS (pH, 7.4) instead of recombinant Clec9A-Fc, were used as control beads for the negative selection steps. Both bead solutions were placed on ice on a see saw rocker (SSL4, Stuart Equipment, New Zealand) for 30 minutes. After incubation, the supernatant was removed by magnetic separation as described above. Then, 200 µL of PBS was added to wash the beads and the wash process described above was performed for a total of three times.

2.2.1.8 Blocking of Empty Protein G Sites

Unconjugated Protein G sites on the beads were blocked with skim milk to minimise non-specific binding of oligonucleotides. This was achieved by adding 0.1 g of skim milk to 5 mL of PBS. The solution was vortexed vigorously and heated in a water bath with periodic mixing to solubilise the skim milk power. The tubes containing the control and target beads, for negative and positive selection respectively, were applied to a magnetic field and the PBS from the last wash step was removed. Each bead preparation was resuspended in 200 µL of the preprepared 2% (w/v) skim milk solution and incubated for 30 minutes at room temperature with gentle agitation on a rotator (SB2, Stuart Equipment, New Zealand). The beads were again magnetically restrained, and the supernatant was removed. The beads were washed three times with 200 µL PBS (pH 7.4) as described previously.

2.2.1.9 Oligonucleotide Incubation with Magnetic Beads

Each SELEX round contained a negative selection step, prior to positive selection. A magnetic field was applied to the tube containing the control beads and the solution was removed. The

beads were resuspended in 200 µL of 1 nM oligonucleotide library diluted in PBS containing complete IMDM medium (see Table 2.7 for details) to ensure the incubation buffer components were present at each selection round. The bead solution was mixed by pipetting and then incubated at room temperature for 1 hour with gentle agitation on a rotator.

After incubation, the control beads were magnetically restrained, and the supernatant was transferred to the tube containing the Clec9A-Fc conjugated Protein G target beads for the positive selection step. The target beads were resuspended by pipetting up and down several times and then incubated with the solution containing the oligonucleotide library for 1 hour with gentle agitation on a rotator. The target beads were magnetically restrained, and the supernatant was removed and discarded

Both the control and conjugated beads were subjected to nine washes with 200 µL of PBS (pH 7.4) containing 0.001% Igepal and then a final wash in PBS only. After the final wash, the beads were resuspended in 200 µL of PBS.

2.2.1.10 Heat Elution of Oligonucleotides

The oligonucleotide sequences were eluted from both bead preparations via heat elution. The tubes were incubated at 95°C for 5 minutes and the beads were magnetically restrained while the supernatants were quickly removed and placed into fresh 1.5 mL tubes. The supernatants from the control and target beads theoretically contained oligonucleotide sequences that had affinity for components on the beads (non-specific) and for the target molecule (specific), respectively.

2.2.1.11 Amplification of Oligonucleotides

The amplification of the starting, and then the enriched, oligonucleotide libraries was performed using a QuantStudio 3 Real-Time PCR System (ThermoFisher Scientific, New Zealand) and SYBR green chemistry. A 200 µL sample of the heat eluted oligonucleotides was used as the template. An aliquot of 5 µL of this template was added to each respective PCR reaction tube containing 20 µL of master mix (Table 2.8). The thermal cycling protocol used included an enzyme activation step at 95°C for 5 minutes, followed by 40 cycles of 95°C for 40 seconds, 58°C for 30 seconds, and 72°C for 15 seconds, followed by a final 1 minute at 72°C

when cycling was complete. The PCR reaction was stopped during the exponential phase of the amplification curve, just before the plateau.

For a PCR reaction at each round, 12 tubes were set up containing 20 µL of master mix and 5 µL of target oligonucleotide template. A further two tubes were prepared in the same way but using the oligonucleotides from the negative selection for the 5 µL template. The controls included in the reaction were a positive control containing 1 µM of the original N40 starting library, a no template control containing Ultra-Pure H_2O as the template and finally a blank containing 25 µL of Ultra-Pure H_2O.

Table 2.8: Table of master mix reagents and volumes for SYBR green qPCR used in SELEX experiments.
The total volume of the master mix varied depending on the number of reactions required.

Stock reagent	x1 reaction (µl)	Final concentration
UltraPure H_2O	15.65 µl	
10X Buffer	2.5 µl	1X
dNTPs (10 mM)	0.5 µl	200 µM
Pf40 (10 µM)	0.55 µl	220 nM
PrB40 (10 µM)	0.55 µl	220 nM
SYBR (30X)	0.1 µl	0.12X
HotMasterTaq (5 units/µL)	0.15 µl	0.75 U
Total volume	20 µl	
Briefly vortex and spin down master mix and pipette 20 µl into each PCR tube		
Add template	5 µl	
Total volume	25 µl	

2.2.1.12 Concentrating the PCR Products

The PCR products from the positive selection steps at each round of SELEX theoretically represent the oligonucleotide sequences that bound to recombinant Clec9A-Fc protein linked to the protein G magnetic beads. These PCR products were concentrated into a smaller volume for gel electrophoresis purification using an Ultracel®30kDA cutoff centrifugal filter in a Amicon® Ultra-0.5 tube (Merck, New Zealand). The total volume (25 µL) of each PCR product from each reaction was pipetted into the centrifugal filter to pool the samples, keeping the oligonucleotides from the positive and negative selection rounds separate. The column was centrifuged at 14,000 x *g* for 5 minutes and the eluate was and discarded. The centrifugal filter containing the amplified PCR product was inverted so that the entrance of the filter was facing

downward inside the tube. The centrifugal filter was then centrifuged at 1,000 x *g* for 1 minute to collect the highly concentrated PCR product.

2.2.1.13 Agarose Gel Electrophoresis

A 4% (w/v) agarose gel was prepared by adding 1.6 g of genetic technology grade (GTG) agarose (NuSieve™,Lonza, New Zealand) to 40 mL of 1x tris-acetate-EDTA (TAE) (0.4 M tris acetate pH 8.3, 0.01 M EDTA) buffer in an Erlenmeyer flask. The flask was placed on a hot plate at 300°C with a magnetic stir bar stirring at 250 rpm. Once the gel crystals had dissolved the gel was poured into a prepared gel cast containing a well comb. The gel was left to polymerise for 45 minutes at room temperature.

A DNA ladder was prepared by adding 1 µL of GeneRuler Low Range DNA Ladder (ThermoFisher Scientific, New Zealand) to 25 µL of Ultra-Pure H_2O. An aliquot of 1.6 µL of 100X SYBR (Invitrogen™, ThermoFisher, New Zealand) was added the DNA ladder preparation and to each concentrated DNA sample. Samples included the PCR products from negative selection, the N40 starting library (positive control), a no template control (negative control), a water blank and PCR products from the positive selection. All tubes were vortexed, briefly centrifuged and incubated for 8 minutes at room temperature. Thereafter, 6 µL of 6X DNA gel Loading Dye (Thermofisher, New Zealand) was added to each tube, which were vortexed and briefly centrifuged.

The polymerised gel was loaded into a gel electrophoresis tank filled with TAE buffer. A 30 µL aliquot of each sample and the ladder was pipetted into respective lanes and electrophoresised at 75 V for 90 minutes to separate DNA fragments of varying size. The gel was then transferred to a UV transilluminator (UV Transilluminator, 2000, Bio-Rad, New Zealand) for visualisation and isolation of the bands of interest. The bands representing the positive selection, observed at approximately 80bp using the DNA ladder as a reference, was removed using a clean scalpel and placed in a pre-weighed 15 mL falcon tube. The tube was weighed again to determine the weight of the gel alone and was stored either at 4°C for same or following day extractions, or at -20°C for longer term storage.

2.2.1.14 Gel Extraction

The double stranded DNA (dsDNA) was purified from the excised agarose gel fragment using the QIAquick® Gel Extraction Kit and protocol (Qiagen, New Zealand). The weight of the gel fragment determined the amount of solubilisation and binding (QG) buffer (Qiagen, New Zealand) to be added to the tube. For example, if the excised gel from gel electrophoresis weighed 200 mg, 600 µL of QG buffer would be added to the tube and placed in a water bath set to 55°C. The tube was incubated for 20 minutes and mixed periodically by vortexing until the gel had completely dissolved and the DNA was released into solution. A 1x volume of isopropanol relative to the excised gel weight was added. The solution containing the dsDNA was split between two MinElute® spin columns (Qiagen, New Zealand). One column was stored as a back-up in case anything went wrong in the following steps. The solution containing the dsDNA was added to the MinElute® column 700 µL at a time and centrifuged at 6,000 x *g* for 1 minute until all the solution had been passed through the column. The eluate was passed through the column three more times before discarding into a hazardous waste container. A 500 µL aliquot of QG buffer was added to the columns and was centrifuged for 1 minute at 6,000 x *g* and the eluate was discarded. Then, 750 µL of wash buffer (PE buffer) (Qiagen, New Zealand) was added to the columns, centrifuged for 1 minute at 13,200 x *g* and then a further two times at 13,200 x *g* for 1 minute, without the addition of anything to the column, to remove any additional traces of ethanol from the columns. The hinge of the column lid was reorientated in the centrifuge to remove any persistent traces of ethanol at each no liquid centrifuge step. The columns were placed in to fresh 1.5 mL tubes and 30 µL of Ultra-Pure H_2O was added to the membrane of the column, incubated for 1 minute at room temperature, and then centrifuged at 13,200 x *g* for 1 minute. Another 30 µL of Ultra-Pure H_2O was added to the membrane and incubated for 1 minute at room temperature. A final centrifugation step at 13,200 x *g* for 1 minute resulted in a 60 µL eluant of purified DNA. A 2 µL aliquot was sacrificed to determine the DNA concentration via Nanodrop spectroscopy and the remaining solution was stored at -20°C for later use.

2.2.1.15 Strand Separation to Retain and Purify Single Stranded DNA

The consequence of using a biotin-labelled reverse primer in the PCR reactions was that each antisense strand is biotin labelled. Thus, single stranded DNA was prepared using a streptavidin magnetic bead strand separation approach. Streptavidin-labelled magnetic beads (New England BioLabs, New Zealand) were resuspended via gentle inversion for 5 minutes and 50 µL of beads were aliquoted into a fresh 1.5 mL tube. The beads were prepared for conjugation with a wash in 100 µL of Ultra-Pure H_2O and two washes in 100 µL of PBS (pH 7.4). The supernatant was removed each time the beads were subjected to a magnetic field After the final wash, the beads were resuspended in 40 µL of the gel extracted dsDNA. The solution was incubated at room temperature for 30 minutes with agitation. The supernatant was then removed by magnetic separation, and the beads were washed in 50 µL of Ultra-Pure H_2O with mixing by pipetting up and down several times. The beads were pulled to the side by magnetic field and the supernatant was removed.

To separate the DNA strands, the beads were resuspended in 30 µL of 0.3 M sodium hydroxide (NaOH) and incubated at room temperature for 3 minutes. The supernatant containing the non-biotin labelled sense strand was removed by magnetic separation and transferred in to a fresh 1.5mL tube.

The Qiagen QIAEX® II Gel Extraction Kit (Qiagen, New Zealand) was then used to remove salts and agarose contaminants from the ssDNA. A 6X volume of Solubilisation and Binding Buffer (QX1) (Qiagen, New Zealand) was added to the 30 µL solution containing the sense DNA and mixed by pipetting up and down. The QIAEX II Suspension Beads (Qiagen, New Zealand) were resuspended in their solution by vortexing for 30 seconds. A 10 µL aliquot of the beads were added to the tubes containing the sense DNA and mixed through the solution by pipetting up and down. The tubes were incubated at 50°C for 10 minutes with mixing by flicking the side of the tube every two minutes. A 20 µL aliquot of sodium acetate was added which changed the colour of the solution from purple to yellow. The tube was centrifuged at 8,000 x *g* for 30 seconds to pellet the beads and the supernatant was discarded. The pellet was resuspended with 500 µL of Buffer QX1 and the tube was centrifuged at 8,000 x *g* for 30 seconds. Again, the supernatant was discarded. The beads were then washed twice with 500 µL of PE buffer. After the final wash, the supernatant was discarded. The pellet was air dried for approximately 20-30 minutes until it became white in appearance.

The pellet was then resuspended in 20 µL of Ultra-Pure H_2O and incubated at 50°C for 10 minutes. Finally, the tube was centrifuged to pellet the beads once more and the supernatant, containing the purified ssDNA was removed with a pipette and placed into a fresh 1.5 mL tube. The resultant solution was then stored at -20°C for the following round of SELEX.

2.2.1.16 Library Preparation

After seven rounds of Protein-SELEX, the oligonucleotide pool should have been enriched enough to perform the selection in a more complex and representative environment. The ssDNA obtained from the final round of Protein-SELEX (Round 7) was split evenly between two tubes and quantified using the NanoDrop spectrophotometer. One of the tubes was used to continue two additional rounds of selection using the recombinant Clec9A-Fc conjugated magnetic bead method as discussed In Sections 2.2.1.5-2.2.1.15, while the other was used for whole Cell-SELEX (Figure 2.8). The subsequent two rounds of Protein-SELEX (Rounds 8 and 9) were performed the same as detailed above, only the oligonucleotide pool was resuspended in 100% IMDM complete medium (Table 2.7).

2.2.1.17 Sorting and Collection of Clec9A$^+$ Mouse Dendritic Cells

To obtain cells for negative and positive selection for the cell SELEX rounds, the spleens from three naïve C57 mice were harvested and processed with the help of Ian Hermans' research group at the Malaghan Institute of Medical Research. Approximately $500x10^6$ cells from the three spleens were run on the AutoMACS® Pro Separator (Miltenyi Biotech) to enrich for CD11c cells using Ultrapure mouse CD11c MicroBeads (Milteyni Biotech). The beads are used to isolate specific, viable mouse DCs from single cell suspensions. The $CD11c^{-ve}$ cells were run through the autoMACS twice, to maximise the $CD11c^{+ve}$ cell population on the beads. The $CD11c^{+ve}$ cells from the AutoMACS sort were prepared for fluorescence activated cell sorting (FACS) to isolate $CD8^{+ve}$ cells that should also express the Clec9A cell surface receptor. The $CD11c^{+ve}/CD8^{+ve}$ splenocytes were purified from the cell sample using FACS on the BD LSRFortessa™ X-20 Cell Analyzer (BD Biosciences, New Zealand) with the BD FASCDiva™ software (BD Biosciences, New Zealand).

The cells were incubated with a multicoloured antibody mix, containing antibodies specific to cell surface markers characteristic of $CD8^{+ve}$ cell morphology, in addition to live/dead sorting using Zombie NIR™. These antibodies used were to bind to B220, CD11c, XCR1 and CD8 and made up to a total volume of 300 µL in FACS buffer. The specific antibodies and detection wavelengths used are listed in Table 2.9.

It was considered that selecting for cells expressing Clec9A using a Clec9A specific antibody would have created downstream issues in the SELEX process, requiring additional manipulation of the fragile cells after sorting. Specifically, a Clec9A surface receptor bound to an antibody is not free to allow for oligonucleotide binding during SELEX. Therefore, Clec9A expressing cells were indirectly selected for using XCR1. XCR1 is a chemokine receptor and is highly correlated with CD8, CD205, and Clec9A/DNGR-1 (Bachem et al., 2012). The final purified splenocyte pool used for positive selection in cell SELEX rounds contained 96% of cells positive for XCR1 and presumably for Clec9A. The cells that did not express XCR1 were retained and used in the negative selection rounds.

Table 2.9: FACS setup.
Table depicts laser colour and channels, type of fluorescent dye used for each marker, antibody clone, catalog number, dilution, and volume of antibody added to staining mix for all antibodies used in FACS sorting. Each antibody was chosen with a different fluorescent dye, thus different to prevent overlapping of dyes in the emission spectrum.

Laser colour / channel	Antibody (fluorescent dye)	Clone	Catalog number	Dilution	Volume (µL)
Blue 515	B220 (FITC)	RA3-6B2	Bioleg 103206	300	1.0
Violet 780	CD11c (BV786)	HL3	BD 563735	200	1.5
Violet 450	XCR1 (BV421, FR)	ZET	Bioleg 148216	200	1.5
Ultra Violet 395	CD8 (BUV395)	53.67	BD 563786	200	1.5
Total volume in buffer (300 µL)					

2.2.1.18 Gating Strategy for FACS Sorting of XCR1⁺ Cells

The FACS sorting was performed by a senior scientist at the Malaghan Institute of Medical Research. The gating strategy for FACS was performed as detailed in Section 2.1.3.5.

2.2.1.19 Incubation of Cells with Oligonucleotide Sequences

In the same way for Protein-SELEX, the oligonucleotide pool for Cell SELEX was linearised by heating at 95°C for 5 minutes and then cooled on ice for 30 minutes. The oligonucleotide pool was diluted to 200 µL in 100% of supplemented IMDM. A negative selection was performed first. For this, 100,000 XCR1^{-ve} cells were added to a 1.5 mL tube and centrifuged at 500 x *g* for 5 minutes to pellet the cells. The supernatant was removed, and the cells were resuspended in 200 µL of oligonucleotide library. The tube was incubated at 4°C for 1 hour with gentle agitation on a rocker. Incubations were performed at 4°C to slow down cellular metabolism and limit internalisation of oligonucleotide sequences by receptor mediated endocytosis (Li et al., 2014; Shangguan et al., 2015). When the negative oligonucleotide incubation with the control cells was finished, the tube was centrifuged at 500 x g for 5 minutes and the supernatant was collected for the positive selection round. The XCR1^{-ve} cells were then washed in 200 µL of PBS and centrifuged twice at 500 x *g* for 5 minutes. The oligonucleotides were eluted from the cells by heating at 95°C for 5 minutes and the tube was centrifuged at 8,000 x *g* to separate the cell debris from the free oligonucleotides. The supernatant was removed and added to a fresh, labelled 1.5 mL tube.

For positive selection, 100,000 XCR1^{+ve} CD11c dendritic cells were added to a new 1.5 mL tube and centrifuged at 500 x *g* for 5 minutes. The supernatant was removed and replaced with the supernatant from the negative selection round and incubated at 4°C for 1 hour. This solution should have contained the oligonucleotides with specificity towards the Clec9A receptor. The cells were pelleted by centrifugation as described above and the supernatant from the XCR1^{+} CD11c cells was transferred in to a fresh, labelled 1.5 mL tube.

Both tubes (from the positive and negative selection rounds) were stored at -20°C until further use. For the second round of cell SELEX, the protocol remained the same, but the negative selection consisted of a 1:5 ratio of CD11c^{-ve} splenocytes to XCR1^{-ve} CD11c cells to increase selection complexity. Finally, the incubation times were reduced to 30 minutes.

2.2.1.20 Preparation of Oligonucleotides for the Next Round of Selection in Cell SELEX

The preparation steps required to amplify, purify, and separate the dsDNA for the following round of selection in cell SELEX remained the same as detailed in Sections 2.2.1.11 to 2.2.1.15.

2.2.1.21 Generation of Sequences to dsDNA for Clean-up Pre-Processing

To provide an appropriate amount of DNA for next generation sequencing (NGS) and to convert the sequences to dsDNA, the ssDNA from the final rounds of selection were amplified using SYBR green PCR. The protocol used is detailed in Section 2.2.1.11 with one exception that the reverse primer was not biotin labelled. Twelve PCR tubes were prepared for each oligonucleotide pool and were amplified in independent reactions with appropriate controls (N40 positive, no template control and blank) so that the reaction could be stopped before the exponential phase of the PCR reaction. This prevented accumulation of aggregates and spurious product formation.

Section 2.2.2 Next Generation Sequencing (NGS)

2.2.2.1 DNA Preparation for NGS

To concentrate the DNA for NGS, the Monarch PCR and DNA clean-up kit (New England BioLabs, New Zealand) was used for dsDNA of <2kb. The PCR products were pooled in a 1.5 mL tube and diluted 1:5 with DNA clean-up binding buffer. A 700 µL aliquot of this solution was added to the kit column within a collection tube and centrifuged for 1 minute at 8,000 x *g*. The eluant was passed through the column a total of three times to ensure all the DNA had bound to the membrane and after the final run, was discarded. The column membrane was washed twice with 200 µL of DNA wash buffer and after each wash, the tube was centrifuged for 1 minute at 8,000 x *g* and the flow through was discarded. The column was transferred to a clean 1.5 mL microcentrifuge tube and 20 µL of Ultra-Pure H_2O was added to the centre of the matrix and centrifuged for 1 minute at 8,000 x *g* to elute the DNA. The eluant was retained and the concentration of the DNA was quantified using the Qubit 3.0 fluorometer (Invitrogen™, ThermoFisher, New Zealand) using the QuBit™ dsDNA HS Assay Kit (ThermoFisher, New Zealand) as per the manufacturer's instructions.

The concentrated DNA from the SELEX pools were sequenced using Illumina NGS by GenXPro, Germany. All samples were read at a sequencing depth of 1 million reads per sample across 100 base pairs (bp), with 20,000 reads per sample.

2.2.2.2 Bioinformation of NGS data

The bioinformatics data was provided in a FASTQ format for pre-processing and was subjected to the bioinformatic pipeline illustrated in Figure 2.9. The computer used to conduct my bioinformatic research was supplied by Victoria University of Wellington. The computer was Ubuntu 20.04.3 LTS GNU/Linux 4.4.0-139-genericx86_64 operating system.

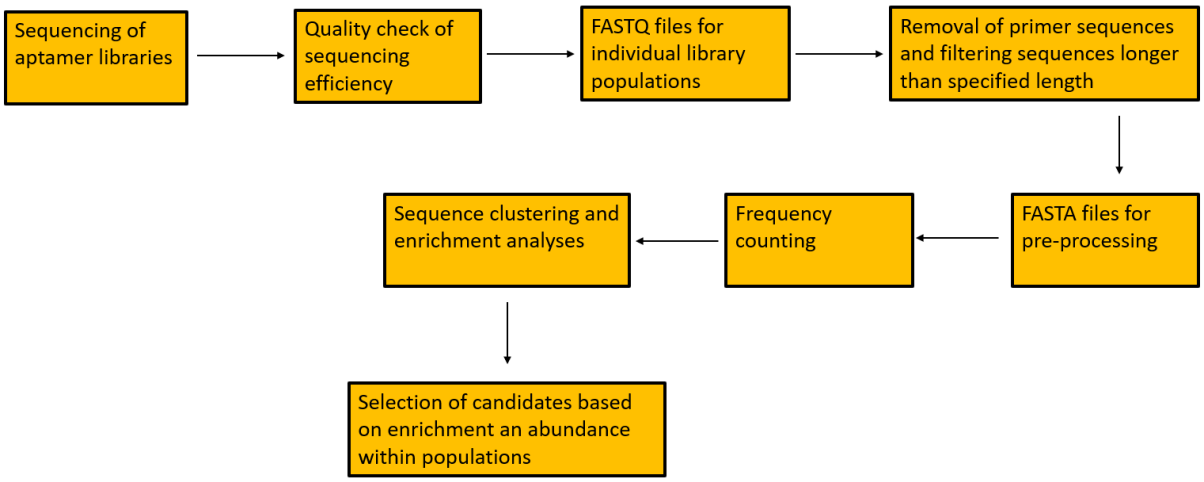

Figure 2.9: Outline of bioinformatic pipeline.
This was created to process the four NGS fastq files that represented significant stages in the hybrid SELEX process, N40 starting oligonucleotide library, Protein-SELEX round 7 and protein and Cell-SELEX round 9.

2.2.2.3 Quality Check

Prior to bioinformatic analysis, the Fastq files provided from GenXPro, Germany, underwent a FastQC quality control check to provide an understanding of the sequencing quality and whether the data has any issues that should be considered during additional analyses. This was performed in addition to the quality control provided by GenXPro as a comparison. The FastQC quality control analysis provides a range of information to assess the quality of the sequencing data. Basic statistics provides the end user with information relating to the name of the file, the type of quality score, total number of reads, read length and GC content. The base sequence quality provides an overview of the quality of a base at each position. Per sequence

quality scores provides information that helps identify whether a group of sequences are of lower quality. Per base sequence content provides the percentage of each nucleotide present at each position for the whole data set. Sequence GC content provides the number of reads versus the GC content within each read. Per base 'N' content details the number of bases where the nucleotide cannot be identified. Sequence length distribution explains the range of sequence lengths across the whole data set. Sequence duplication levels identify whether there is the presence of any overrepresented sequences. Finally, adapter content provides information around the proportion of reads where an adapter sequence has been identified within the library. There should be no adapter sequences present for Illumina sequencing.

2.2.2.4 Library Pre-Processing

To identify the aptamer candidates that fulfil theoretical characteristics based on enrichment and abundance within the populations, bioinformatic applications were used. This allowed for the isolation of sequences with conserved characteristics, suggestive of enrichment towards the target, for further characterisation for target binding. FASTAptamer, a bioinformatic toolkit for high-throughput sequence analysis of combinatorial selections, was used to achieve this (Alam et al., 2015). Prior to bioinformatic analyses, the datasets required pre-processing to ensure information obtained was accurate and representative. This included primer removal and further filtering of sequences of inconsistent length to the desired N40 region after the primers had been removed. Incorrect amplification of sequences may result in sequences of undesired length and thus required filtering from the population.

The conserved primer sequences were removed using a bash script (see Appendix 4) with the cutadapt feature to simplify the downstream analyses (Eaton et al., 2015). This script removed both primer sequences and retained sequences of a specified length. Thus, sequences that were incorrectly amplified were removed at a pre-defined error rate. This pre-analyses step yielded only sequences that were the length of the random region (i.e. 40 nucleotides in length).

2.2.2.5 Bioinformatics Pipeline

Subsequent to library pre-processing, bioinformatic analyses were performed following a classic bioinformatics pipeline (Figure 2.9). This pipeline included calculating the number of

unique and total sequences within each library, performing cluster analyses to group sequences within populations that harbour sequence similarity, sequence conservation analyses to understand the total number of sequences that were conserved between libraries, and finally, enrichment analyses to identify fold enrichment ratio between a population and its parent population. The command lines and bioinformatic scripts used in all analyses are detailed in Appendix 4.

The total number of sequences and total number of unique sequences were calculated using the fastaptamer-count feature in FASTAptamer. Identifying the total number of sequences from each library provides an initial indication of enrichment or selection towards the target during selection. If a reduction in total number of unique sequences was observed between the starting and enriched libraries, it would infer that target-specific selection was occurring.

The number of conserved sequences between populations were compared using the fastaptamer-compare feature in FASTAptamer. This feature allowed for the comparison of two sequences and provided total reads, reads per million (RPM) and rank. Fastaptamer-compare was used to understand sequence conservation between Protein-SELEX Round 7 Protein-SELEX Round 9 and Cell-SELEX Round 9.

All sequences within a library were clustered into families based on the seed sequence and the defined Levenshtein edit distance of seven. The sequence with the highest number of reads became the seed sequence for Cluster One. All the sequences that were found to be within the Levenshtein edit distance, i.e. the maximum number of insertions and deletions/substitutions that are required to change one sequence into the seed sequence, were grouped into this cluster. This was achieved using fastaptamer-cluster and was a computationally intense process which required multiple days to weeks of processing. The cluster analyses provided information on the rank, size, reads, RPM cluster number, rank in cluster and edit distance. Up to three library cluster files were able to be analysed using the fastaptamer-enrich feature. This compared the enrichment of each sequence within each library. Due to the wealth of sequences produced through NGS, not all could be characterised in the time given for this project. Therefore, sequences were chosen that appeared to exhibit the most enrichment to the target based on preliminary data (see Section 3.3.5).

2.2.2.6 Computational Secondary Structure Prediction

To determine whether the candidate aptamers had similar or conserved secondary structures, the top nine candidates were folded using ViennaRNA. This is a free software package that uses a range of algorithms to predicts the secondary structure using an aptamers sequence primary. The command line is provided in Appendix 4.

Section 2.3 Characterisation of candidate aptamers

2.3.1 Gold Nanoparticle (AuNP) Assay

The gold nanoparticle (AuNP) assay is a colorimetric assay that relies on the association of aptamer to citrate capped AuNP and the disassociation of the aptamer from the AuNP upon addition of its target molecule. Colorimetric detection of this dissociation is observed through the addition of salt (NaCl), which aggregate the AuNP, causing a colour change of red to blue (Tao et al., 2020) (Figure 2.10). The colour change is induced by a reduction in the distance of one AuNP to another. Electrostatic forces keep the AuNP spaced apart and in red appearance. Upon NaCl addition, AuNPs destabilise via electrostatic interference, thus forcing the AuNP closer together and changing its visible colour. When aptamers are added to the AuNP solution, the aptamers adsorb onto the AuNP surface resulting in electrostatic stabilisation due to an interaction between ssDNA and AuNP (Li & Rothberg, 2004). Following the addition of NaCl, the AuNP are protected from aggregation and the colour remains red. However, in the presence of the target molecule, the aptamer undergoes a conformational change to bind the target causing it to dissociate from the AuNP. When NaCl is added, the AuNP are no longer protected by the aptamer and aggregation occurs, confirming the specificity of the aptamer.

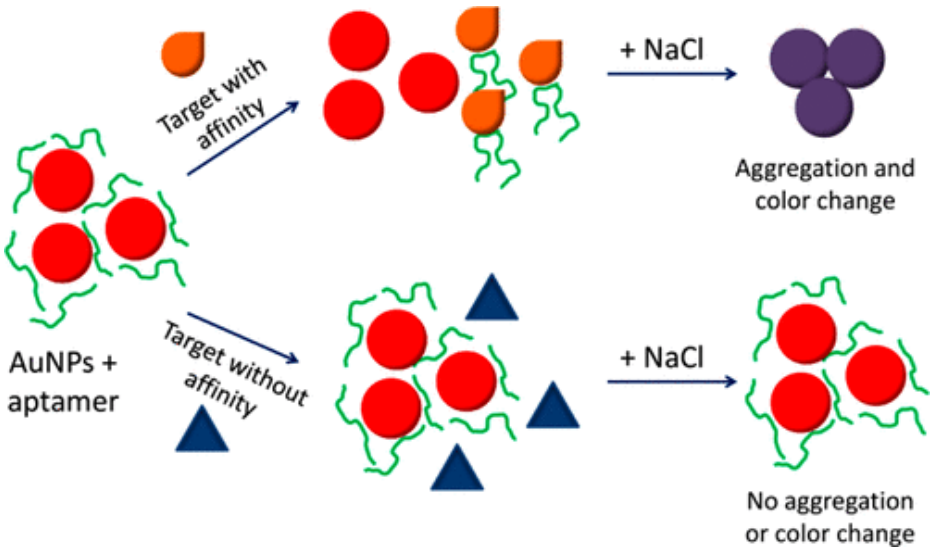

Figure 2.10: Schematic representation of colorimetric detection of aptamer/target binding using the gold nanoparticle (AuNP) assay

Aptamer electrostatically absorbs to the surface of the AuNP providing colloidal stability. Under the addition of NaCl, the aptamer protects the AuNP from aggregation and colour change. If aptamer-specific target is added, the aptamer will undergo a conformational change to bind the target. When NaCl is added in this case, the AuNP will not have protection from the aggregation effects of NaCl and thus, the AuNP become closer in contact, causing a colour change from red to blue.Figure adapted with permissions from RightsLink.

2.3.1.2 Preparation of Glassware for use in Gold Nanoparticle Development

To ensure the AuNP are prepared to a high standard, all the glassware used must be put through the dishwasher using an acid wash solution as well as dishwasher detergent. The day before the AuNP preparation protocol, all glassware was placed in the dishwasher (Undercounter FlaskScrubber Glassware Washer, Labconco, New Zealand) and washed on the glass and plastic setting. Decomatic and Acid Rinse (Decon, New Zealand) were loaded into the dishwasher and the cycle was run for approximately one hour.

2.3.1.3 Acid Wash for 1L Schott Bottle

An acid rinsed 1 L Schott bottle (Schott, Australia, ThermoFisher, New Zealand) was used in the AuNP preparation process for rinsing of glassware with double distilled water (ddH_2O) and for use during the AuNP assay. The AuNP are extremely sensitive, dust and any debris within the glassware cause the AuNP to behave inconsistently and are more subject to degradation. Thus, an acid wash for all glassware mitigates this risk. To prepare the 1 L acid washed bottle, 9mL of 37% hydrochloric acid (HCl) and 3mL of 70-72% nitric acid (HNO_3) was added to the bottle in the order listed. This solution was left in the bottle until it became a golden yellow colour. The solution was then swirled around in the bottle to coat all areas with the acid. To coat the

sides of the bottle, up to the neck, the bottle was held horizontally and gently rotated for final disposal into a neutralisation tub containing sodium bicarbonate ($NaHCO_3$) and approximately 100 mL H_2O. While working with acid, all appropriate personal protective equipment (PPE) was worn such as a double layer of gloves, lab coat and goggles. The acid washed bottle was rinsed with 2 L of ddH_2O using a 1 L bottle acid washed bottle from previous AuNP preparations.

2.3.1.4 Glassware Preparation Continued

Paper towels were set up on the bench for transfer of glassware to dry. Before transfer, each piece of glassware from the dishwasher was rinsed with 500 mL ddH_2O from the newly acid washed bottle. After rinsing, glassware was blotted dry with a Kimwipe, and openings were covered with a Kimwipe to dry. Glassware was left overnight to dry. When dry, the Kimwipes were replaced with tinfoil to cover openings.

2.3.1.5 Second Acid Wash for Glassware

On the following day, an acid wash solution was prepared in a 50 mL conical flask by combining 21 mL of 37% HCl and 7 mL of 70-72% HNO_3 in the order listed. The aqua regia solution was left in the fume hood for approximately one hour until the solution was golden yellow in colour. Then, a 500 mL Erlenmeyer flask (used to boil the gold III chloride trihydrate solution), condenser, and connector used for AuNP synthesis were rinsed with the acid wash solution. Half of the acid solution was added to the 500 mL Erlenmeyer flask while the connector was placed in a beaker underneath the condenser and clamped upright so that the acid poured into the condenser would pass through the connector and into the beaker. The other half of the acid solution was passed through the condenser into the connector. This was left for one hour and then the acid was passed through the condenser to the connector once more and all acid was added to the neutralisation tub and stirred to neutralise. The Erlenmeyer flask, condenser and connector glassware were rinsed a second time with 500 mL ddH_2O from the 1L acid washed bottle. Glassware was blotted with Kimwipes, and openings were covered with tinfoil.

2.3.1.6 Preparation of Gold III Chloride Trihydrate

While the glassware was being prepared, as described in Section 2.3.1.5, 30 mg of gold III chloride trihydrate was weighed of gold III trihydrate into a small plastic culture dish. A 5 mL aliquot of ddH_2O was added and the solution was transferred into the 50 mL acid washed conical flask. An additional 5 mL of ddH_2O was added to the culture dish and then into the conical flask. To the conical flask, 85 mL of ddH_2O was added using a 100 mL acid washed measuring cylinder. The solution was stored with tinfoil on the opening and in the dark until use while the gold III chloride trihydrate solution requires storage under nitrogen gas. The bottle containing the gold II chloride trihydrate stock was nitrogen purged by attaching a hose with a sawn-off pipette tip on the end to the N_2 gas tap. A gentle flow was used and held in the bottle for 30 seconds. The lid was screwed tightly and stored for later use.

2.3.1.7 Preparation of Trisodium Citrate Dihydrate

A trisodium citrate dihydrate solution was prepared by measuring 2.05 g of trisodium citrate dihydrate into a weigh boat and adding to a 100 mL volumetric flask. The volumetric flask was filled halfway with ddH2O. The solution was made up to 100 mL to prepare a 70.54 mM solution. The trisodium citrate dihydrate solution was filtered through a 0.2 µM filter (Corning®, Sigma Aldrich, New Zealand) and stored in a Schott bottle until further use.

2.3.1.8 Synthesising the AuNP

The 0.8 mM AuNP solution was prepared by heating 95 mL of the gold III chloride trihydrate solution in a 500 mL Erlenmeyer flask to 400°C on a heating plate with a magnetic stir bar at 370 rpm. A condenser and connector were placed in the opening of the Erlenmeyer flask and clamped to hold the condenser upright, on top of the flask. The condenser was required to prevent evaporation of the solution due to heating at 400°C. the condenser was connected to the water tap using rubber tubing. Cold water was passed through the outside tube which cooled the evaporating solution in the inner tube causing the transition back to liquid state and thus returning to the flask. When droplets began to appear on the connector, this indicated that the gold solution was at boiling point. Once it had reached the boiling point, a 30-minute timer was set and the trisodium citrate dihydrate solution was placed in a water bath set to

95°C. At 30 minutes, 5 mL of the trisodium citrate dihydrate solution was removed via syringe. The condenser and connector were removed from the top of the flask, while the flask remained on the heat with stirring. The 5 mL of trisodium citrate dihydrate was added to the gold III chloride trihydrate and a timer was set for a further 15 minutes. During this time, the colour of the solution changed from colourless, to grey/blue, to wine red. After 15 minutes, the flask was removed from the heat and taken to the bench while swirling. The stir bar was removed with a magnet and the flask was capped with tinfoil. The flask, containing the AuNP solution was placed in the dark to cool for approximately 4 hours. Once completely cool, the AuNP solution was placed in an acid washed Schott bottle, covered with tinfoil, and placed in the fridge until use. Each AuNP preparation had a shelf life of one week, after which the sensitivity begins to degrade.

2.3.1.9 Preparation of AuNP for AuNP Assay

For the AuNP assay, a 12 nM solution of AuNP is required. This is prepared by adding 500 µL of the 0.8 mM AuNP solution to 500 µL ddH_2O into 1.5 mL tubes. A total of 24 tubes were centrifuged at 17,000 x *g* for 18 minutes and 700 µL of the supernatant was removed and discarded. The pelleted AuNP solution was resuspended by pipetting up and down and pooled into an acid washed glass vial covered with tinfoil. The concentration of the AuNP was determined by NanoDrop under the UV-Vis feature. The solution was measured at wavelengths of 520 nm and 625 nm and the concentration of the AuNP solution was determined using the absorbance at 520 nm and the Beer-Lambert law:

$$A = \varepsilon bC.$$

Where 'A' is the absorbance, 'Ɛ' is the extinction coefficient 'b' is the length of the light path and 'C' is the concentration. The equation is rearranged to find C:

$$C = A \div (\varepsilon \times b).$$

The AuNP solution was then diluted to 12 nM in 1 mL aliquots for each experimental condition.

2.3.1.10 Optimisation of NaCl Concentration for Aggregation

As variability exists between AuNP batches, preliminary optimisation experiments must be performed after each preparation of AuNP to determine the stability of the AuNP and thus, the

optimal concentration of NaCl to aggregate the AuNP. A concentration range of NaCl, from 0.5 M to 0.8 M, was set up in a 96 well plate. A with aptamer and without aptamer AuNP solution is prepared. A 3.6 µL aliquot of the 10 µM aptamer solution is added to a 1 mL 12 nM AuNP solution in 1.5 mL tubes and mixed by inversion several times. The no aptamer condition uses Ultra-Pure H_2O in place of the aptamer volume. After mixing, 100 µL of each AuNP/aptamer solution is added to 8 wells and incubated at room temperature for 30 minutes. At 30 minutes, 12 µL of PBS is added to all wells using a multichannel pipette. The PBS is incubated with the AuNP solution for 30 minutes at room temperature. Following the incubation with PBS 8 µL of a known concentration of NaCl is added to labelled wells via multichannel pipette. The plate was left for 10-30 minutes to aggregate and then read on the spectrophotometer (SPECTROstar Nano, Absorbance plate reader, BMG Labtech, New Zealand) using the SPECTROstar Nano software (BMG Labtech, New Zealand) at wavelengths of 520 nm and 625 nm to determine the optimal aggregation NaCl concentration. The assay also allows for visual detection of aggregation. In this optimisation assay, the aptamer should protect the AuNP until an excess amount of NaCl is added. There should be a concentration dependent increase in aggregation when no aptamer is present. The best NaCl concentration to use is the lowest concentration that fully aggregates the bare (no aptamer) AuNP.

2.3.1.11 AuNP Assay to Determine Aptamer/Target Interactions

The AuNP assay is set up similarly to the NaCl AuNP optimisation experiment, except this assay investigates the aptamer and target interactions using different concentrations of target. This assay was intended to be optimised using human alpha thrombin (ThermoFisher, New Zealand) and the thrombin binding aptamer, HD22 (Pica et al., 2017) (Sangon Biotech, China), to then be applied for the screening of oligonucleotide candidates with Clec9A Clec9A .

A target concentration range was set up for each experimental condition from 50 to 1000 nM. Each assay contained a no aptamer control, where the volume of aptamer was replaced with ddH_2O, and a non-specific aptamer control. The non-specific aptamer control used was OM5C6, a methamphetamine aptamer that has been used in the AuNP protocol by the Pitman Lab previously (Odey, VUW, unpunished results). The AuNP were prepared to a 12 nM concentration as described in Section 2.3.1.9. A 3.6 µL aliquot of 10 µM aptamer was added to 1mL of 12 nM AuNP in 1.5 mL tubes and mixed by inversion. The no aptamer condition uses

Ultra-Pure H_2O in place of the aptamer volume. A 100 µL aliquot of the AuNP/aptamer solution was added across 8 wells and incubated for 30 minutes at room temperature. At 30 minutes, 12 µL of a known concentration of target, prepared in 0.001 M PBS is added to all wells using a multichannel pipette, mixed by pipetting up and down and incubated with the AuNP for 30 minutes. At 30 minutes, 8 µL of the optimised NaCl concentration is added to the wells via multichannel pipette and mixed by pipetting up and down. The solution is left for 10-30 minutes to aggregate. The plate is read on the spectrophotometer at wavelengths 520nm and 625nm.

The AuNP assay was originally optimised to characterise the binding interactions between aptamer and small molecules. It was not clear how proteins would interact with the AuNP assay. Because they are larger molecules, they may interact with the assay rather than the aptamer, providing false positive results. To address this, the thrombin binding aptamer, HD22, known to bind human alpha thrombin was used to optimise the current protocol. Unfortunately, under these experimental conditions, the thrombin binding aptamer did not appear to exhibit binding affinity to thrombin and human thrombin alpha did appear to interact with the assay to non-specifically bind to the AuNP and protect them from salt-induced aggregation in a concentration dependent manner (Figure 2.11).

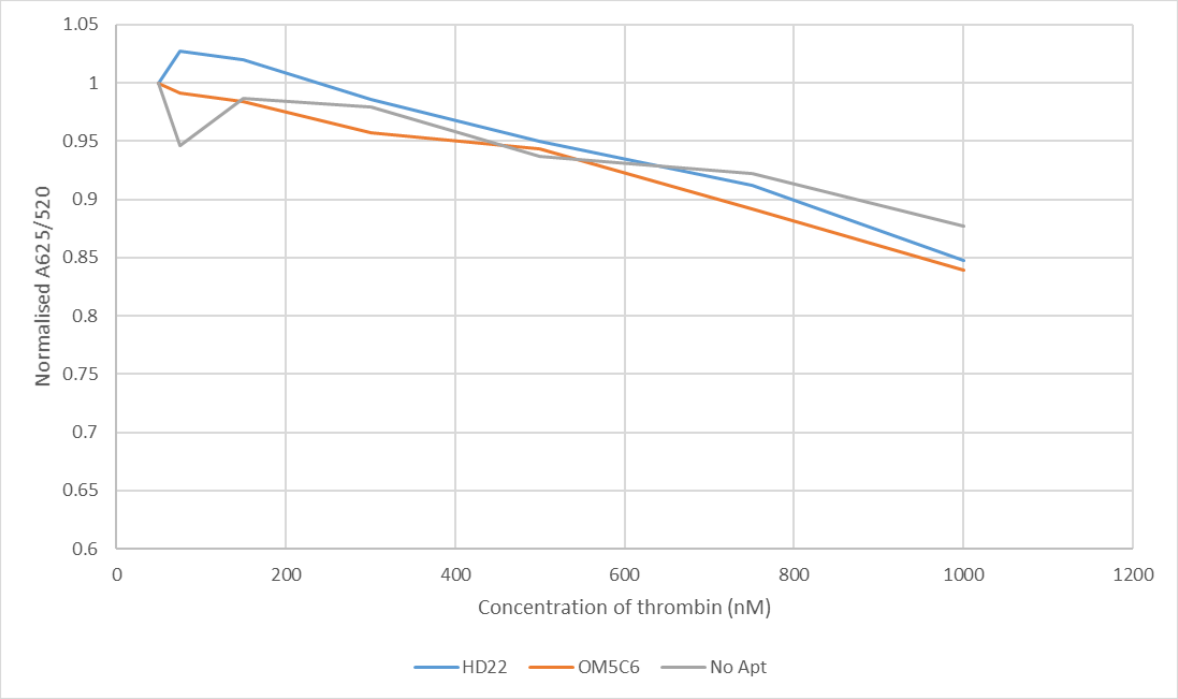

Figure 2.11: Optimisation of AuNP assay for proteins.
Optimisations were performed using the thrombin binding aptamer (TBA), HD22 and its target, human alpha thrombin showing that thrombin is interacting with the AuNP assay in a concentration dependent manner. The graph plots the normalised 625/520 absorbance values with increasing concentration of thrombin for three aptamer conditions. Blue is HD22, specific to thrombin, orange is a non-specific aptamer OM5C6, specific to meth and grey is the no-aptamer condition.

2.3.2 Circular Dichroism (CD) Spectroscopy to Investigate Binding Interactions Between Candidate Aptamers and Clec9A.

To avoid the limitations involved with the AuNP assay, circular dichroism (CD) spectroscopy was used. CD spectroscopy is a technique that provides information around the formation of secondary structures of molecules by subjecting those molecules to left and right circular polarised light. The difference in absorbances of this polarised light is used to predict the formation of different secondary structures (Kypr et al., 2009; Ladokhin et al., 2010). This method was used as an additional aptamer characterisation technique.

2.3.2.1 Preparation of Aptamer and Target Samples for Analysis using CD Spectroscopy

Aptamer candidates were prepared after confirming the concentrations of the 2 µM stock preparations by NanoDrop spectrophotometry. From the 10 µM aptamer stock, 2 µM aptamer stocks were prepared in PBS (0.01 M) to a total volume 40 µL in 0.5 mL tubes and mixed by vortexing. The tubes were briefly centrifuged to bring the contents of the tube to the bottom. After NanoDrop spectrophotometry measurements, the concentrations were adjusted if necessary. In new 0.5 mL tubes, 16 µL of 2 µM aptamer solution was combined with 16 µL of

2 µM recombinant Clec9A in PBS to make a final concentration of 1 µM of each in a total volume of 32 µL. For the no target blank, 16 µL was taken from each 2 µM aptamer preparation and combined with 16 µL PBS. For the no aptamer blank, 16 µL of 2 µM recombinant Clec9A was combined with 16 µL PBS. Non-specific target experiments were carried out using the same aptamers and thrombin as the target molecules under the same conditions.

2.3.2.2 Preparing the CD Spectroscopy Machine for Use

Prior to use of the CD spectroscopy machine (Chirascan Plus, AppliedPhotophysics, New Zealand), the machine required purging with nitrogen gas (N_2) for one hour or half a day depending on the last time it was used. This was performed by turning on the N_2 gas and setting the pressure at 400kPa. Once purged, the light was turned on in the machine and left to equilibrise for 15 minutes. After this point, the rest of the machine could be turned on along with the software.

2.3.2.3 Measuring Samples Using CD Spectroscopy

A background blank was measured first which measured the background noise with no sample or cuvette within the system. This interfering background noise was automatically subtracted from all subsequent measurements. All measurements were performed using the 0.5 mm pathlength glass cuvette (Quartz SUPRASIL®, Hellma Analytics, Sigma Aldrich, New Zealand). A water blank was then measured by pipetting 30 µL of Ultra-Pure H_2O at the bottom of the cuvette. A glass coverslip was placed over the top and the cuvette was placed inside an aluminium spacer (Hellma Analytics, Sigma Aldrich, New Zealand). The cuvette with spacer was placed in the machine. The absorbance was measured over a wavelength spectrum of 200 nm to 320 nm. The bandwidth, the amount of data that can be collected at each time point, was set at 2 nm and the step scanning feature was set at 2. The time set for the accumulation of each data point was set to 1 second, where the approximate scan time was 87 seconds. Five repeat measurements were taken of each sample and averaged. The data was smoothed using an increase of one smoothing window. Following the water blank, a PBS only, and a Clec9A only blank were also performed under the same conditions, as were the experimental samples.

Each aptamer was measured firstly with no target present, followed by measurements with the target present.

2.3.2.4 Analysis of CD Spectrophotometry Data

The data was exported from Chriascan plus software (AppliedPhotophysics, New Zealand) into excel comma separated values (csv) files. The differential absorbance was provided at each wavelength and presented as ellipticity (mdeg). For the aptamer measurements with no target, the measurements from the PBS blank were subtracted. This value was then normalised by subtracting each blank corrected value to the blank corrected value at 320 nm for aptamer and target conditions, the blank subtraction was performed using the Clec9A only blank. The data was plotted with the normalised ellipticity on the Y-axis and the wavelength on the X-axis.

CHAPTER 3: RESULTS

Section 3.1 Characterisation of the DC2114 Cell Line

This section addresses Objective 1 and shows the results of two characterisation procedures to evaluate the gene expression levels of *Clec9A* and the presence of Clec9A on immortalised DC2114 cells in culture. The results from this section of work were critical for assessing the appropriateness of using DC2114 cells for use in a Cell-SELEX experiment (Objective 2) for the generation of an aptamer to Clec9A.

These results were obtained through the employment of SYBR green qPCR to determine the expression levels of *Clec9A* mRNA of DC2114 cells over six passages in three independent replicate experiments. Flow cytometry was used to determine the proportion of DC2114 cells that presented the Clec9A receptor on their extracellular surface. The inclusion of a negative (JAWS II) and positive (fresh splenocytes) control proved to be critical to the success of Objective 2.

3.1.1 Gene Expression Profiles of Clec9A *in DC2114 Cells with Increasing Passage Number*

The changes in mRNA expression levels of *Clec9A* in incubated DC2114 cells relative to passage number were assessed. The relative expression levels of *Clec9A* were normalised against the reference gene, *Rpl19* using the $2^{-\Delta\Delta Cq}$ method.

Figure 3.1 shows that expression levels of *Clec9a* were variable between independent replicate experiments. The first replicate experiment showed no change in expression of *Clec9a* across passage numbers. These results imply that in biological replicate 1, expression levels remained stable and were not affected by passage.

The second replicate experiment showed an overall main effect ($P<0.05$) of passage number on *Clec9a* mRNA levels. Post-hoc tests showed that cells in Passages 4 and 5 exhibited lower *Clec9a* mRNA levels compared to that in Passage 3 ($P=0.007$, 0.007, respectively).

The third replicate experiment also showed an overall main effect ($P<0.05$) of passage number on *Clec9a* mRNA levels. However, in this case, the post-hoc test showed that cells in Passages 4 and 5 exhibited higher *Clec9a* mRNA levels compared to that in Passage 1($P= 0.024$ and $P=0.010$, respectively).

Whilst the results in Experiments 2 and 3 show opposing relationships between expression levels and passage number, in both cases, significant differences were observed at Passages 4 and 5, compared to earlier passages.

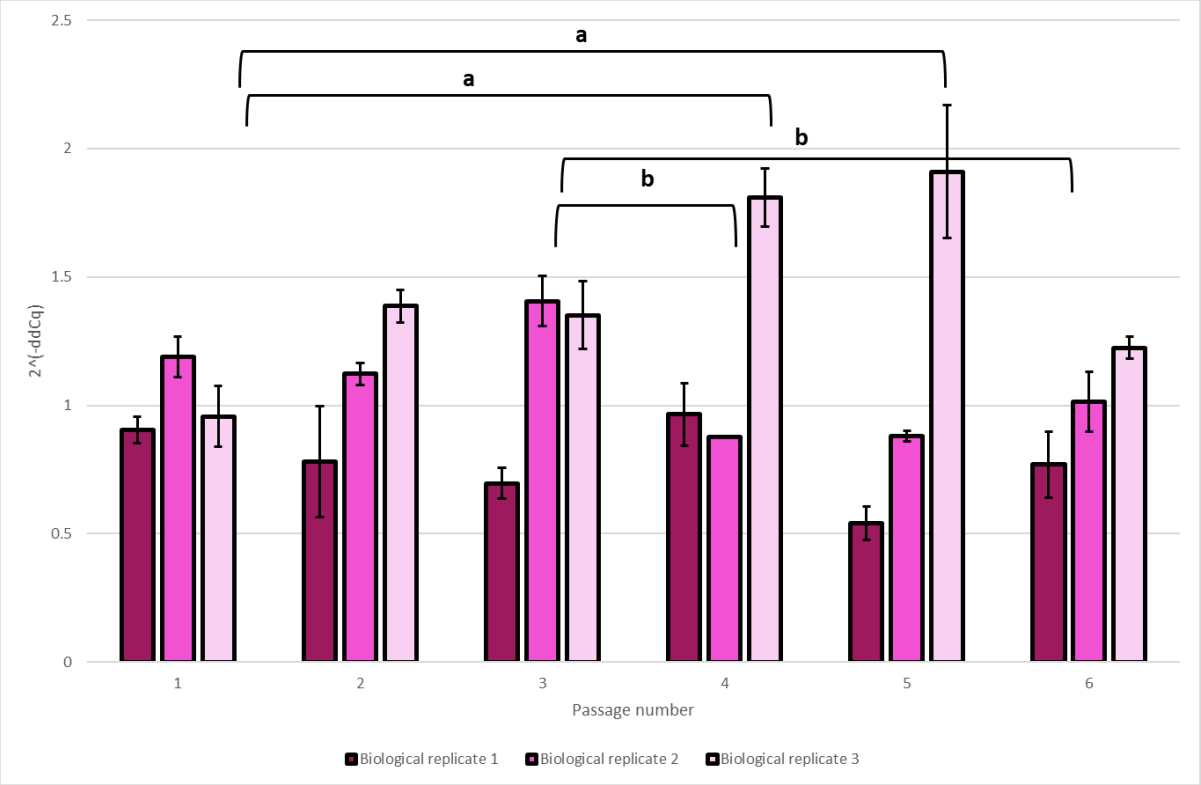

Figure 3.1: Relative mean ± SEM Clec9A mRNA expression levels of DC2114 over six passages.
The error bars represent the standard error of the mean (SEM) from three experimental replicates of each independent replicate experiment (N=3). Significant differences are denoted as (a for biological replicate 2 (P=0.007 for both compared to passage 1) and (b for biological replicate 3 (P=0.024 and 0.010 respectively, compared to passage 1). (a and (b = significance level of P<0.05.

3.1.2 Clec9A Receptor Presence on DC2114 cells

Figure 3.2 represents the histograms for the presence of the surface receptor Clec9A on fully- and FMO-stained cell populations of DC2114, JAWS II (negative control) and CD8+ sorted splenocyte (positive control) cells. The digested spleen preparation has had contaminating connective tissue removed so a greater proportion of Clec9A positive cells were expected.

Figure 3.2A depicts fully- and FMO-stained DC2114 cells and the results are almost completely superimposed. This implies that the fluorescence of Clec9A specific antibody in the fully stained sample does not exceed the background fluorescence in the FMO condition. Thus, there is little to no Clec9A present on the surface of the DC2114 cells.

Figure 3.2B depicts fully- and FMO-stained JAWS II cells (negative control). Similar to the DC2114 cells, the fully-stained JAWS II cell population is nearly totally overlapped with the FMO-stained JAWS II cell population. One difference is that the peak for the FMO-stained JAWS II cell population is broader, relating to varying levels of background fluorescence. This confirms that the JAWS II cells act as an appropriate negative control, demonstrating negligible expression of Clec9A.

Figure 3.2C and D depict fully- and FMO-stained digested (C) and undigested (D) splenocyte samples. Both graphs show a dramatic shift in fluorescence between the fully- and FMO-stained cell populations, with the fully-stained cells displaying a much higher fluorescence. Figure 3.2C presents a much narrower peak compared to Figure 3.2D. this can be explained by the procedures used to obtain the splenocyte samples. Digested splenocyte populations result in a much purer and more enriched cell population compared to undigested splenocyte cells. the contamination of cells and connective tissue in the undigested cell sample contributes to greater background fluorescence and thus a broader peak is observed. This implies that both populations of $CD8^{+}$splenocytes are positive for Clec9A staining.

Collectively, these results reveal that DC2114 cells do not express Clec9A on their cell surface which is surprising given they express *Clec9a* mRNA. Given that the splenocytes presented high levels of Clec9Aexpression above the relative background fluorescence, the decision was made

to use these cells for the Cell-SELEX strategy. Digested splenocytes were used as they were purer and more enriched with DCs.

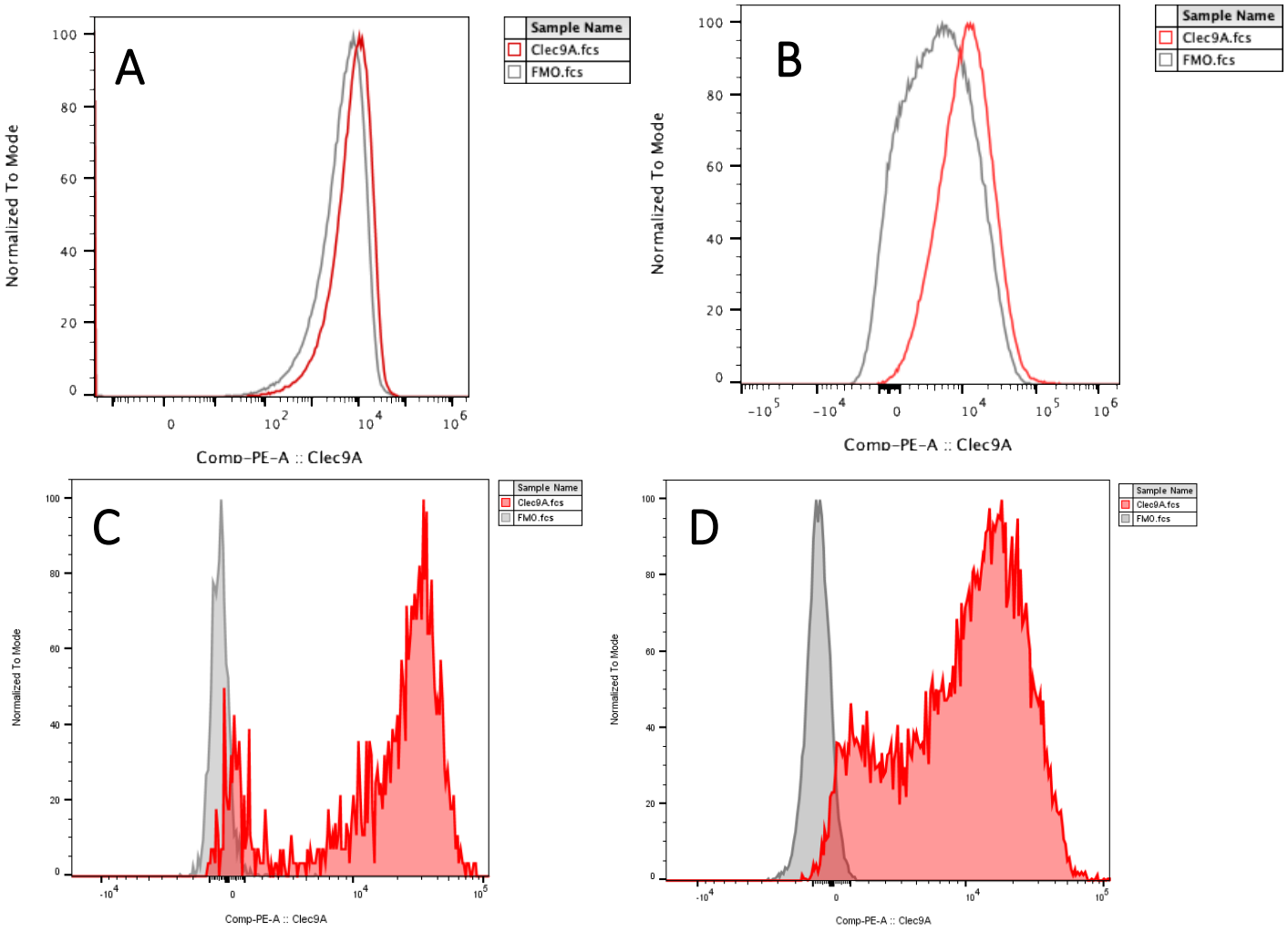

Figure 3.2: Single colour flow cytometry histograms.
Histograms present the fluorescence intensities and proportion of cells expressing Clec9A against a fluorescence minus one (FMO) control for A) DC2114, B) JAWS II, C) Splenocytes digested and D) Splenocytes undigested. Fluorescence intensities of Clec9A are presented on the X-axis for each condition while the normalised modal number of counts are depicted on the Y-axis. Grey lines for each figure represent the FMO cell population while red represent the fully stained cell population.

Section 3.2 Hybrid SELEX

3.2.1 Hybrid SELEX Experimental Outline

This section addresses Objective 2 and describes the use of a hybrid-based SELEX method to generate aptamers specific to mouse Clec9A receptor as summarised in Figure 3.3.

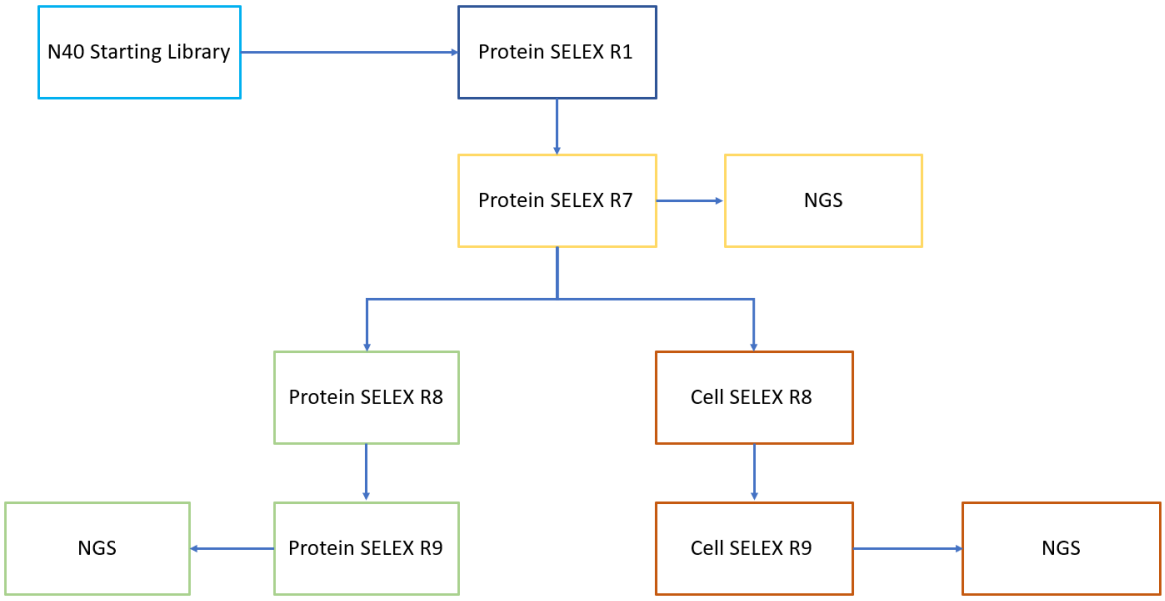

Figure 3.3: Schematic for Hybrid-SELEX and sequencing.
7 rounds of Protein-SELEX are performed initially. After round 7, the library is split, and SELEX is continued with two rounds of Protein-SELEX and Cell-SELEX in parallel. Along with the N40 oligonucleotide starting library, Protein-SELEX Round 7 and Protein- and Cell-SELEX Round 9 are sequenced using Illumina NGS.

3.2.2 Successful Conjugation of Recombinant Clec9A to Protein G-Coupled Magnetic Beads

A Nanodrop spectrophotometer was used to determine the conjugation success of recombinant Clec9A-Fc onto the Protein G conjugated magnetic beads. The Nanodrop readings were obtained of the Clec9A solution before and after the conjugation steps and were 0.16 and 0.07 µg/mL, respectively. The decrease in Clec9A concentration after the conjugation step indicates the conjugation was successful.

3.2.3 Optimisation of Primer Annealing Temperature for Use in SELEX PCR

Figure 3.4 shows the results of the N40 oligonucleotide library using the primers at three different annealing temperatures (54, 56 and 58°C). All temperatures amplified at similar rates which indicated that any of these temperatures would be suitable to use. An annealing temperature of 58°C was used for all SELEX PCR experiments hereafter.

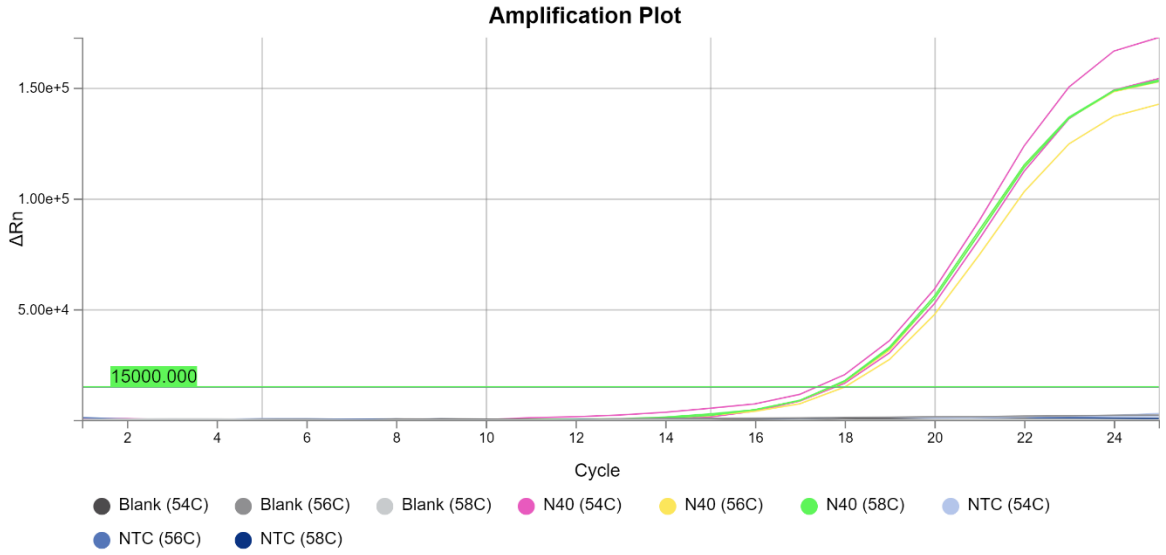

Figure 3.4: Real-Time PCR amplification plot assessing the effect of annealing temperature on PCR amplification.
Forward and reverse SELEX primers with melting temperatures of 55.5 and 56.2°C were assessed for their efficiency to amplify 1 nM N40 library under three annealing temperatures in the same reaction using VeriFlex™ technology. The temperatures were 54, 56 and 58°C, shown in pink, yellow and green respectively. The cycle threshold is set at halfway up the amplification curve in the log phase.

3.2.4 Validation of Blocking Step to Minimise Non-Specific Binding to Beads during SELEX

Figure 3.5 shows the effect of blocking unconjugated protein G sites on magnetic beads after conjugation with recombinant Clec9A. There was a large difference in amplification between the blocked and non-blocked conditions. The mean Cq value of the non-blocked condition was 9.80, compared to 14.79 for the blocked condition. These results show that there is a greater number (~ 32-fold more) of amplicons produced from the un-blocked conditions. Without a blocking step, there would be a greater number of binding sites for oligos to non-specifically bind to and thus remain in the pool despite not having specificity to the target. These results confirm that blocking the protein G conjugated magnetic beads with skim milk is necessary to minimise non-specific binding of oligonucleotide library to free protein G sites on the magnetic beads and thus retain a more target-specific oligonucleotide pool.

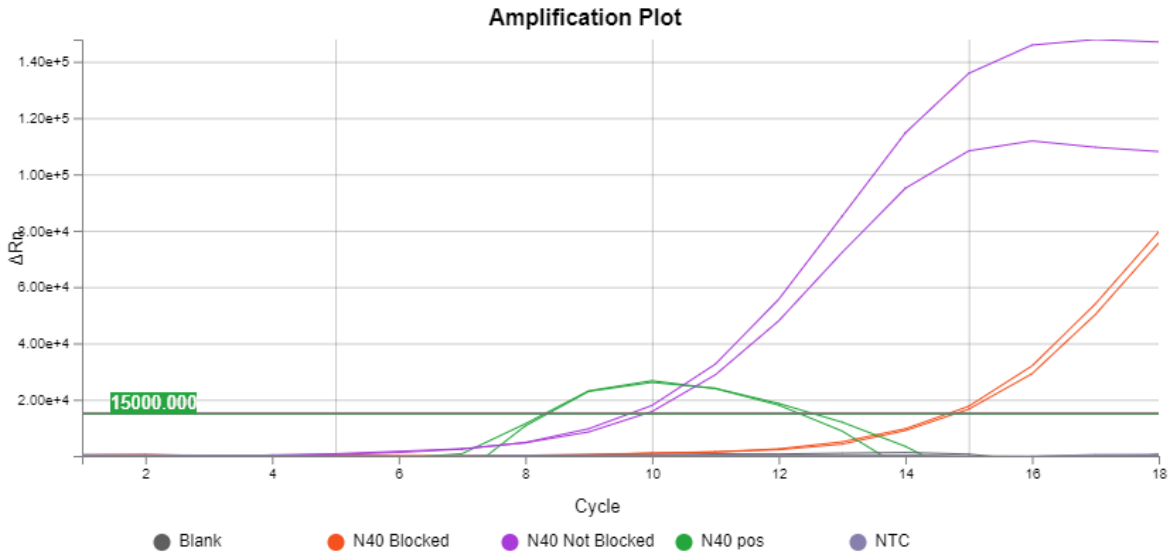

Figure 3.5: Real-Time PCR amplification plot assessing the influence of blocking for the reduction of non-specific binding.
1 nM of N40 oligonucleotide library was incubated with Clec9A conjugated beads either blocked or non-blocked with 2% w/v skim milk and the amplification was assessed. The lines green, purple, and orange represent the N40 positive control, non-blocked condition, and blocked condition respectively. The horizontal line represents the cycle threshold which is set at the halfway point of the amplification curve in the log phase.

3.2.5 Nucleotide Library Enrichment for Clec9A using Hybrid SELEX

The concentration of ssDNA present in solution following a round of positive SELEX (incubation with the target) was estimated by Nanodrop spectrophotometry to crudely track the amplification of DNA and inform on the progression of SELEX. Figures 3.6 A, B, C, and D show the amplification curves of SELEX Rounds 1, 7 and 8 for Protein-SELEX and Cell-SELEX, respectively.

At the beginning of the SELEX process, the library is random and not specifically enriched towards a target molecule. As expected, there was a greater number of oligonucleotides present in the negative, compared to the positive, selection pool due to the unlikelihood that many sequences would exhibit specificity to Clec9A in the initial rounds (Figure 3.6A). A comparison of the Cq values of 16.60 and 19.33 suggest that there were ~8-fold more amplicons present in the negative reaction in SELEX Round 1. These results confirm that the negative SELEX step is effective at removing sequences from the selection pool that exhibit binding to molecules other than the target.

By SELEX Round 7, the oligonucleotide library should be enriched towards the target molecule. The results from SELEX Round 7 show that the positive SELEX reaction exhibits a lower Cq value than the negative SELEX reaction (*i.e.* mean Cq values of 17.19 and 18.00, respectively) (Figure

3.6B). These results show that there were fewer oligonucleotides being retained in negative SELEX, implying that enrichment has occurred towards recombinant Clec9A due to an increase in the number of oligonucleotide sequences present in the positive SELEX condition.

The results from Protein-SELEX Round 8 were expected to show continued enrichment of oligonucleotide sequences that bind Clec9A. However, the results showed that the negative SELEX reaction has ~4-fold more amplicons (Cq of 15.89 *c.f.* 17.57) than that in the positive SELEX reaction (Figure 3.6C). This is interesting as it shows that there was little change in the Cq values for positive SELEX reactions from SELEX Round 7, indicating that the number of target-specific oligonucleotides between selection rounds was similar. However, a greater number of oligonucleotides present in the negative SELEX reaction, compared to the previous round, suggests that the mutational PCR is working to diversify the oligonucleotide population between SELEX rounds.

The results from Cell SELEX Round 8, the first round performed with fresh mouse splenocytes, were expected to show the oligonucleotide library being enriched sequences that bind Clec9A in the state it is presented on the surface of the cell. Additionally, the negative SELEX condition includes cells that do not express Clec9A, the two sub-types of splenocytes (*i.e.* Clec9A^{+} and Clec9A^{-}) may exhibit divergent expression patterns of other cell-surface receptors and proteins. Thus, although the library enrichment suggests the presence of sequences with affinity to Clec9A (Figure 3.6D), they may also exhibit specificity to new molecules present on the Clec9A^{+} cells that have not been removed in the negative SELEX step. There is a 2-fold greater number of amplicon products in the negative, compared to the positive, SELEX conditions (mean Cq of 12.55 and 13.69, respectively) indicating that new binding sites were present on the Clec9A^{-} cells, as opposed to the magnetic beads. Compared to SELEX Round 7, there were a greater number of amplicons, as demonstrated by lower Cq values, indicating a greater number of oligonucleotides were retained on the cells. This may be resultant of a broader range of molecules in both cell SELEX rounds that retained sequences within the pool.

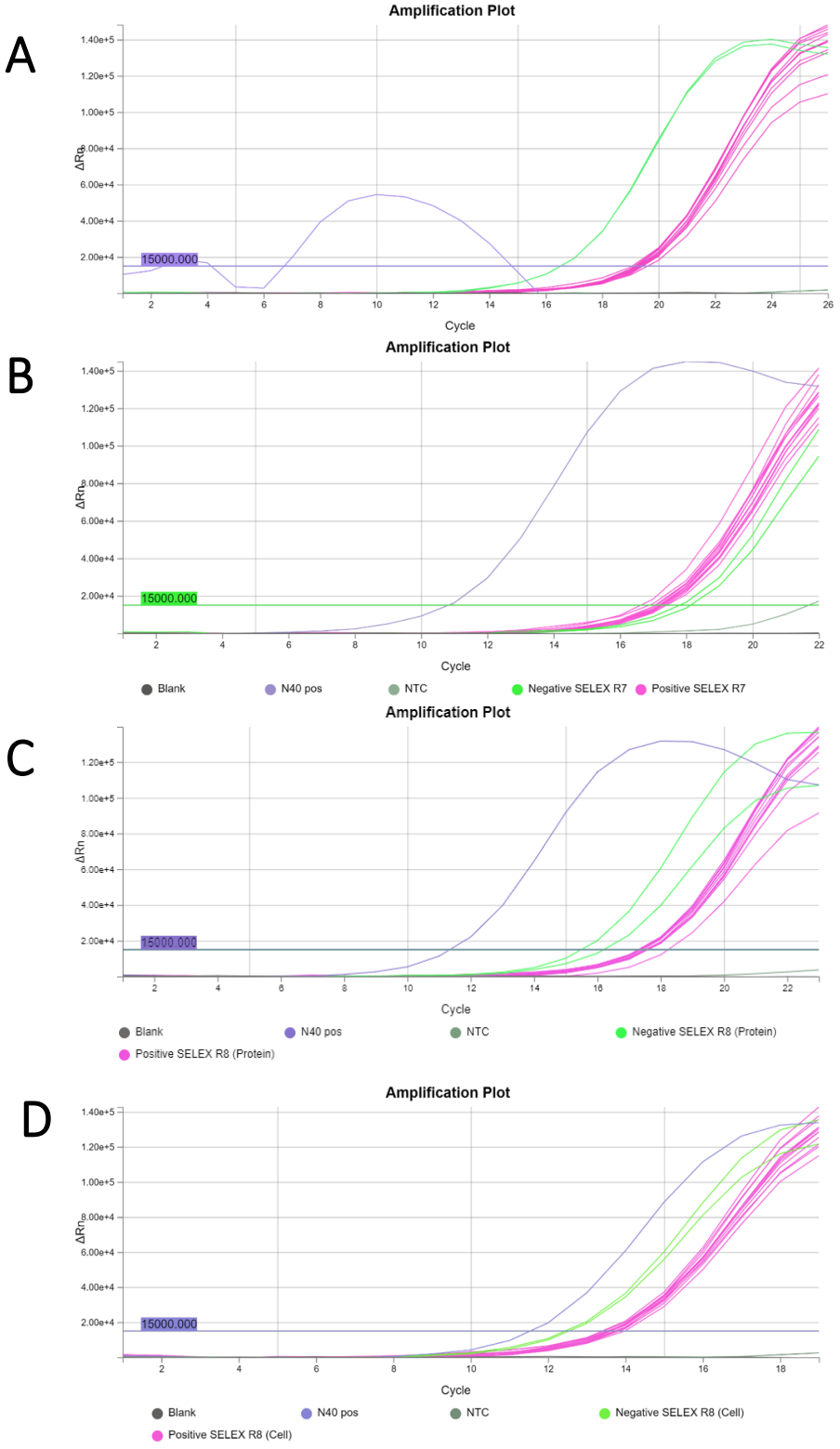

Figure 3.6: Real-Time PCR amplification curve for SELEX experiments

A) protein SELEX R1 B) protein SELEX R7 C) protein SELEX R8 and D) cell SELEX R8. Each plot depicts the amplification of the oligonucleotide library at different stages of enrichment towards the target molecule. Purple, green and pink represent the N40 positive control, the negative SELEX condition and positive SELEX condition respectively. The horizontal line represents the cycle threshold which is set at halfway up the amplification cure when in log phase

3.2.6 Agarose Gel Electrophoresis and Extraction of Positive SELEX DNA

Following each PCR amplification, the amplicon products from each reaction were run on an agarose gel to purify the oligonucleotides by size and eliminate potential PCR contaminants. Figures 3.7 A, B and C show the gel electrophoresis images relating to SELEX Rounds 1, 7 and 8 for Protein-SELEX and Cell-SELEX, respectively.

Figure 3.7A depicts the presence of a strong fluorescent band of approximately 80 base pairs in size in the positive reaction from SELEX Round 1 (Lanes 7 and 8) and shows that the sequences that successfully bound to Clec9A conjugated magnetic beads were of the expected size. Furthermore, the visualisation of a faint grey band in the negative SELEX reaction (Lane 2) indicates the successful removal sequences with specificity to non-target molecules.

The oligonucleotide library at SELEX Round 7 should be enriched towards Clec9A, resulting in a large amount of product in the positive SELEX reaction, as is observed by the thick bands observed in Lanes 7 and 8 in Figure 3.7B, indicating the presence of oligonucleotides in the positive SELEX condition. Compared to SELEX Round 1 (Figure 3.7A), the band appears thicker implying the oligonucleotide pool has enriched for sequences that bind Clec9A.

Figure 3.7C reveals thick fluorescent bands of approximately 80 base pairs in size in the positive SELEX reactions from both the Protein- and Cell-SELEX experiments (Lanes 10-11 and 14-15, respectively). The results from the Round 8 Protein SELEX remains similar to previous rounds showing a thick band (Figure 3.7C). Interestingly, there appears to be a thicker band in the negative reaction from Protein-SELEX Round 8, compared to Round 7 (Lane 2). This result aligns with the amplification plot (Figure 3.6C) showing an increase in the number of oligonucleotides in the negative SELEX step. These results together suggest that there was a greater number of non-target sequences in Round 8 of the Protein-SELEX strategy, likely due to error-prone PCR.

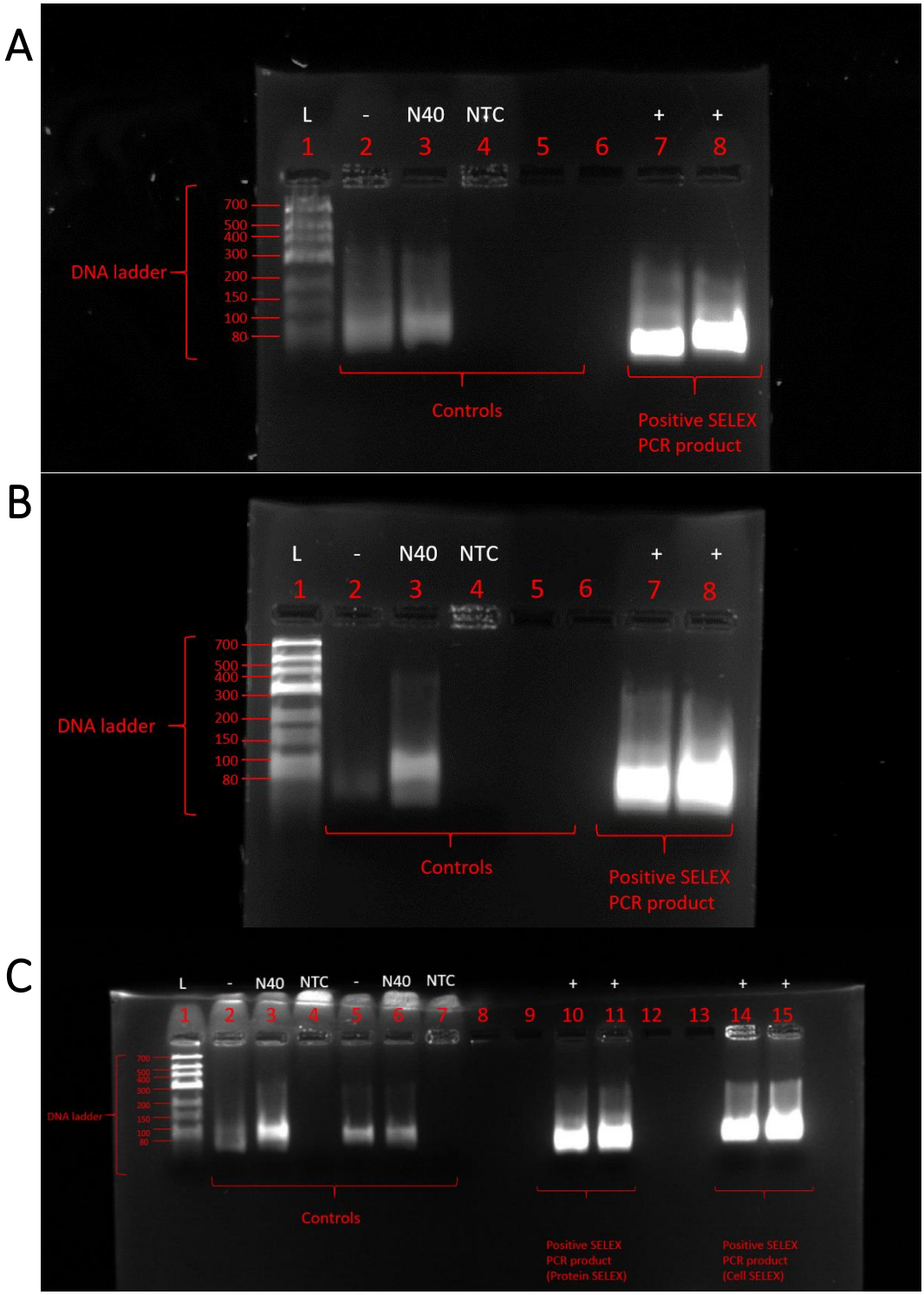

Figure 3.7: Agarose gel electrophoresis images of SELEX rounds.

Agarose gel electrophoresis was used to purify DNA for the following round of SELEX, A) Protein-SELEX R1 B) Protein-SELEX R7 C) Protein- and Cell-SELEX Round 8. Target specific sequences from positive selection were amplified via real-time PCR and ran through an agarose gel to purify the DNA and remove any contaminating and unwanted PCR products. This fluorescent bands labelled on the image as positive PCR product indicate target-specific sequences from the previous SELEX round and were removed using a scalpel and used for the following round of SELEX. For images A) and B), the lanes 1-5 are as follows: DNA ladder, negative SELEX PCR product, N40 positive control, and no template control. Lanes 7-8 are the positive SELEX product. For image C) lanes 1-7 are as follows: DNA ladder, negative selection product, N40 positive control, no template control for protein SELEX R8 (lanes 1-4), negative selection product, N40 positive control and no template control for Cell- SELEX Round 8 (lanes 5-7). Lanes 10-11 and 14-15 are the positive SELEX product from Protein- and Cell-SELEX Round 8 respectively.

3.2.7 Freshly Sorted and Purified Mouse Splenocytes Provided Relevant Clec9A$^+$ and Clec9A$^-$ DCs for Positive and Negative Cell-SELEX.

Flow cytometry results of the DC2114 cell line surprisingly showed negligible numbers of cells that exhibited surface expression of Clec9A, despite having encoded mRNA expression of *Clec9a*. Thus, this cell line could not be used for the Cell-SELEX strategy. Luckily, the positive control cells, the mouse splenocytes, could be used in the place of the DC2114 cells. As the Clec9A receptor needed to remain free for oligonucleotide binding in the SELEX experiments, the cells could not be sorted using a Clec9A antibody. Thus, cells were sorted for XCR1 receptor expression which is a chemokine receptor secreted by CD8$^+$ DCs and is understood to correspond with the co-expression of Clec9A (Bachem et al., 2012).

Figures 3.8A and B present dot-plots depicting the surface expression of XCR1 and Clec9A, respectively for cells specifically sorted for XCR1 using FACS. Figure 3.8A illustrates the proportion of cells, sorted for XCR1, expressing the receptor against forward scatter area (FSA) which allows for the discrimination of cells by size. There is a dense population of cells at the top centre of the dot-plot which indicate these cells exhibit high levels of XCR1 surface expression as expected. The sorting report found the XCR1 sorted cell population was 96% pure for XCR1.

To confirm the presence of the Clec9A receptor on XCR1$^+$ cells, cells were then stained with Clec9A antibody and the proportion of cells expressing Clec9A were measured using flow cytometry. Figure 3.8B depicts the dot plot for Clec9A expression of XCR1$^+$ cells. The dot plot measures the fluorescence intensity for Clec9A of XCR1$^+$ cells on the Y-axis, against FSA on the X-axis. There is a concentrated region of cells present in the upper centre of the dot plot which indicates that the XCR1 cells also express high levels of Clec9A.

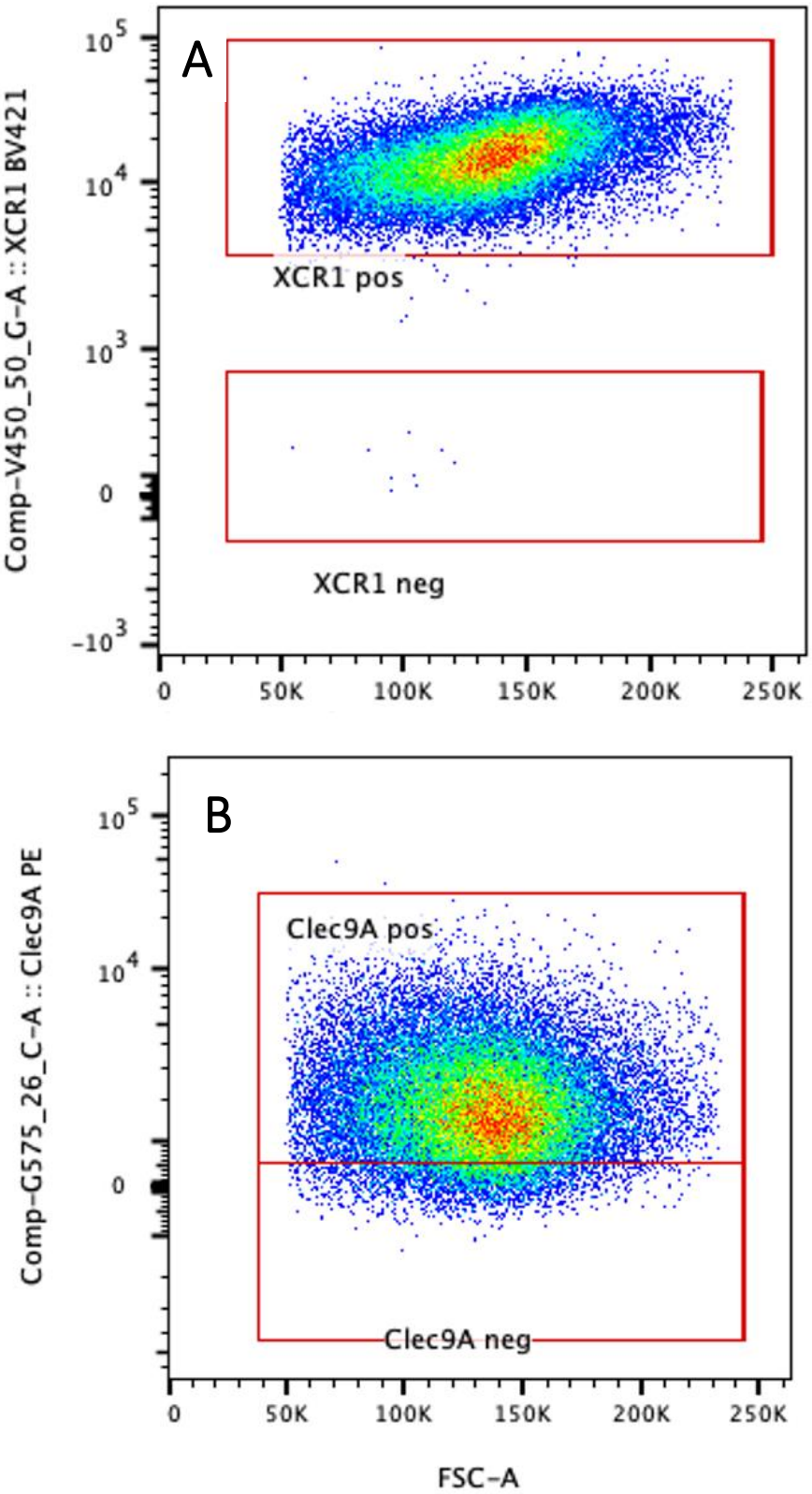

Figure 3.8: Single colour flow cytometry purity dot-plots.
Plots present A) the proportion of XCR1 cells, expressing XCR1 and B) the proportion of XCR1 cells expressing Clec9A. The fluorescence intensity of the selected markers on each plot are represented on the Y-axis and compared with FSA on the X-axis to ensure cells are similar size.

Section 3.4 Bioinformatic Processing of Data for Selection of Candidates

Four libraries were sequenced using Illumina sequencing and included the N40 starting library, Protein-SELEX Round 7, and Protein-SELEX Round 9 and Cell-SELEX Round 9.

3.4.1 Unique Sequences

Sequence uniqueness is useful to assess the efficiency of the SELEX process to evolve an oligonucleotide library towards a target molecule. A reduction in unique sequences within the library, i.e. the sequence complexity, is inversely related to enrichment. Thus, the fewer unique sequences present, the more enriched the library (Alam et al., 2015).

Figure 3.9 compares the number of unique sequences for each SELEX library sequenced. As expected, the N40 starting library had the greatest number of unique sequences as it should represent the maximum possible diversity of oligonucleotide sequence combinations. The Protein-SELEX Round 7 library contained the fewest unique sequences implying that the oligonucleotide library was being enriched towards sequences that bind recombinant Clec9A. As expected, there was a minimal difference in the numbers of unique sequences between libraries from Protein-SELEX Rounds 7 and 9. However, there are discernible differences in the numbers of unique sequences in libraries between Protein-and Cell-SELEX Round 9. During Cell-SELEX, the oligonucleotide library was likely to be exposed to a range of novel interfering receptors and surface chemistries. Thus, it would be expected that the number of unique sequences would increase, and this would perhaps be further exacerbated by the negative selection cells expressing receptors other than Clec9A that are not present on Clec9A^{+} cells.

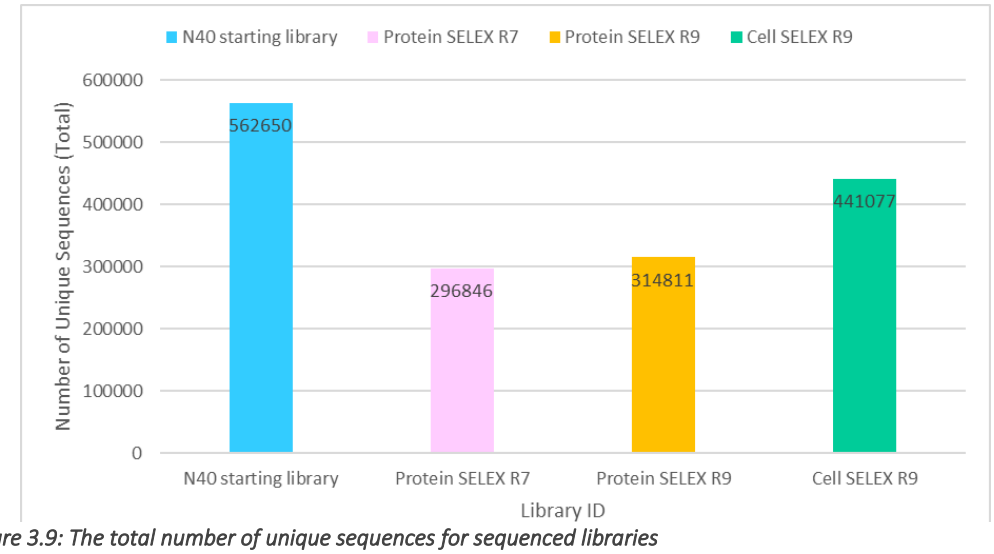

Figure 3.9: The total number of unique sequences for sequenced libraries
N40 starting library (blue), Protein-SELEX Round 7 (pink), Protein-SELEX Rounds 9 (orange) and Cell-SELEX Round 9 (green). The total number of unique sequences were obtained using Fastaptamer-count

Therefore, oligonucleotides that do not exhibit specificity to Clec9A were likely to be carried across and remained within the library population, causing an increase in the number of unique sequences.

3.3.2 The Number of Conserved Sequences Across SELEX Libraries

Fastaptamer-compare was used to compare the number of conserved sequences between libraries to help understand the amount of enrichment occurring between SELEX rounds. For Protein-SELEX, the oligonucleotide library was enriched towards recombinant Clec9A under near-identical experimental conditions. However, there was a large degree of variability between Protein- and Cell-SELEX conditions. Thus, high levels of sequence similarity would be expected between Protein-SELEX rounds, but not between Protein- and Cell-SELEX rounds.

Table 3.1 shows the number of conserved sequences between Protein-SELEX Rounds 7 and 9 and Cell-SELEX Round 9. There was a higher number of conserved sequences between Protein-SELEX Round 7 and Cell-SELEX R9, than compared to the two Protein-SELEX rounds. This supports the suggestion that a greater number of oligonucleotides are being retained in the Cell-SELEX strategies as there were more novel molecules present, increasing the number of non-specific oligonucleotide sequences.

Table 3.1: Table listing the number of conserved sequences.
Conservation observed between Protein-SELEX Rounds 7 (PR7) and 9 (PR9) and Cell-SELEX Round 9 (CR9). Data was obtained using Fastaptamer-compare.

	PR7	PR9	CR9
PR7		90869	136112
PR9	90869		101245
CR9	136112	101245	

3.3.3 Sequence Reads

To determine enrichment within the aptamer libraries, the reads per million (RPM) of each aptamer library were plotted and compared and is essential when comparing sequencing data for libraries of differing sizes. Previous studies discovered that the relationship of replicate sampling and sequencing of the same population was tight and linear whereas comparison between populations separated by a single round of selection showed a broadened

distribution indicating enrichment s sequences become greater or less in abundance (Alam et al., 2015)

Figure 3.10A compares the RPM of sequences in the Protein-SELEX Round 7 and Cell-SELEX Round 9 libraries and were expected to have the greatest differences. There was a linear relationship between the libraries which indicate that the shared sequences are present in similar abundance within both libraries. This implies that the sequences present in the Protein-SELEX Round 7 were not further enriched under the Cell-SELEX conditions with the most abundant sequence at 1893.39 and 1897.78, respectively. The high abundance of this sequence in both libraries suggests this sequence has persisted due to amplification bias. This is the phenomenon where specific sequences have a greater ability to amplify under PCR conditions meaning they are retained in the pool due to amplification efficiency rather than enrichment towards the target molecule.

Figure 3.10B compares the RPM of sequences in Protein-SELEX Rounds 7 and 9 and were expected to have the fewest differences. The results showed a linear relationship between both libraries; however, the data is skewed with higher abundance observed in the Round 9 library. A high RPM is either related to enrichment towards the target molecule or amplification bias during PCR reactions. The greater RPM values for most of the conserved sequences in the Round 9 library implies that abundance is due to target-specific enrichment rather than amplification bias.

Figure 3.10C illustrates the relationship between Protein-SELEX and Cell-SELEX Rounds 9. There was a broader distribution of sequences between the two libraries suggesting the presence of moieties and interactions that were unique to each SELEX method, which results in different sequence representations within each library pool.

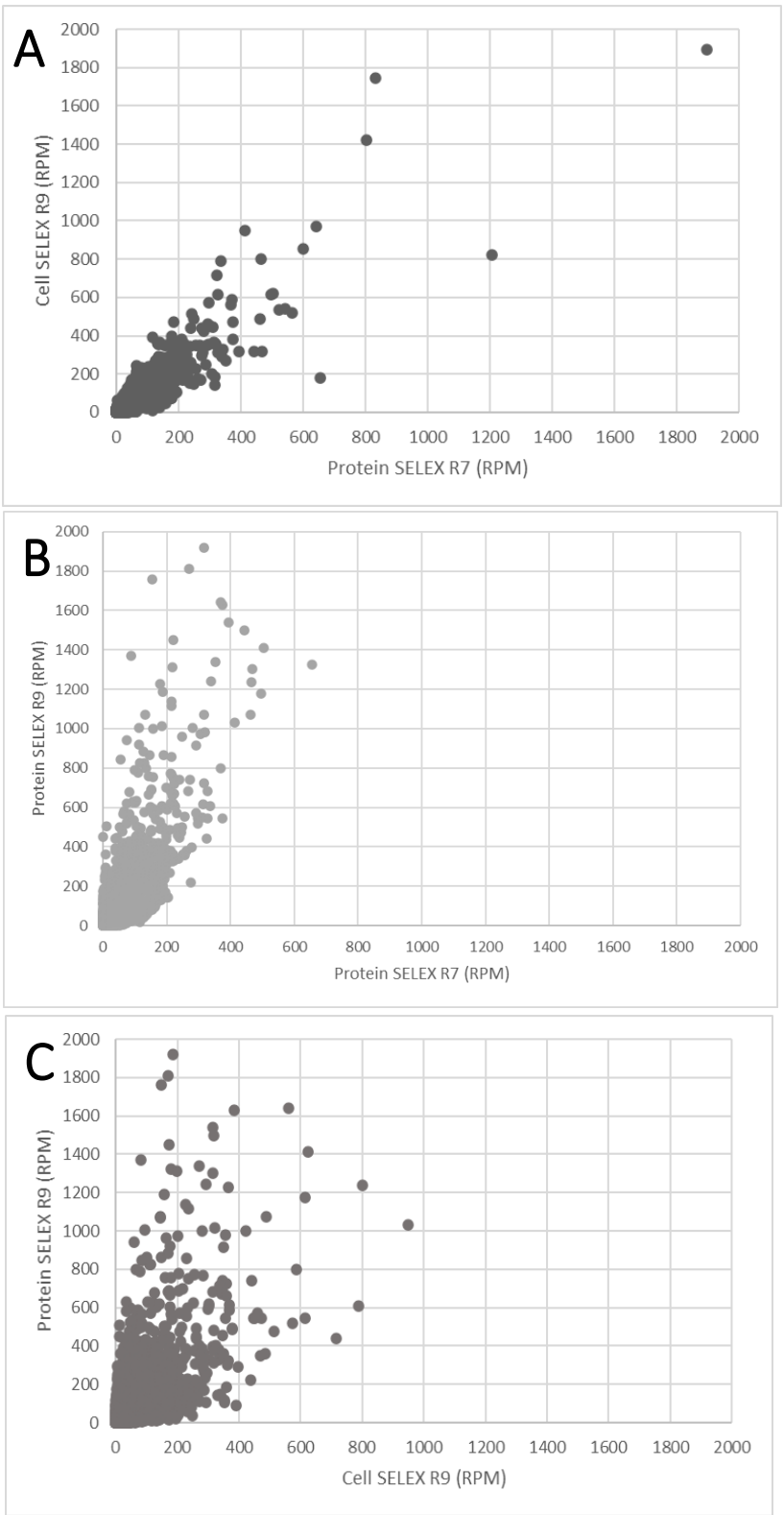

Figure 3.10: The reads per million (RPM) values of conserved sequences for SELEX Libraries.
A) Cell-SELEX R9 and Protein-SELEX R7, B) Protein-SELEX R7 and Protein-SELEX R9, and C) Protein-SELEX R9 and Cell-SELEX R9. RPM values were obtained using Fastaptamer-cluster using a Levenshtein edit distance of 7.

3.3.4 Comparison of Top 100 Sequences Based on RPM with SELEX Libraries

Enrichment of the oligonucleotide library across SELEX rounds was assessed using the RPM values for the top 100 sequences for Protein-SELEX Round 7 and were compared to the respective RPM of the same sequence within the Protein- and Cell-SELEX Round 9 libraries (Figure 3.11). Enrichment is demonstrated by the difference in sequence abundance between SELEX rounds. An oligonucleotide library that is enriched towards a target molecule should exhibit variation in the enrichment and thus depletion of sequences within the library. Since the 100 most abundant sequences present in Protein-SELEX Round 7 library were ranked based on RPM, it was expected that the top 100 sequences will present a linear trend as the subsequent sequence will be present in the population with less abundance.

The results show variability between the two Round 9 libraries, when compared to the Protein-SELEX Round 7 library. There are sequences with similar RPM values in the Cell-SELEX Round 9 library as there were in the Protein-SELEX Round 7 library, with most ranging between 300 and 2000 reads. This suggests that the target-specific sequences in the Protein-SELEX library did not enrich towards Clec9A on the cells. The Cell-SELEX library may have evolved to find sequences that bind the receptor under new conditions and thus would not be observed in the Protein-SELEX R7 library.

The greatest variability in RPM between libraries was observed when the two Protein-SELEX libraries were compared. The greater abundance in RPM for sequences found in the Protein-SELEX Round 9 indicates selective amplification of sequences with the affinity to bind recombinant Clec9A. Some of the sequences also presented the same or lower RPMs in Round 9, compared to 7 which is a further indication of enrichment occurring due to the depletion of specific sequences.

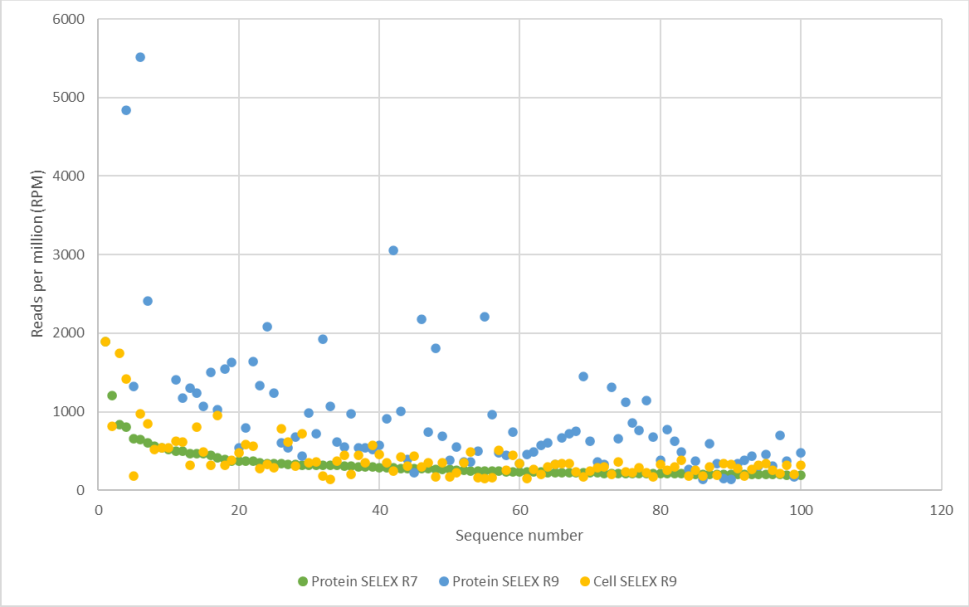

Figure 3.11: Reads per million (RPM) of the top 100 sequences for protein SELEX R7
Protein SELEX R7 (green) compared with the RPM for the same sequence in Protein-SELEX R9 (blue) and Cell-SELEX R9 (yellow) to illustrate enrichment for the most abundant sequences in Protein-SELEX R7 towards the target molecule. RPM values were obtained using the bash script Fastaptamer-cluster using a Levenshtein edit distance of 7.

3.3.5 Selection of Aptamer Candidates based on Bioinformatic Data

After analysing the bioinformatic data within the SELEX populations, aptamer candidates were selected on a range of criteria to experimentally assess their affinity for Clec9A. A range of criteria were used to select sequences most likely to represent enrichment for binding to Clec9A as selection based on one category may produce false results. For example, selecting sequences purely on highest read number or RPM, may only identify sequences that are abundant in the population due to PCR amplification bias rather than target specificity. Therefore, reads and RPM are considered but are not ultimate. Secondly, conservation of sequences between libraries can indicate target binding under a range of moieties and so would be desirable for aptamer end use.

The top five most abundant and five most conserved sequences were selected across all three libraries, as well as the most enriched sequences and those with the greatest reads within the final Round 9 libraries. This resulted in 18 candidate sequences (Table 3.2). Cluster number was employed as a measure to understand the enrichment and distribution of sequences across selection libraries with Cluster 1 containing sequences with similarities to the most abundant sequence in the population.

Figure 3.12 shows the candidate sequences, 1 to 18 and their cluster number within each library. Based on Figure 3.12 and Table 3.2, all sequences are present in each library but at varying cluster numbers. Cluster number, in combination with cluster rank, is a measure of abundance. Therefore, the lower the cluster number and cluster rank, the more abundant this sequence is in the population.

Most of the candidate sequences for all libraries have Cluster numbers below 50, which indicate that these sequences are present in each library with good abundance. Sequence 1 has the same cluster number for Protein-SELEX Round 7 and Cell-SELEX Round 9. Furthermore, this sequence is present at a similar abundance as observed in the RPM for Table 3.2. This may suggest this sequence is prevalent in the population due to PCR bias. Sequences 7 for Cell-SELEX Round 2 (219) and Sequences 12, 14 and 17 for Protein-SELEX Round 9 have higher cluster numbers (87, 142 and 142, respectively). The cluster number for sequence 12, 14 and 17 in Cell SELEX Round 9 is 9, 10 and 10, respectively. This indicates that these specific sequences may have been more highly enriched within this library and may exhibit affinity for moieties expressed on the cell. Whether this is target specific or due to other interfering molecules within cell SELEX, is unknown.

Regardless, the presence of each sequence across all three libraries indicates there could be conserved moieties between SELEX conditions that may result in specificity to the target. At this stage, it is not clear whether any of these sequences are present in the population due to amplification bias.

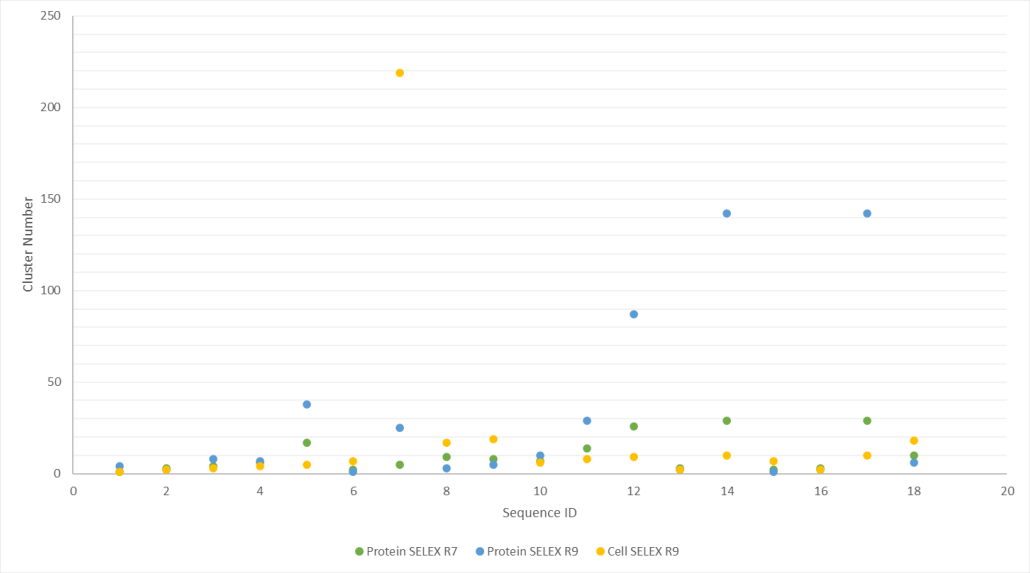

Figure3.12: Cluster number for the top 18 candidate sequences.
Candidates were chosen based on criteria that suggest binding to the target molecule. candidate oligonucleotide sequences were selected based on bioinformatic data for: top 5 sequences from each library, top 5 conserved sequences across libraries, greatest enrichment, and greatest number of reads. Green: protein SELEX R7, Blue: protein SELEX R9 and Yellow: cell SELEX R2. Cluster data was obtained using the bash script, Fastaptamer-cluster using a Levenshtein edit distance of 7.

Table 3.2: Candidate aptamer sequences.
RPM and cluster number for protein SELEX R7 and protein and cell SELEX R9 are listed in the table.

Sequence	RPM			Cluster Number		
	PR7	PR9	CR9	PR7	PR9	CR9
ACACGGGTTTGTGCATCCCACGACTTCGGCCAGCATCACC	1897	10256	1893	1	4	1
GACATCCACACCCTCTCCCCTTCCGATAAGCACCCCCATC	834	27834	1745	3	2	2
CCCTGTGAACTCCGATGCCCTGTGGACTTGCCTGCTACCC	804	4835	1421	4	8	3
TACGCCGTGAATTGTCTATGCACCACCTCCAACCCAATCC	643	5515	969	6	7	4
ACGTACATCTTATGACATGAACAACACCCCCTGCGCACCG	412	1030	950	17	38	5
TCCGTATCACTTCATACCGCTCCTACCTTTACCCACCAAT	1206	41033	821	2	1	7
ACCAAATGGTGACAGTACCACCTGTTGTGTATGCAATTCC	654	1325	178	5	25	219
TAATCTCGATCTAGTCCGCTCACCCACTCACCTCCCTTCC	541	16178	540	9	3	17
TCCCATTTCCCCCATTACCTCCAATGATATGCCTGTGCCA	564	8536	518	8	5	19
ACATCCAATTACATGATGGGACAGTACCCCCCACCTCCCC	600	2410	852	7	10	6
ACACAGATACCTGGATACTCATCGATCAACTCATTCCGCC	464	1235	802	14	29	8
ACCATACAACATCACGCACAGACCGCTACCGCAGCAATCC	337	606	788	26	87	9
GACATCCACACCCTCTCCCCTTCCGATAAGCACGCCCATC	0.57	172	14	3	2	2
GAACGTGTAAGCCCACCAACGCGCCACCAGACTCTCTTGC	0.57	1.36	14.44	29	142	10
TCCGTATCACTTCATACCGCTCCTACCTTTACGCACCAAT	0.57	449	12.03	2	1	7
GACATCCACACCCTCTCCCCTTCCGATAAGCGCCCCCATC	0.57	150	7.7	3	2	2
GAACGTGTAAGCCCACCAACGCGCCACCAGACTCTCCTGC	324	439	716	29	142	10
GTAATCCCTCGAACTTGCCTGAACATCTCTCCGCCCACTT	522	7239	537	10	6	18

Section 3.4 Characterisation Results

This section addresses Objective 3 and presents the results of two characterisation procedures used to evaluate the candidate aptamers, chosen in Objective 2, for their ability to bind to recombinant Clec9A.

The first characterisation method utilised a gold nanoparticle (AuNP) assay and assessed whether candidate aptamers, pre-adsorbed onto the surface of AuNP in solution, underwent a conformational change to bind Clec9A when introduced into the solution. This was tested through the mechanism of salt-induced aggregation of AuNP which aptamers, if remained attached, provided protection again. Thus, bare AuNP under salt conditions resulted in a colour change from red to blue, implying that there is an interaction between aptamer and target. Circular dichroism (CD) spectroscopy was the second characterisation method, and this investigated whether Clec9A resulted in a change in secondary structure formation suggestive of an interaction occurring between the aptamer and Clec9A. This relied upon the formation of secondary structures within the candidate aptamers which was unknown.

Section 3.4.1 Gold Nanoparticle (AuNP) Assay

3.4.1.2 Interaction of Clec9A in AuNP assay

The in-solution AuNP assay is beneficial for small molecules where there may only be a few binding sites as immobilisation may use or block these few sites (Chatterjee et al., 2020). However, the use of the AuNP assay for assessing aptamers against protein targets has not been attempted previously. My preliminary investigations with a positive control, an aptamer known to bind thrombin, did discover an interaction between AuNP and the protein, thrombin. Unfortunately, thrombin bound the AuNP and protected it from salt-induced aggregation in a concentration dependent manner (Figure 2.11, Section 2.3.1.11).

The AuNP assay is measured via the A625:A520 absorbance ratio which measures the proportion of aggregated particles. Thus, an increase in A625:A520 absorbance ratio upon target molecule addition would signify a binding interaction between the aptamer and its target molecule.

Figure 3.13A and B shows the effect of increasing concentrations of recombinant Clec9A on the aggregation of the AuNP before (Figure 3.13A) and after (Figure 3.13B) the addition of salt, respectively. Immediately after the addition of Clec9A but before the addition of NaCl, a colour

change was observed at the higher concentrations (Final well concentration of 50-100 nM) from a lighter red to a deeper purple colour, regardless of which aptamer was added. There is some variability between (aptamers) and within (Clec9A) rows, but this is likely due to a variability in the number on AuNP added to each well. The salt-induced aggregation was present at varying intensities relative to Clec9A concentration and furthermore, at higher concentrations the aggregation is visually more purple than the characteristic blue. The observable colour change before and after the addition of NaCl regardless of the presence of a specific aptamer candidate for Clec9A (Row A; BP01), a methamphetamine aptamer (Row B; OM5C6) or no aptamer (Row C; bare AuNP) indicates that Clec9A was interfering with the AuNP to destabilise their electrostatic interactions, resulting in change of colour in a concentration dependent manner.

Figure 3.14 confirms the results illustrated in Figure 3.13, as measured by a spectrophotometer plate reader. The A625:A520 absorbance ratio of AuNP increases with increasing concentrations of recombinant Clec9A, regardless of the presence or absence of aptamers. This confirms that the salt-induced aggregation observed is increasing concurrently with the increasing concentrations of Clec9A. An aptamer (i.e. OM5C6) that is not specific to the target molecule would be expected to remain bound to the surface of the AuNP and protect from salt induced aggregation. An AuNP solution without the presence of a protective aptamer layer (bare AuNP) would be expected to aggregate completely, regardless of Clec9A concentration. These results suggest that the increase in absorbance is due to the interaction of Clec9A with the AuNP, instead of a specific interaction between aptamer and Clec9A, causing AuNP aggregation.

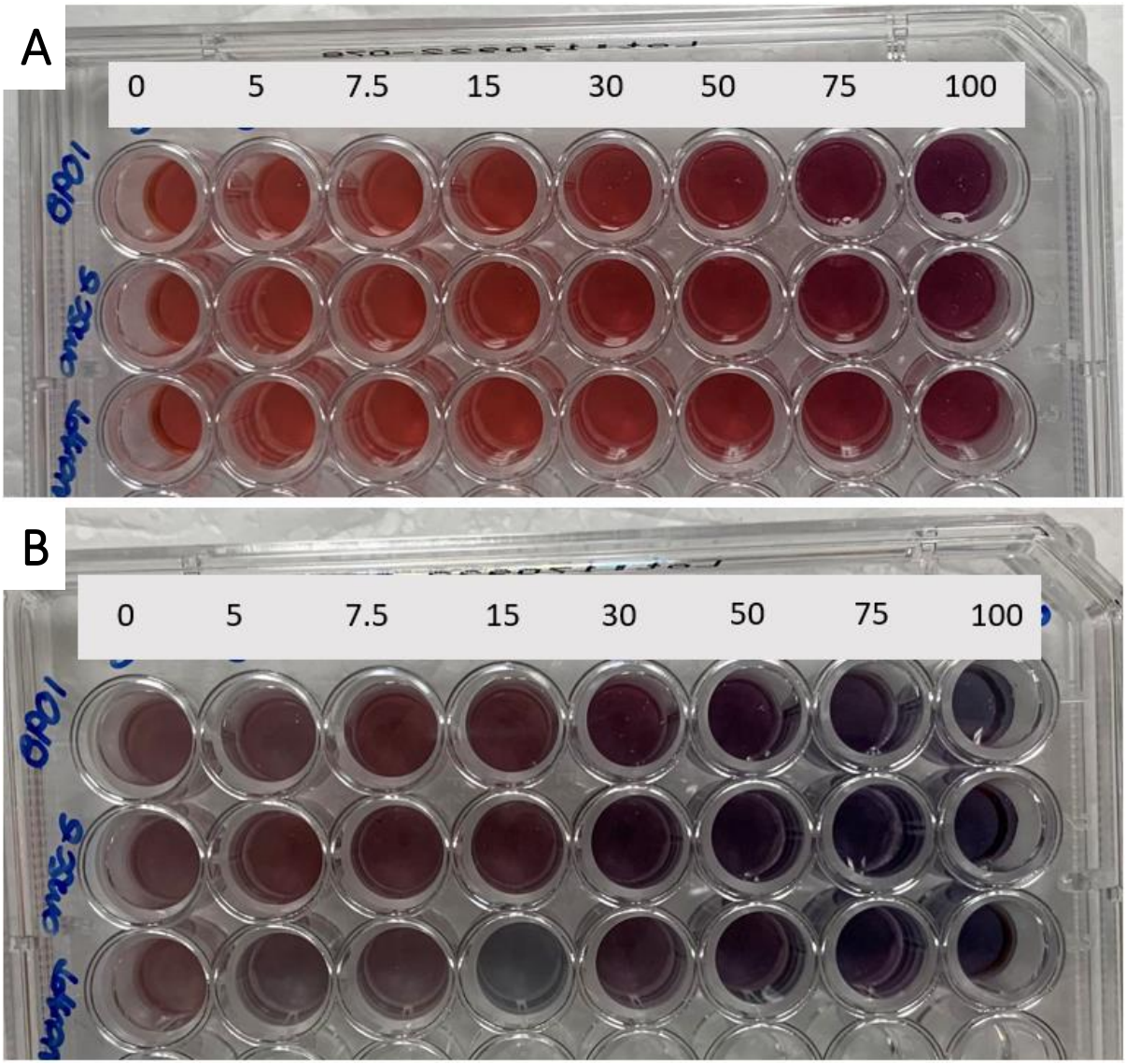

Figure 3.13: Visible AuNP aggregation of aptamer conditions.
A) after the addition of Clec9A and B) following the addition of NaCl. For both figures, the aptamer used for the association on to the AuNP surface in row 1 was BP01, a Clec9A candidate aptamer from hybrid SELEX, row 2 was OM5C6, a meth-specific aptamer and row 3 was no aptamer. The final Clec9A concentrations are depicted above each figure.

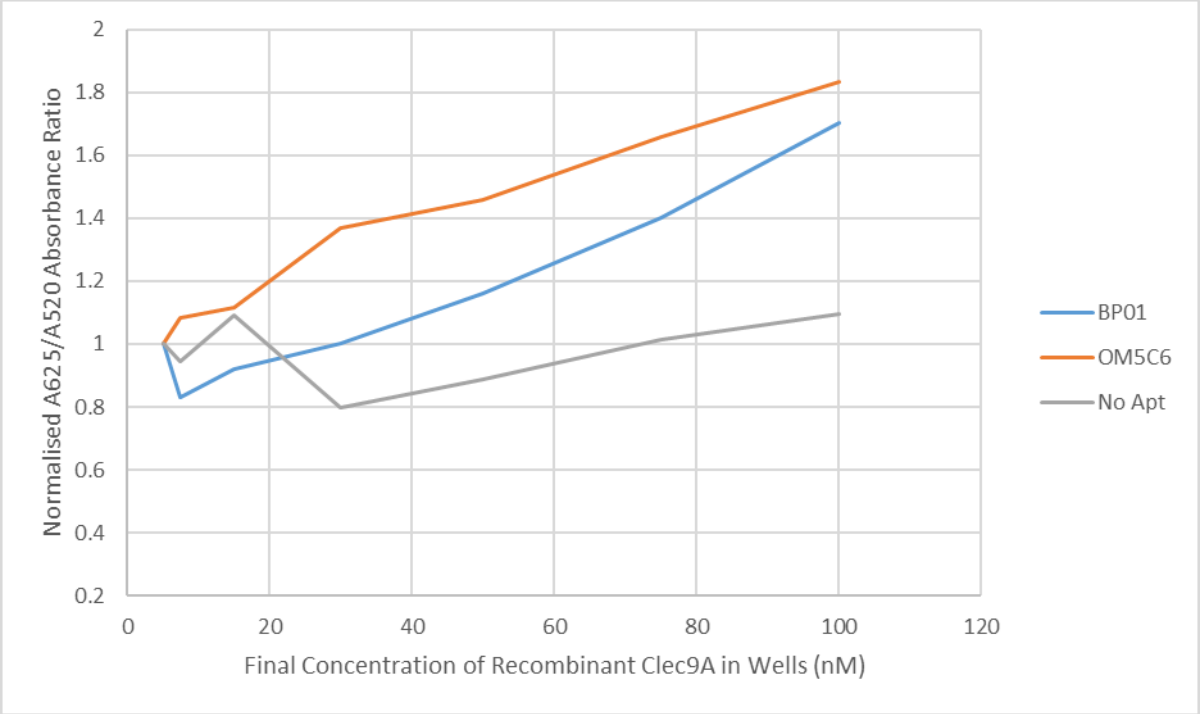

Figure 3.14: Aggregation of AuNP, measured as A625/A520 under different aptamer conditions across a concentration range of Clec9A

The normalised A625/A520 ratio is represented on the Y-axis where the final concentration of Clec9A in the wells is represented on the X-axis. The blue line shows the AuNP aggregation with surface association of BP01, a Clec9A candidate aptamer resultant of hybrid SELEX, orange is the meth-specific aptamer, OM5C6, while grey is no aptamer.

Despite the fact that proteins interfere with the AuNP assay, several of the Clec9A aptamer candidates were screened using this assay in the hope that an aptamer with good binding properties could still be identified from those that don't bind Clec9A.

3.4.1.3 Screening Candidate Aptamers Using AuNP Assay

Although higher concentrations of Clec9A appeared to interact with the AuNPs (Figure 3.13A), there was no observable interference with the AuNP of Clec9A at concentrations of up to 30 nM. Therefore, for candidate screening experiments, the concentration range was reduced to 0 to 30 nM.

Figure 3.15 shows the A625/A520 absorbance ratios for the top nine candidate aptamers with a concentration range of Clec9A from 2.5 to 30 nM. These candidates were chosen as they would be tested using CD spectroscopy later. Furthermore, due to consumable limitations, these were the only sequences that could be screened in duplicate. These nine sequences exhibited high RPM values and therefore, may exhibit target binding characteristics. Importantly, OM5C6 (non-specific meth aptamer) and no aptamer are included as negative

controls. The results show variability in the A625/A520 absorbance ratios across all aptamers and dilutions.

The non-specific control (OM5C6) exhibited little difference in absorbance ratio compared to the candidate aptamers BP02, BP03, BP04, BP05, BP06, BP07, and BP08. These candidates, including OM5C6, have A625/A520 values above one, and there is a concentration dependant increase at higher concentrations of Clec9A, indicative of greater aggregation occurring. Furthermore, the no aptamer control exhibits the least concentration-dependant change in aggregation at each concentration when compared to the lowest concentration of Clec9A. Since aggregation is present in all wells for the no-aptamer control, there will be minimal differences in aggregation (A625/A520) between wells which is observed for this condition in Figure 3.15. The presence of large error bars in all conditions demonstrate the variability and inconsistency of this data.

The fact that the non-specific control aptamer (OM5C6) exhibits A625/A520 absorbance ratios similar to the candidate aptamers implies that the candidate aptamers do not display measurable specificity towards Clec9A. However, due to the inconsistency observed within the controls, it may also be inferred that the aggregation observed could be occurring due to an interaction between Clec9A and the AuNP, resulting in the destabilisation, and thus aggregation, of the AuNP in all conditions. Due to the variability observed with these results, no conclusions can be drawn regarding NaCl-induced aggregation caused by aptamer and target interactions.

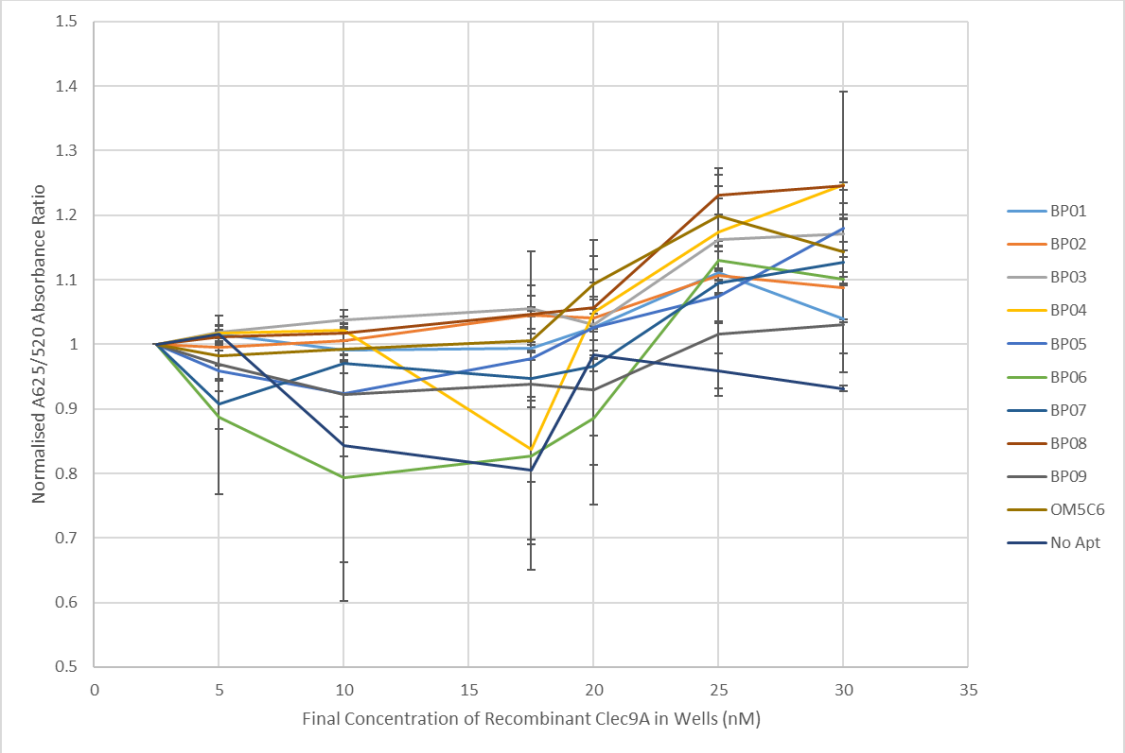

Figure 3.15: NaCl induced aggregation of AuNP, measured as A625/A520 of aptamer candidates across a concentration range of Clec9A.

The aptamer candidate ID is represented on the right-hand side of the graph where the controls, OM5C6 and no aptamer are light brown and dark blue respectively. The error bars are representative of the standard deviation of two replicates. The normalised A625/A520 ratio is depicted on the Y-axis while the final concentration of Clec9A in the well is presented on the X-axis.

Table 3.3: Visual representation of NaCl induced aggregation of AuNP.

Aggregation is assessed under surface association of different candidate aptamers. The aptamer candidate ID is listed on the left column of the table where the final concentration of Clec9A in each well is described at the top of the table.

Final Concentration of Clec9A Target in Wells (nM)							
	0	2.5	5.0	10.0	17.5	20.0	25.0	30.0
BP01								
BP02	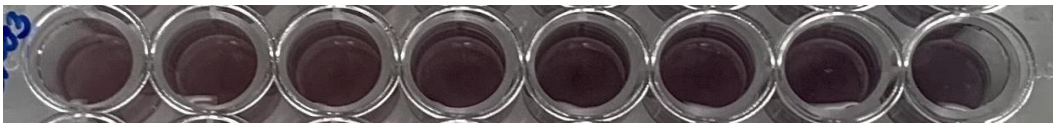							
BP03								
BP04								
BP05	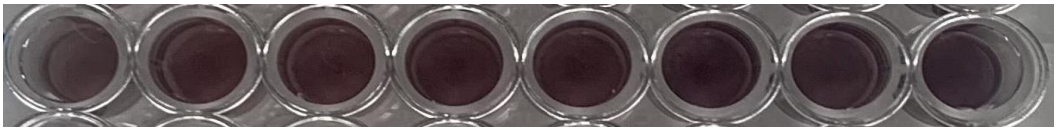							
BP06								
BP07	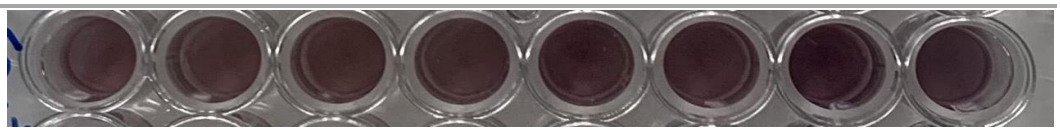							
BP08								
BP09								
OM5C6								
No Apt	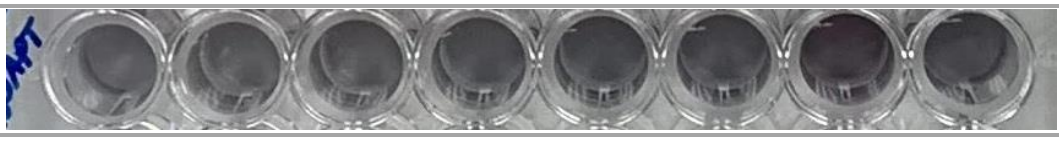							

Section 3.4.2 Investigation of Aptamer and Target Interactions Using CD Spectroscopy

3.4.2.1 Comparison of Top Nine Candidate aptamers with Clec9A and Thrombin Targets

CD spectroscopy was employed as the second characterisation method to investigate the aptamer interactions with Clec9A. This method has the limitation that it relies on the formation of secondary structures. Candidates one to nine were tested with their target molecule Clec9A and a non-specific target molecule, human α thrombin (which is a similar size to Clecc9A).

Given the delivery delays of more recombinant Clec9A protein, the lowest volume cuvette has to be used to enable all nine aptamer candidates to be screened. Thus, the highest concentrations of aptamer and target that could be used and provide a measurable spectrum was 1 µM of aptamer and 1 µM Clec9A or human α thrombin.

Figure 3.16 shows the spectral data of the nine aptamers, which are measured in ellipticity across a spectrum of wavelengths from 200 to 320 nm, in the presence (orange) and absence (blue) of Clec9A (left) or human α thrombin.

All candidate aptamers present spectral data characteristic of B form DNA. This is the most common structure of helical DNA and reflects the DNA conformation identified by Watson and Crick (Bansal, 2003). The helix is right-handed and more elongated with a wide major groove that provides access for the binding of proteins (Kypr et al., 2009). This helical structure is characterised in CD spectroscopy data by a broad positive band at 280 nm and a broad negative band at 245 nm (Kypr et al., 2009).

Changes in ellipticity between the aptamer candidate with Clec9A, compared to the aptamer alone, is used to measure conformational change and the strength of a binding event. This would be further supported by no changes in ellipticity between the aptamer candidate with human α thrombin, compared to the aptamer alone. If both proteins (Clec9A and human α thrombin) produced changes in ellipticity when combined with an aptamer candidate, compared to aptamer alone, but that the spectral data was different between the aptamer candidate binding Clec9A and human α thrombin, the result would be inconclusive.

A significant separation in the spectral peaks with and without Clec9A was observed for candidates BP01 (Figure 3.16A), BP04 (Figure 3.16D), BP05 (Figure 3.16E), BP06 (Figure 3.16F), and BP07 (Figure 3.16G). This was noted as a separation at the negative 245 nm peak. Candidate BP01 (Figure 3.16A) and BP04 (Figure 3.16D) showed a shallower, more positive

spectra at 245 nm in the absence of Clec9A, and a deeper, more negative spectra at 245 nm with Clec9A. Candidates BP05 (Figure 3.16E), BP06 (Figure 3.16F) and BP07 (Figure 3.16G) all share a similar trend of a large separation at 245 nm, a more defined spectra in the presence of Clec9A and an attenuated spectra in its absence. All other aptamer candidates BP02 (Figure 3.16B), BP03 (Figure 3.16C), BP08 (Figure 3.16H) and BP09 (Figure 3.16I) showed a close relationship between the spectra with and without Clec9A, where some separation was observed around 220 nm for candidates BP03 (Figure 3.16C), and BP08 (Figure 3.16H). This can be attributed to noise generated from measuring at low concentrations with a small cuvette pathlength. The differences observed in the spectra with Clec9A and without for candidates BP01, BP04, BP05, BP06, and BP07 may be related to a specific interaction with their target molecule.

The CD spectroscopy spectral data for all aptamer candidates with and without Clec9A were also compared to that of a non-specific target, human α thrombin. Furthermore, to confirm the presence of target specific binding of candidates BP01, BP04, BP05, BP06, BP07, a non-specific target comparison was essential. As observed for Clec9A, all candidates exhibited a B form characteristic peak at 280 and 245 nm. The aptamer BP04 (Figure 3.16D), with and without thrombin, found a large distance between the spectra at around 245 nm, where the ellipticity values with thrombin become positive. This implies that the differences observed with BP04, in the presence of Clec9A, is unlikely to be a target specific interaction. The spectral data with and without thrombin for candidates aptamers BP01 (Figure 3.16A), BP05 (Figure 3.16E), BP06 (Figure 3.16F), and BP07 (Figure 3.16G) showed a close relationship and marginal spectral separation around 220 nm for BP05 and BP06. The differences observed between the spectral data for Clec9A and thrombin, suggest that the spectral differences observed with and without Clec9A are related to a specific interaction of the aptamer with Clec9A. Furthermore, as described, candidates BP05 (Figure 3.16E), BP06 (Figure 3.16G) and BP07 (Figure 3.15G) present an attenuated spectra in the absence of Clec9A. This could suggest that Clec9A is stabilising the secondary structure of the aptamer, resulting in a defined spectra.

BP03 (Figure 3.16C) showed similar trends in the spectra with thrombin and without thrombin, suggesting that this candidate does not display affinity to either target. These results were important for gaining confidence that the differences in spectral data for BP05, BP06, and BP07 could indeed be attributed to a target specific interaction.

The aptamers BP02 (Figure 3.16B) and BP08 (Figure 3.16H) and BP09 (Figure 3.16I) had been identified to not exhibit specificity to Clec9A due to minimal differences between the spectra with and without Clec9A. However, the spectral data for thrombin shows a separation of the spectra with and without thrombin around 245 nm. For these candidates, the spectra without thrombin is more attenuated suggesting stabilisation of the aptamers secondary structure in the presence of thrombin. These data suggest that BP02 and BP08 and BP09 may not have an affinity to Clec9A but may instead demonstrate specificity towards thrombin.

Predicted secondary structure of these aptamers were generated using ViennaRNA and are presented in Figure 3.16. The structure contains the predicted positional entropy shown by the colour scale and the colour at each base. Aptamers BP01 BP05, BP06, and BP07 were suggested to present a specific affinity to Clec9A and interestingly have similar predicted secondary structures. BP01 and BP07 are the most structurally similar, consisting of a long-stemmed region and small loop residues throughout the stem. Similarly, BP05 and BP06 also contain a long-stemmed region but a larger loop residue is observed closer to one end. Contrastingly, the sequences that exhibited binding to thrombin, BP02 BP08, share similarities between one another that are different to those that present Clec9A binding while BP09 has a disparate predicted secondary structure to BP02 and BP08. BP02 and BP08 consist of a large loop residue, followed by a stemmed region and a smaller open looped residue. BP09 has more loop residues within the stemmed region and a larger loop towards the end. Similarly, it displays the same opened loop residue at one end. These similarities observed within both groups suggest the influence of conserved secondary structures on binding ability.

The results presented suggest that candidate aptamers BP01, BP05, BP06, and BP07 may exhibit an affinity to Clec9A. However, further characterisation methods would need to be performed to confirm these results.

A


Ellipticity (mdeg)
Wavelength (nm)
BP01 No Target
BP01 With Clec9A

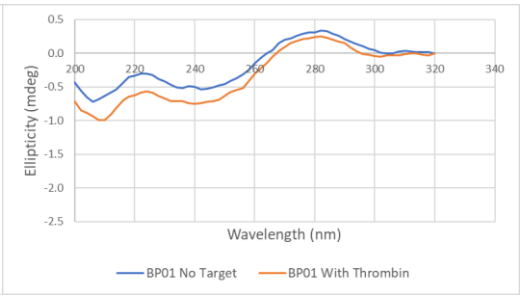
Ellipticity (mdeg)
Wavelength (nm)
BP01 No Target
BP01 With Thrombin

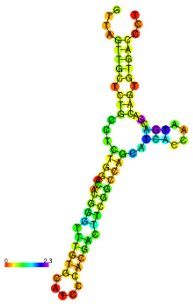

B

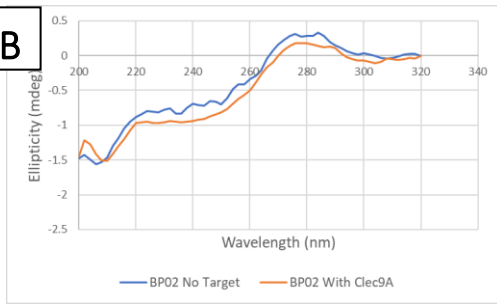
Ellipticity (mdeg)
Wavelength (nm)
BP02 No Target
BP02 With Clec9A

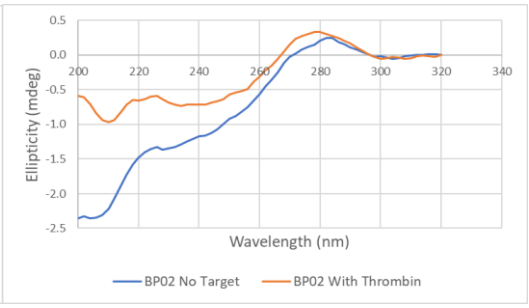
Ellipticity (mdeg)
Wavelength (nm)
BP02 No Target
BP02 With Thrombin

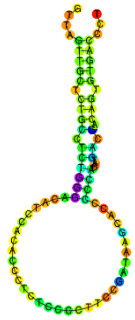

C

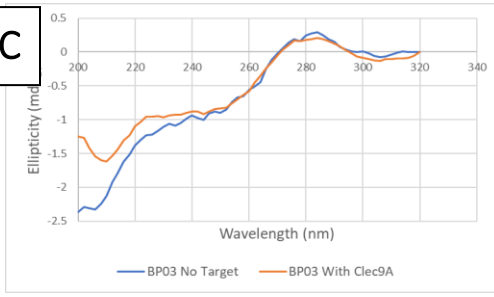
Wavelength (nm)
BP03 No Target
BP03 With Clec9A

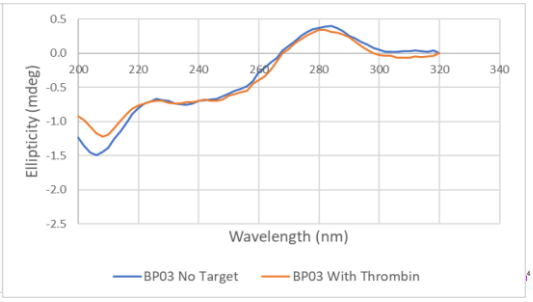
Ellipticity (mdeg)
Wavelength (nm)
BP03 No Target
BP03 With Thrombin

D

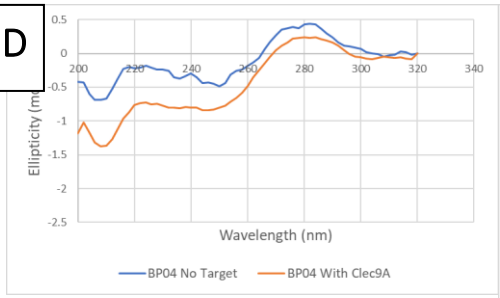
Wavelength (nm)
BP04 No Target
BP04 With Clec9A

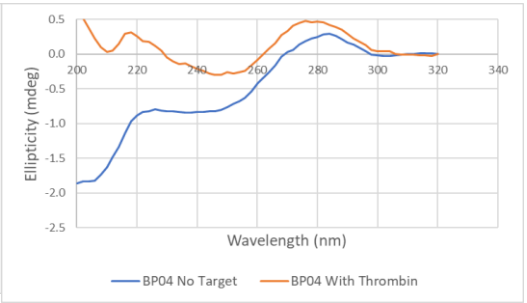
Ellipticity (mdeg)
Wavelength (nm)
BP04 No Target
BP04 With Thrombin

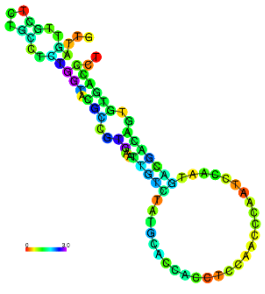

E

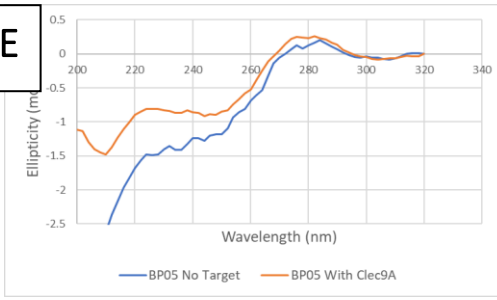
Wavelength (nm)
BP05 No Target
BP05 With Clec9A

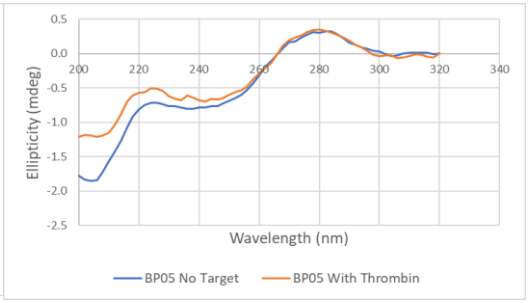
Ellipticity (mdeg)
Wavelength (nm)
BP05 No Target
BP05 With Thrombin

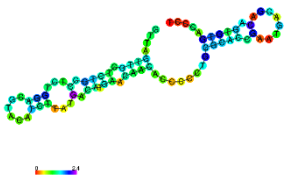

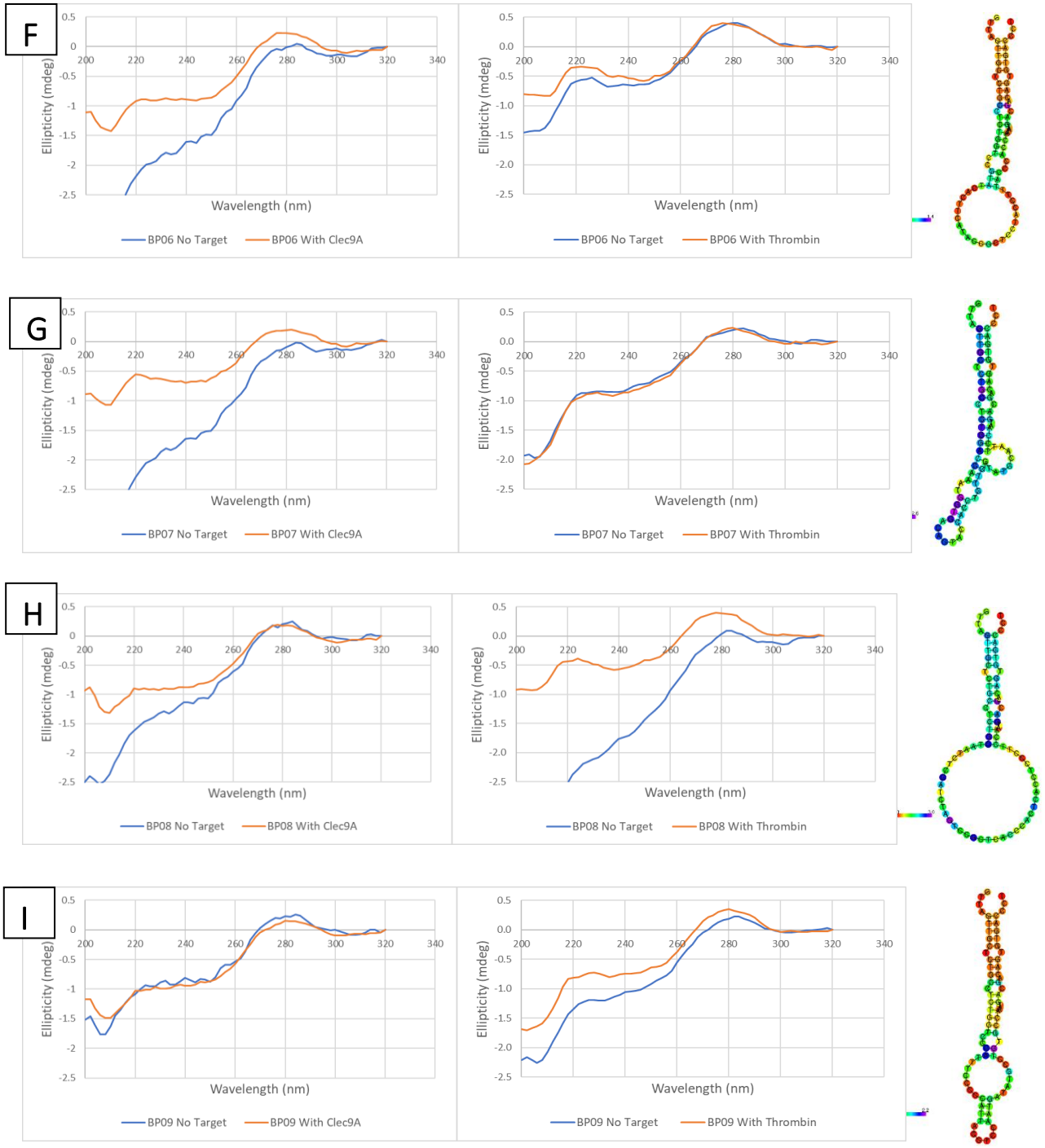

Figure 3.16 A-I: CD spectroscopy data of top 9 candidate aptamers.

Spectral data illustrates the differential ellipticity, measured in mdeg of the interaction of aptamers with Clec9A (left figure) and thrombin (right figure), across a spectrum of wavelengths from 200 to 320 nm. Computational prediction of secondary structure for each candidate is presented on the right.

CHAPTER 4: DISCUSSION

Section 4.1. General Discussion

This study was a proof of concept study, utilising aptamer technology to create aptamers towards Clec9A. Success of developing a Clec9A aptamer could have downstream applications within the field of immunotherapy. The use of an aptamer specific to molecules associated with immune cross-presentation such as Clec9A could target and direct an immune response through specific delivery of peptides, adjuvants, or immunotherapeutic drugs.

This study employed a hybrid SELEX approach to generate aptamers towards Clec9A. The hybrid SELEX method was performed by first enriching the oligonucleotide library towards recombinant Clec9A, followed by further enrichment towards primary cells expressing Clec9A on their surface.

To perform the Cell-SELEX component, an immortalised DC line was initially identified for use as the positive cell target. The DC2114 cell line was selected due to its published characteristics of a $CD8^+$ cDC1 subset expressing Clec9A (Dunand-Sauthier et al., 2014; Dunand-Sauthier et al., 2011; Fuertes Marraco et al., 2012; Seguín-Estévez et al., 2014). Herein, my data initially supported the selection of the DC2114 cell line due, to its expression of *Clec9a* mRNA. However, flow cytometry analyses found negligible levels of Clec9A protein receptor expressed on its surface. This was an unexpected and intriguing result as it suggested that DC2114 cell morphology had been affected through their subculture, despite using identical conditions used to originally characterise this cell line (Fuertes Marraco et al., 2012).

Following completion of the hybrid SELEX experiments herein, four oligonucleotide libraries, including the N40 starting library for comparison, were sequenced using Illumina NGS. Bioinformatic analyses found 18 candidate aptamers conserved within the Protein SELEX Round 7, and Protein- and Cell-SELEX Round 9 libraries. Due to several delayed reagents caused by the ongoing COVID-19 pandemic, only the top nine candidates were able to be characterised using both a modified AuNP assay and CD spectroscopy. Results for measuring the interactions between candidate aptamers and Clec9A using the AuNP assay were inconclusive as Clec9A was thought to be directly interacting with the AuNPs, thus altering their ability to aggregate in the presence of salt. However, CD spectroscopy results suggested a possible specific interaction of the candidate aptamers BP01, BP05, BP06, and BP07 with Clec9A. The

discrepancies observed between the characterisation methods may relate to the suitability of the characterisation method, and the design of the hybrid SELEX method to generate aptamers with specific characteristics (e.g. structure switching attributes).

These results contribute to the body of knowledge surrounding aptamer-based immunotherapy and the progression of aptamer science. One of the most significant factors hindering the progression of aptamer science is the efficacy of characterisation strategies used to produce reliable and true results. In the years since the discovery of aptamer technology, there have been many reports on aptamers, previously illustrated as gold standard, not functioning as published (Daems et al., 2021). This may be attributed to the characterisation method. The lack of standardised methods for identifying aptamer and ligand interactions ultimately stunts the advancement of aptamer technology and damages their reputation as robust agents of biosensing. This chapter will address the findings of this study in addition to limitations and potential future directions.

Section 4.2 Characterisation of DC2114 cells

4.2.1 qPCR for Clec9a *Genetic Expression in DC2114 Cells*

In this study, the mRNA expression levels of *Clec9a* in DC2114 cells and the influence on its expression across six passages was assessed using qPCR. The third biological replicate presented the greatest differences in expression of *Clec9a* across passage number where there was an upregulation of *Clec9a* expression at Passages 4 and 5, when compared to Passage 1. Overall, the results exhibited large variability between replicates and therefore, these differences in expression cannot be linked with any certainty to passage number. The expectation was that increasing the number of passages would influence the phenotype, and thus expression levels of genes, within cells. The difference in expression levels may be attributed to freeze/thawing where initial levels of expression were not reflective of genetic expression in cells during repeated sub-culturing. Lower levels of expression have been observed in cells post thaw, compared to fresh (Karimi-Busheri et al., 2013). Though, it is likely that variability observed with these results is associated with the experimental design, all biological replicates originated from different frozen cryovials, of which their original passage number was unknown. This immediately creates variability between replicates relating to differences in freeze/thaw conditions, different passage techniques and variation of complete medium recipes, on top of general batch-to-batch variability. Reasons for differences between

replicates by cause of passage, cell age and culture number would not be known. A more robust and scientifically accurate experiment would involve the comparison of samples that were treated from the original Passage 1 under the same conditions. Splitting a cryovial three ways after thawing would achieve this. Of course, there is still the chance that due to the unknown starting passage number, these cells may have already exceeded their 'safe' number of passages, after which and the cell line loses key genetic functions, thus no longer exhibiting phenotypic and genetic identity to its primary counterpart (Hughes et al., 2007). In which case, performing experiments with these cells will produce unrepresentative results.

4.2.2 Flow Cytometry for the Identification of Clec9A Cell Surface Expression

The results from this study found only negligible, if any, Clec9A on the surface of DC2114 cells. The expression profile of Clec9A on DC2114 cells was most like the negative control cells, JAWS II. The use of DC2114 cells was determine not to be suitable for their intended use in hybrid SELEX. Immortalised cell lines are sometimes thought to have infinite subculturing properties, but each cell line retains a finite number of divisions before it loses key genetic functions. Cell lines can also be contaminated with fast proliferators that outcompete others, eventually creating a cell line that no longer provides its original function. This risk is exacerbated by poor record-keeping and tracking. For example, 2004 study found HeLa cell lines were negligently contaminated into a range of cell lines and out-competed the original line (Masters, 2004).

The inconsistencies observed in both qPCR and flow cytometry experiments may in part be attributed over subculturing influencing the expression characteristics of Clec9A on the surface. It is clear that the DC2114 cells express *Clec9a* mRNA from gene expression experiments. However, over subculturing may have affected protein processing and folding mechanisms so the receptor is no longer efficiently presented onto its plasma membrane. Studies have identified a similar effect with passage and culture conditions on the functional expression of the Caco-2 cell line (Chantret et al., 1994; Sambuy et al., 2005). Cell lines should be routinely authenticated to ensure the cell line still harbours the same characteristics as originally established. Furthermore, the use of passports could aid in the verification of cell lines, where history and authenticity are documented (Drexler et al., 2003). Additionally, issues identified with donated cell lines can be overcome when the cells are acquired from a repository instead as cells are routinely authenticated and documented. Furthermore,

licensing agreements, maintenance and shipping is all centralised and mediated from a repository.

Section 4.3 Hybrid SELEX Methodology

The beginning of any SELEX experiment should contain a greater proportion of oligonucleotides that do not have specific affinity to the target molecule. This is because the starting library is expected to consist of all possible sequence combinations. As SELEX progresses, this proportion decreases as the pool becomes enriched with sequences specific to the target molecule (Djordjevic, 2007). Steps to reduce 'noise' created by non-specific binders within oligonucleotide pools include negative SELEX. This section will discuss whether the hybrid SELEX design with negative selection steps resulted in the enrichment of oligonucleotide pools specific to Clec9A.

4.3.1 Efficacy of Hybrid SELEX to enrich the library for Target-Specific Aptamers

The qPCR amplification plots for each SELEX round showed that the Protein-SELEX Round 1 library demonstrated higher Cq values for positive selection than negative selection. As this is inversely related to amplicon concentration, these results indicated that there was a greater proportion of oligonucleotides present in the negative selection round. Since negative SELEX was employed at the beginning of each SELEX cycle, the large proportion of oligonucleotides exhibited in the negative selection pool indicated that negative SELEX was effective in removing non-specific binders from the pool thereby minimising 'noise' and allowing the opportunity for specific binders to interact with the target. However, there is a possibility that performing negative SELEX at the beginning of every round from Round 1 may have removed sequences that actually did have specificity to the target (Lyu et al., 2016). Since the starting library has the maximum diversity, it is theorised that there is only a small number of copies of each sequence and that high affinity target binders are already present in the starting population (Djordjevic, 2007). Therefore, removing at the onset, or before, library mutation compromises the ability for the library to highly evolve towards the target. The sequences that had been removed in negative selection were removed due to their interaction with the selection matrix through non-specific electrostatic absorption or a specific interaction using Van der Waals or hydrogen bonding. In either case, if these sequences had been allowed to persist in the population for longer, they may have the opportunity to evolve, thus retaining target binding and losing matrix binding.

As SELEX progressed, the concentration of oligonucleotides increased after positive selection and decreased after negative selection. This marked a sufficient enrichment of the positive SELEX pool with sequences that should have specificity for Clec9A, as fewer were being retained through negative SELEX. It is suggested that adequate pool enrichment is met when the number of oligonucleotides is maintained at a constant concentration between rounds (Kolm et al., 2020). This was observed between Protein SELEX Rounds 7 and 8. Unexpectedly, the Cell-SELEX retained a greater proportion of oligonucleotides in the positive SELEX round in Round 8, compared to the concentrations of oligonucleotides in the Protein-SELEX rounds. The increased proportion of oligonucleotides found in the positive pool of Cell-SELEX is likely attributed to inadequate negative SELEX methods to screen and remove non-specific oligonucleotides from the pool, coupled with an increase in potential binding sites from other receptors.

4.3.2 Efficacy of Hybrid SELEX analysed by Next-Generation Sequencing Data

Bioinformatic analyses support the conclusions suggested above. There was a general increase in the number of unique sequences in the Protein- and Cell-SELEX Round 9 libraries, compared to the Protein-SELEX Round 7 library. However, it is reasoned that as enrichment towards the target molecule occurs, the sequence diversity should decrease as the pool evolves to contain specific sequences (Beier et al., 2014). Further bioinformatic results for the Protein-SELEX Round 9 library suggests that enrichment has occurred from Protein-SELEX Round 7, due to the increased RPM of most conserved sequences. These results may be linked to two phenomena.

Firstly, the implementation of mutational PCR should have evolved sequences throughout Rounds 7 to 9, resulting in more sequences with enhanced binding to the target molecule. This creates a final pool with greater sequence diversity and enrichment. Error-prone (mutagenic) PCR has been suggested to improve binding properties by approximately 1-10% (Bittker et al., 2002).

Secondly, the optimal rounds of Protein-SELEX have been exhausted at Round nine, which is leading to an increase in mis-amplification and selective enrichment due to PCR bias. As established with qPCR results, a near-identical concentration of oligonucleotide product was present within the libraries from Protein-SELEX Rounds 7 and 8. Since only three rounds are suggested to be sufficient in identifying high-affinity binders, exceeding the number of optimal

rounds could be detrimental to the pool representation (Kohlberger & Gadermaier, 2021). It may be that both phenomena are occurring concurrently since it is difficult to assess biased amplification of libraries with large heterogenicity and since mutational PCR makes the library even more heterogenic.

In line with the qPCR results, bioinformatic data for Cell-SELEX suggested minimal enrichment of conserved sequences from Protein-SELEX Round 7, and greater sequence complexity within the pool. Interestingly, there was a greater proportion of conserved oligonucleotides between Protein-SELEX Round 7 and Cell-SELEX Round 9 libraries, than for libraries at Protein-SELEX Rounds 7 and 9. Unfortunately, it is not likely that this was resultant from target specificity and these results are more likely a repercussion of inadequate Cell-SELEX design.

The major outcome of Objective One was that the majority of DC2114 cells did not express the Clec9A receptor on their surface. Therefore, the use of primary cells (splenocytes) expressing Clec9A was required and the non-expressing counterparts, $CD8^{-ve}$ DCs, were used for negative selection. The use of non-isogenic cells for negative selection likely impaired the efficacy of Cell-SELEX. Specifically, negative SELEX was inadequate in separating non-specific binders from specific ones in the positive selection pool. An effective negative control cell would harbour all the surface molecules present on the positive cell, aside from the molecule of interest (Takahashi et al., 2016). Heterogeneity in cell morphology means that there were different surface receptors present in the positive cell that the oligonucleotides have not been subjugated to in the negative SELEX round. This would result in the carryover of non-specific sequences from the positive pool. For example, lineage and characteristic markers that were used to specifically obtain Clec9A $CD8^{+ve}$ DCs such as XCR1 and CD11c. To overcome this, surface receptors could be depleted using microRNA mediated silencing. This would result in an isogenic pair of cells that can be used in negative and positive selection, creating a more specific and enriched oligonucleotide pool (Takahashi et al., 2016).

Furthermore, the result obtained from the Cell-SELEX experiments may be related to the presence of density-dependent cooperative binding. Since the cell surface has a wealth of interacting receptors, sequences can be non-specifically retained due to co-localised binding if the interaction of the oligonucleotide with another receptor does not result in unfavourable entropy loss. This results in the retention of unwanted oligonucleotides that exhibit low target affinity (Ozer et al., 2013). Uptake of non-specific sequences is also observed in the presence

of dead cells that may be present in the population due to intensive treatment such as FACS (Kaur, 2018). Hybrid SELEX has great potential for the isolation of highly specific aptamers with the ability to operate in complex physiological conditions. Appropriate negative and counter selection tools, along with the deliberate monitoring of SELEX progression is required in order for this to be successful.

Section 4.4 Characterisation of Candidate Aptamers Using AuNP Assay and CD Spectroscopy

4.4.1 Applicability of Modified AuNP Assay

The final element of this study involved the characterisation of candidate oligonucleotides identified using bioinformatics analyses of NGS data using two characterisation techniques, the AuNP assay and CD spectroscopy. Success has been demonstrated in the Pitman group with the AuNP assay for aptamer and methamphetamine interactions, while CD spectroscopy has routinely been implemented to investigate binding interactions of aptamers (Prante et al., 2019; Schilling-Loeffler et al., 2021). In total, 18 aptamer candidates were chosen. However, due to limitations in reagent availability, only nine were able to be investigated with both methods.

Aggregation of AuNP was observed in the AuNP assay after the addition of the Clec9A protein but before the addition of NaCl. This suggested that Clec9A interfered with the adsorption of the protective aptamers on the surface of the AuNP, instead adsorbing to the surface of the AuNP itself and contributing to the destabilisation of the AuNP. This inference was observed in a concentration-dependent manner, where higher concentrations of Clec9A contributed to a greater intensity of aggregation. Using lower concentrations of Clec9A to reduce its impact of AuNP aggregation still resulted in variability of results, suggesting that Clec9A was still interfering with the assay. Thus, any colour change observed was not indicative of target binding, making this an inappropriate method to determine aptamer and Clec9A interactions, and most likely an interaction using proteins as the target molecule. One study found that target molecules that contain amines or other metal-binding groups such as kanamycin or melamine were strongly bound to the AuNPs and inhibited accurate detection of aptamer binding events (Zhang & Liu, 2021). Furthermore, surface modification of AuNP such as citrate capping as described in our method can increase the AuNPs attraction to molecules such as proteins that have oppositely charged functional groups (Wang et al., 2015a).

4.4.2 CD Spectroscopy

CD spectroscopy was employed as a second method to investigate potential binding events for the top nine aptamer candidates. Differential shifts in ellipticity between aptamer alone and aptamer with Clec9A suggested specific binding interactions for aptamers BP01, BP05, BP06 and BP07. This was indicated by a shift in the spectra of the aptamer with Clec9A to form stronger peaks associated with B form DNA suggesting a greater stabilisation of the aptamer secondary structure. However, if this was the case, the same no target spectra should be observed in the thrombin controls, which it was not. These differences observed are likely attributed to different day processing. All aptamer candidates were screened on one day with Clec9A, while they were screened with thrombin on a different day. This introduces variability to the experimental design as aptamer preparations will be different, resulting in observed differences in the results and thus inconsistent/unrepresentative conclusions. Retrospectively, all aptamers should have been prepared for both targets at the same time and then screened one after the other on the same day.

Aptamer candidates BP05, BP06 and BP07 exhibit similar spectral trends and exhibit high RPM values for protein SELEX libraries. Interestingly, the candidates belong to different clusters within each library suggesting that sequential motifs are not responsible for the efficiency of target binding. Aptamer candidates BP05, BP06 and BP07 exhibit similar secondary structure predictions obtained by ViennaRNA. Aptamers BP05 and BP06 consist of a long-stemmed region with a loop towards one end, whereas aptamers BP07 consists of a long stem and a smaller loop at one end. Thus, although harbouring differences in the primary sequence, the conservation of a similar secondary structure motif across presumed target binders may be a characteristic attributed to their ability to bind Clec9A. The ViennaRNA structure predictions and the similarity of the secondary structures of these sequences could explain why CD spectral data was so similar between the four. It is likely that the predicted structures were conserved as they facilitate stabilisation of the aptamer around the target. Published analyses of structural conservation identified efficient cell internalising aptamers that would have otherwise been overlooked when performing traditional abundance-based informatics (Thiel et al., 2012).

Aptamer BP01 was a sequence identified in the bioinformatic results to possibly be an artefact of PCR bias as it was present at high RPM values within each library and has very similar RPM

values between Protein-SELEX Round 7 and Cell-SELEX Round 9 (1897.78 and 1893.39 respectively). This sequence was chosen since it was thought to be preferentially amplified but not harbour specificity towards the target molecule. Interestingly, it appears to display binding properties towards Clec9A in solution. However, for BP01 the trends in the spectra where the peaks are split do resemble the spectra obtained with thrombin. Therefore, this observation may be a result of artefacts of the experiment rather than an evident binding event occurring. If the experiment was performed again with available reagents and no spectral shift was observed, it could be concluded that this sequence was present in the population due to PCR bias. Thus, highlighting a limitation of SELEX where evasion of these sequences is not possible and so selecting a broad range of sequences that have different bioinformatic characteristics in addition to structural motifs are important to identify specific binders (Kohlberger & Gadermaier, 2021; Thiel et al., 2012).

When comparing both spectra, some sequences were suggested to exhibit binding towards the non-specific target of thrombin, namely BP02, BP04 and possibly BP08. This could be linked to the erroneous negative screening conditions that were not effective at limiting background noise attributed to conservation of non-specific oligonucleotides where efficacy is unknown and it is not possible to specifically separate binders from non-binders if they are within the same positive selection pool (Djordjevic, 2007). Therefore, weaknesses in selection strategies result in a greater proportion of 'noise' within positive selection pools resulting in a disproportional representation of an enriched pool. Likewise, although the likelihood of selecting non-specific binders is low (around 10^{-3}), imperfections in design will increase this likelihood. This phenomenon may be observed with the sequences that present possible binding to thrombin. If there were similarities between the amino acid sequence of proteins, this could explain the ability for these sequences to bind thrombin. Furthermore, this would highlight the importance of a counter selection step to remove sequences that could bind similarly structured molecules. However, a sequence alignment was performed that showed no similarity between amino acid sequences (Appendix 5), and thereby this observed binding is likely due to non-specificity.

Section 4.5 Limitations

4.5.1 Differences Between Target Molecules

This study utilised the strengths of both Protein-SELEX and Cell-SELEX to isolate aptamers that retained specificity towards Clec9A under physiological conditions. A major limitation of this study was the presentation of the target molecule under each condition. The differences between a recombinant protein and a surface-expressed protein may be too extreme to be representative of one another resulting in non-specificity (Kerrigan & Brown, 2010). In Protein-SELEX, the intracellular, transmembrane, and extracellular domain of the Clec9A protein are exposed. This selection strategy could result in the enrichment of an oligonucleotide pool that exhibits specificity towards an inaccessible region of the protein under *in-vivo* conditions. Furthermore, an enriched library towards Clec9A protein may not be able to bind the cell surface receptor as it may be expressed in a modified state or rely on the co-presentation of other receptors, thus changing its morphology to the recombinant protein (Dua et al., 2011).

The receptor Clec9A on the $CD8^{+ve}$ lineage of cDCs interacts with RNF41 (Tullett et al., 2020). This interaction may change the cell surface expression profiles and folding properties which would not be represented with an isolated recombinant protein. The conservation of these sequences into Cell-SELEX rounds will contribute to increased non-specificity of sequences. Several receptor-specific aptamers have been shown not to have specificity towards their cognate ligand when presented on live cells (Chen et al., 2016). Their inability to bind is likely related to differences between the presentation of the target molecule in recombinant and cell surface form. To overcome these differences between the recombinant protein and the protein expressed on the cell, oligonucleotides could be incubated with a peptide of the target molecule that are involved with binding. For Clec9A, this is known because antibodies towards it have been established prior. Successful SELEX experiments have involved the selection of aptamers to small peptides such as brain natriuretic peptide and neuropeptide Y (Mendonsa & Bowser, 2005; Wang et al., 2015b).

4.5.2 Bioinformatics Analyses

Bioinformatic approaches to aptamer technology have provided efficient processing of a wealth of information and thus, based on sufficient pipelines, provide representative information of each library. Analysing high throughput sequencing data provides information on sequence enrichment and general trends relating to abundance. As established, the risk

with assessing sequences with relation to abundance is the inclusion of non-specific sequences that are prevalent in a population due to amplification bias. Furthermore, as shown with CD spectroscopy data, sequences that were suggested to exhibit binding shared predicted secondary structure similarities. Studies have identified that specific secondary structures such as stem-loops can enhance the binding of aptamers to their target (Carothers et al., 2004; Carothers et al., 2006). This suggests that screening for candidates based on structural motifs may provide more detailed information relating to target binding rather than abundance-based information.

To generate a complete profile of an oligonucleotide library, it could be appropriate to employ several bioinformatics approaches, such as investigating the patterning of libraries and primary sequence cluster analyses (Kinghorn et al., 2017) in addition to abundance-based informatics. Apta Trace is a structural motif clustering-based tool that confers SFOLD secondary structure prediction software to a library, where each sequence is clustered and ranked within families that harbour the same secondary structure characteristics and these structures are ranked based on enrichment (Dao et al., 2016). This would be a useful tool to employ in the future.

4.5.3 Characterisation Methods to Reflect the Target Molecule

The non-specific binding to thrombin addresses the necessity for effective characterisation techniques that can be standardised across a range of different target molecules. A wealth of research has been placed on investigating ways to improve current detection strategies, yet there is a lack of effective methods to demonstrate the success of other aptamers. Based on the interaction of Clec9A to the surface of the AuNP, it is unlikely that this method would be effective in determining aptamer and target interactions for this or other proteins. There was variability in the efficacy and sensitivity of the AuNP assay, and batch to batch variations in the AuNP synthesis may alter their sensitivity to NaCl-induced aggregation. This leads to irreproducible results if all factors are not optimised. Furthermore, the assay relies on complete dissociation of aptamers to bind the target and thus a conformational change is required. Since these candidate aptamers were not selected based on their ability to undergo a structural change, this may result in some sequences being retained on the AuNP while others dissociate. This incomplete desorption of the aptamers from the AuNP will lead to weak assay performance and inconsistent results (Thevendran & Citartan, 2022). A more reflective method should be used to investigate binding interactions.

A multifaceted approach should be employed to investigate aptamer and ligand interactions relevant to their end-use. This aids in strengthening the identification of a true binding event if data obtained by different methods provides the same outcome. The success of aptamers within science hinges on their ability to demonstrate function. Without standardised characterisation techniques, characterisation data cannot be adequately compared leading to an over-production of aptamers that do not exhibit binding.

Techniques such as isothermal titration calorimetry (ITC) can be employed to investigate target bindings irrespective of the type of target by measuring the amount of heat exchange generated through a binding event (Plach & Schubert, 2019). ITC is an effective characterisation approach as it provides a binding profile of the aptamer and target interaction in the form of dissociation constants, thermodynamics, and stoichiometry and has investigated the thermodynamic interactions of aptamers with a range of different targets (Amano et al., 2016; Daems et al., 2021; Potty et al., 2009). The employment of three methodologies to obtain a detailed profile of characteristics attributed to an aptamer's molecular interactions has proved successful. The methods of ITC, followed by CD spectroscopy, and finally, aptamer linked immobilised sorbent assay (ALISA) or enzyme-linked immunosorbent assay (ELONA) identified aptamers specific to a histone-like protein (HupB) in Mycobacterium tuberculosis (Kalra et al., 2018). For the characterisation of Clec9A binding aptamers, the characterisation methods used had been pre-established within the Pitman Lab group. The intention was to employ ITC following identification of binders though preliminary methods however, the ITC machine was not functional when required for this work.

Section 4.6 Future Directions

From the findings obtained in this study, it would be interesting to further investigate the candidate aptamers that presented binding. This would involve establishing their ability to bind through CD spectroscopy using higher concentrations and volumes of both Clec9A and aptamer. Since similarities were observed in the predicted secondary structure of the binding aptamers, this structure may be an evolutionary characteristic for target binding. It would be interesting to perform bioinformatic analyses on the aptamer libraries to investigate the conservation of other conserved structural motifs to find better target binders. Sequences with conserved characteristics could be utilised in a 'doped' oligonucleotide library, performing SELEX to enhance target binding and specificity (Hall et al., 2009).

If sequences were found to exhibit binding under CD spectroscopy, other characterisation methods that are physiologically representative could be employed to test binding. This would involve investigating their capacity to interact with the target presented on cells. Techniques such as flow cytometry could be considered for this information. Aptamers could be tagged with a fluorescent label and incubated with target expressing cells. The aptamer and target interaction could then be measured by fluorescence intensity using flow cytometry (Suh et al., 2014; Tang et al., 2007). Following efficient binding to cell surface Clec9A, internalisation studies could be performed to investigate the aptamer's ability to be endocytosed by the receptor. This could be achieved similarly using confocal laser scanning microscopy through labelling or staining with fluorescent probes or tags (Berg et al., 2016; Zhao et al., 2017).

Section 4.7 Concluding Remarks

To conclude, the studies reported herein demonstrate the implementation of a hybrid SELEX method to enrich an oligonucleotide library to contain sequence that bind the dendritic cell surface receptor Clec9A. The hybrid SELEX method consisted of oligonucleotide library incubation with recombinant Clec9A and subsequent selection against cells expressing Clec9A. While the original cell line intended for use in positive selection, DC2114 cells, expressed *Clec9a* mRNA, they were found not to express Clec9A on their surface, which may be related to over subculturing and loss of morphology to the primary line. Real-time PCR and bioinformatics information found that the oligonucleotide library exhibited enrichment towards Clec9A in the Protein SELEX rounds, however the Cell-SELEX component presented minimal enrichment of sequences. This could be related to the differences in presentation of the target molecule between SELEX techniques and overwhelming oligonucleotides with potential binding sites in cell SELEX. Using bioinformatics data, the top nine were able to be characterised using both an AuNP assay and CD spectroscopy. Three potential aptamer candidates (BP05, BP06, and BP07) were identified for binding towards recombinant Clec9A using CD spectroscopy whilst BP01 was thought to be non-specifically interacting with Clec9A due to its persistence within the population resultant of amplification bias. Further characterisation experiments will need to be performed to confirm the specificity of the binding characteristics of these aptamers to Clec9A. Overall, these findings demonstrate the ability to create aptamers towards Clec9A through a modified hybrid SELEX approach. These findings can be taken and applied to future research within this area.

CHAPTER 5: APPENDICIES

Appendix 1: PCR and Gel Electrophoresis Figures for SELEX Rounds

SYBR Green PCR was employed in each round of SELEX to amplify the oligonucleotide sequences retained in the positive SELEX round for the implementation of the amplified oligonucleotides into the following round of SELEX in single-stranded form. These plots are reported below.

A

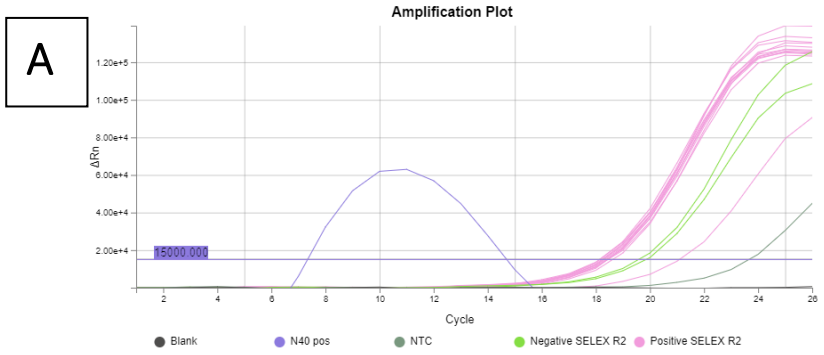

B

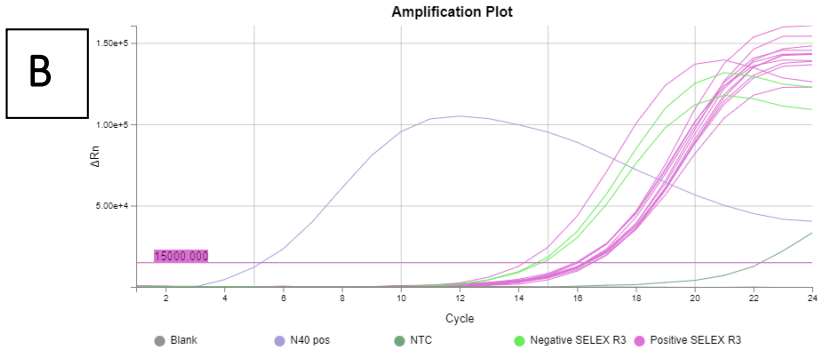

C

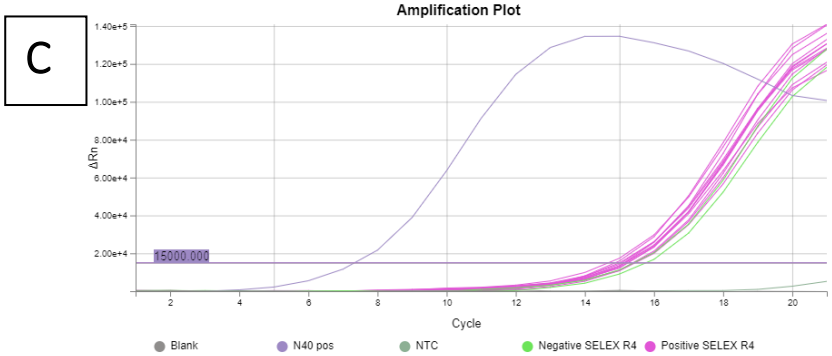

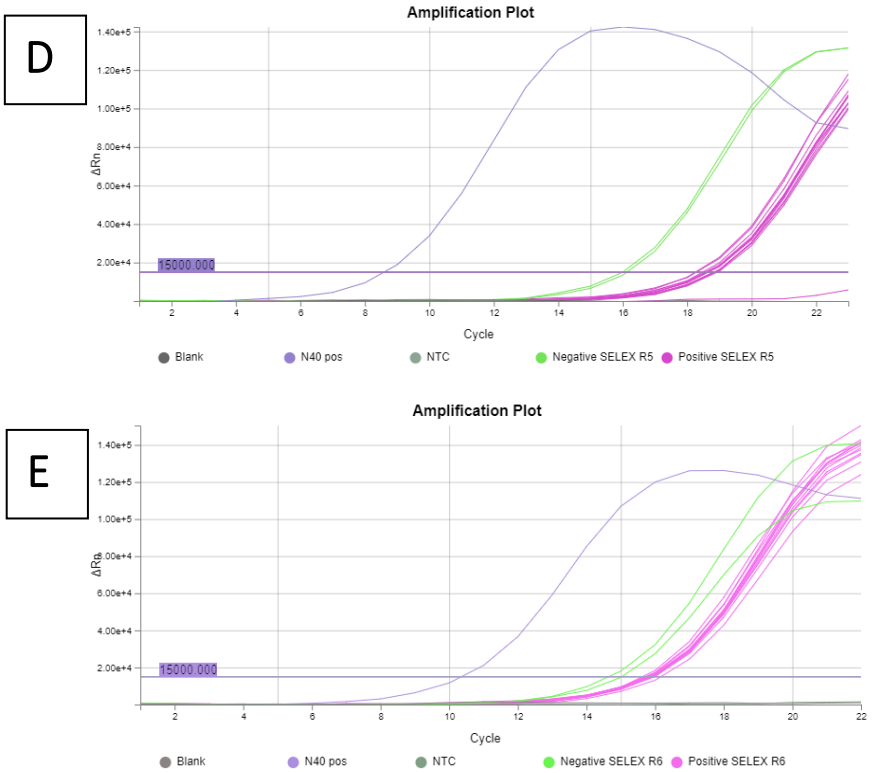

Figure 5.1: Real-Time PCR amplification curve for SELEX experiments

A) SELEX R2 B) SELEX R3 C) SELEX R4 D) SELEX R5 E) SELEX R6. Each amplification plot depicts the amplification of the oligonucleotide library at different stages of enrichment towards the target molecule. All amplification plots are from Protein-SELEX. Purple, green and pink represent the N40 positive control, the negative SELEX condition, and the positive SELEX condition respectively. The horizontal line represents the cycle threshold which is set at halfway up the amplification cure when in the log phase.

Gel electrophoresis was used in each round of SELEX to purify the dsDNA resultant of PCR amplification. The isolation and purification of the dsDNA obtained from these rounds are detailed in Section 2.2.1.13 – 2.2.1.14. Gel electrophoresis images for SELEX rounds 2, 3, 4, 5, and 6 are reported below.

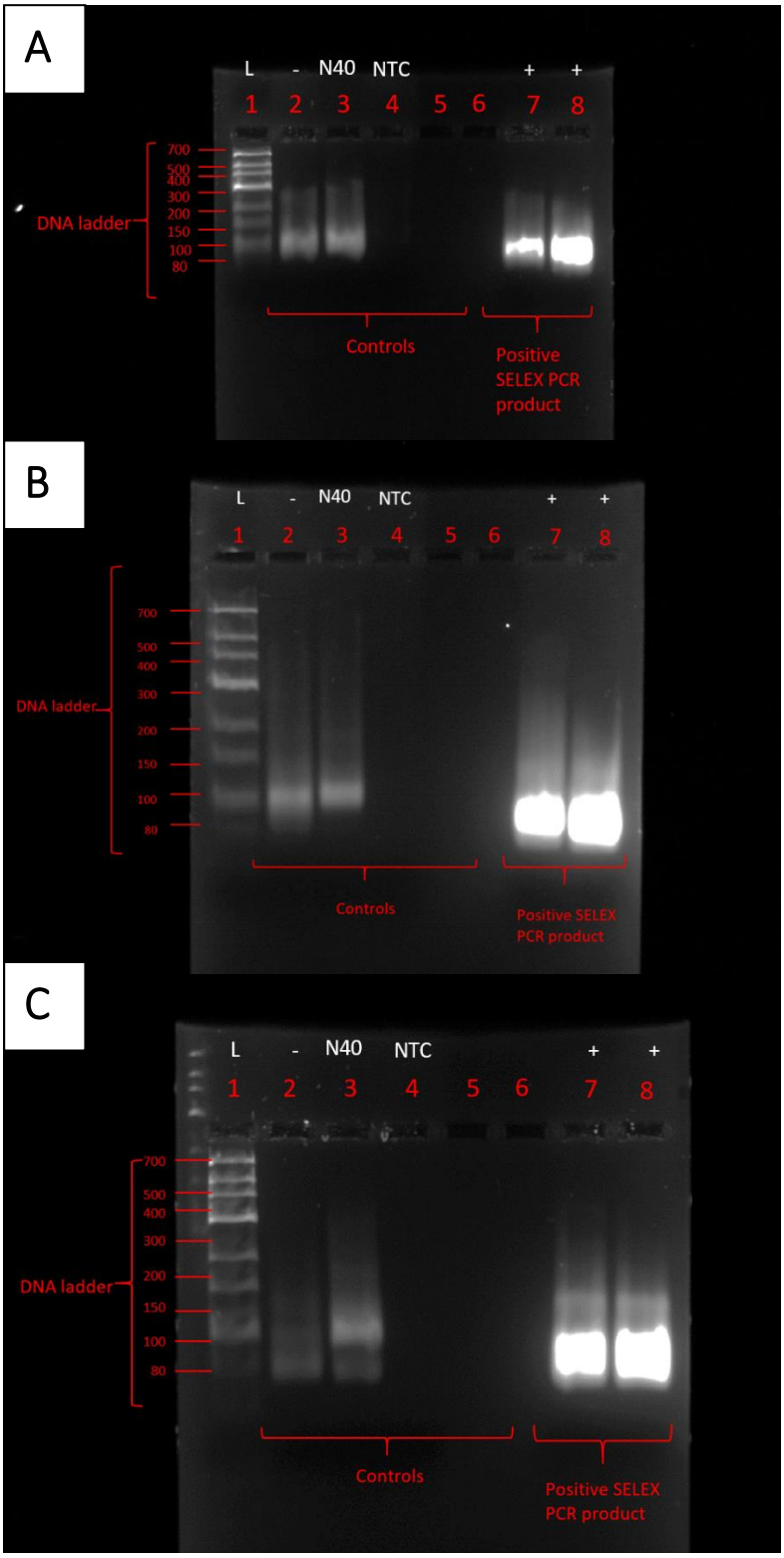

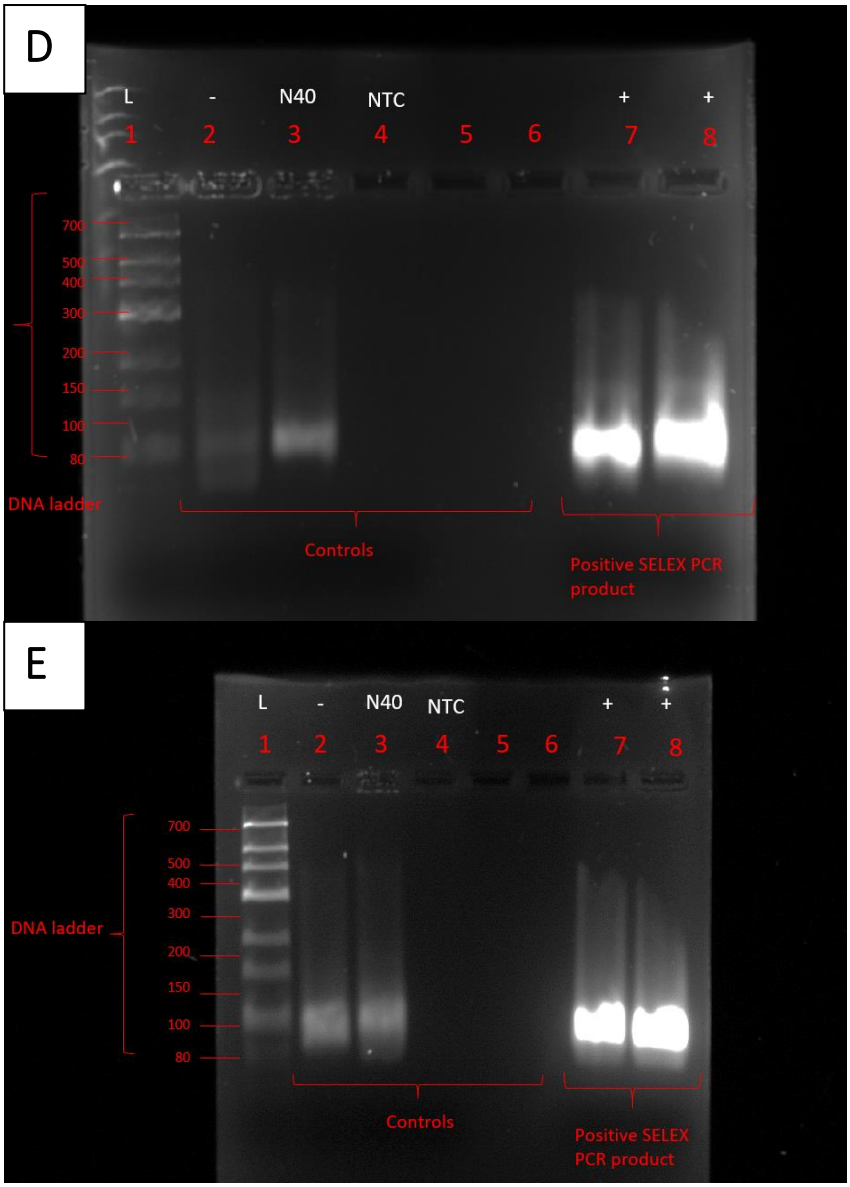

Figure 5.2: Agarose gel electrophoresis images for SELEX experiments.
Gel electrophoresis was used to purify DNA for the following round of SELEX, A) SELEX R2 B) SELEX R3 C) SELEX R4 D) SELEX R5 and E) SELEX R6. Target specific sequences from positive selection were amplified via real-time PCR and ran through an agarose gel to purify the DNA and remove any contaminating and unwanted PCR products. These fluorescent bands labelled on the image as positive PCR products indicate target-specific sequences from the previous SELEX round and were removed using a scalpel and used for the following round of SELEX. Lanes 1-5 are as follows: DNA ladder, negative SELEX PCR product, N40 positive control, and no template control. Lanes 7-8 are the positive SELEX product

R&D SYSTEMS
a bio-techne brand

Recombinant Mouse CLEC9a Fc Chimera

6776-CL-050

Certificate of Analysis

Size: 50 µg
Lot: TNM0320081

Description

Source	Chinese Hamster Ovary cell line, CHO-derived mouse CLEC9a protein

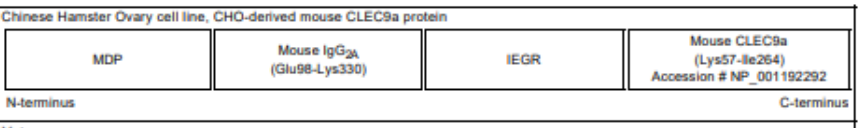

N-terminal Sequence Analysis	Met
Structure / Form	Disulfide-linked homodimer
Predicted Molecular Mass	50.8 kDa (monomer)

Specifications

SDS-PAGE	60-65 kDa, reducing conditions
Activity	Measured by flow cytometry for its ability to bind a ligand expressed in necrotic EL-4 mouse lymphoblast cells. When 100 ng of Recombinant Mouse CLEC9a Fc Chimera is added to 5 x 10^5 EL-4 cells, >50% of necrotic EL-4 cells bind to the protein.
Purity	>95%, by SDS-PAGE under reducing conditions and visualized by silver stain.
Endotoxin Level	<0.10 EU per 1 µg of the protein by the LAL method.
Formulation	Lyophilized from 27.3 µL of a 0.2 µm filtered solution in PBS, pH 7.3.

Preparation and Storage

Reconstitution	Reconstitute at 100 µg/mL in PBS.
Shipping	The product is shipped at ambient temperature. Upon receipt, store it immediately at the temperature recommended below.
Stability & Storage	**Use a manual defrost freezer and avoid repeated freeze-thaw cycles.** • 12 months from date of receipt, -20 to -70 °C as supplied. • 1 month, 2 to 8 °C under sterile conditions after reconstitution. • 3 months, -20 to -70 °C under sterile conditions after reconstitution.
Date Bottled	8/5/2020

It is hereby certified that the above product has been tested for proper performance and function under our established Quality Control testing criteria.
It is authorized by our Quality Assurance program to be released for sale.

Diane R. Wotta, Ph.D.
Sr. Director, Quality and Regulatory Affairs
This C of A was updated on 8/7/2020, Rev. 0.

For research use only
Not for use in humans

Page 1 of 1

bio-techne
Global bio-techne.com info@bio-techne.com techsupport@bio-techne.com TEL +1 612 379 2956
USA TEL 800 343 7475 Canada TEL 855 668 8722 China TEL +86 (21) 52380373
Europe | Middle East | Africa TEL +44 (0)1235 529449

Figure 5.3: Certificate of Analysis for Recombinant Clec9A.
Recombinant Clec9A was purchased from R&D Systems via In Vitro Technologies and was used for all experiments were recombinant Clec9A was described.

Appendix 3: Quantification of Library Concentration for NGS

The concentration of dsDNA was quantified using Qubit 3.0 and the HS Assay Kit and provided as information to GenXPro, Germany when processing for Illumina NGS sequencing.

Table 5.1: Concentrations of libraries for Illumina NGS by GenXpro.

SELEX round and target description	Concentration (ng/µL)	Volume (µL)
N40 (Pre-SELEX)	12.0	19
Protein R7	25.0	19
Protein R9	13.0	19
Cell R9	14.8	19

Appendix 4: Bioinformatic Scripts

The following scripts were used to conduct bioinformatic analyses from Illumina NGS Fastq data.

#Quality control

#FastQC

Provides a quality control for raw high throughput sequence data. Provides a set of analyses such as sequence quality scores, GC content, sequence length distribution, sequence duplication levels, and phred scores. This will provide an immediate impression of any problems within the data.

Command line: fastqc → open file

#Removal of primer sequences

Filters were applied to sequences within the raw data to specifically remove primer sequences from the data to provide efficient processing. The minimum (-m) and maximum (-M) were chosen as 37 and 41 to span the N40 random region and account for any insertions or deletions in the sequences. The minimum overlap of 14 was chosen to find any adaptors within the sequence.

Command line: cutadapt -j 0 -m 37 -M 41 --untrimmed-output N90_RS_output.fastq -a "GTTAGTTGCTCTGCCTCTGG;min_overlap=14;max_error_rate=0.3"..."AATGACGACAGTGTGACCCT;min_overlap=14;max_error_rate=0.3" -o N90_RS.trimmed.fastq N90_RS.fastq

#Frequency counting and conversion of files to FASTA format

Fastaptamer-count was used to determine the number of unique and total sequences within a library and convert FASTq files to supported FASTA format.

Command line: fastaptamer_count -i CR_2BP_trimmed.fastq -o CR_2BP_count.fasta

#Comparing conserved sequences between SELEX library populations

Fastaptamer compare was used to understand sequence conservation between SELEX libraries at different stages of the SELEX process. This would be used as a measure of enrichment. Fastaptamer-compare provided information on reads, reads per million (RPM) and rank.

Command line: fastaptamer_compare -x CR_2BP_count.fasta -y PR_9BP_count.fasta -o compare_CR9vPR9.tsv

#Clustering of sequences based on conserved sequence similarity

Fastaptamer-cluster was used to cluster closely related srquences based on a Levelnshtein edit distance of seven. This provided information on cluster number rank within-cluster, RPM, and reads.

Command line: fastaptamer_cluster_xs -i PR_9BP_count.fasta -o PR_9BP_cluster.fasta -d 7 > PR9_cluster.tsv

D is the Levenshtein edit distance

#Assessing fold enrichment of sequences between libraries

The enrichment of sequences was assessed between Protein-SELEX Round 7, Protein-SELEX Round 9 and Cell-SELEX Round 9.

Command line: fastaptamer_enrich -x PR1_RP_cluster_xs.fasta -y PR_9BP_cluster.fasta -z CR_2BP_cluster.fasta -o PR1_PR9_CR2_enrich.tsv

#ViennaRNA computational secondary structure prediction based on primary sequence

The most probable secondary structure was computationally predicted using ViennaRNA. This also provided a colour scale for per sequence probability

Command line: RNAfold --noconv -p --MEA < 18.seq seq.18

relplot.pl rna.ps dot.ps > 18_rss.ps

MEA is the maximum expected accuracy

Noconv prevents the conversion of ‘T’ bases to ‘U’ bases

Appendix 5: NCBI Blast of Amino Acid Sequences for Thrombin and Clec9A

A sequence alignment was performed to compare similarities between the amino acid sequences of Human Alpha Thrombin and mouse Clec9A. No similarities were observed between the two sequences (Figure 5.4).

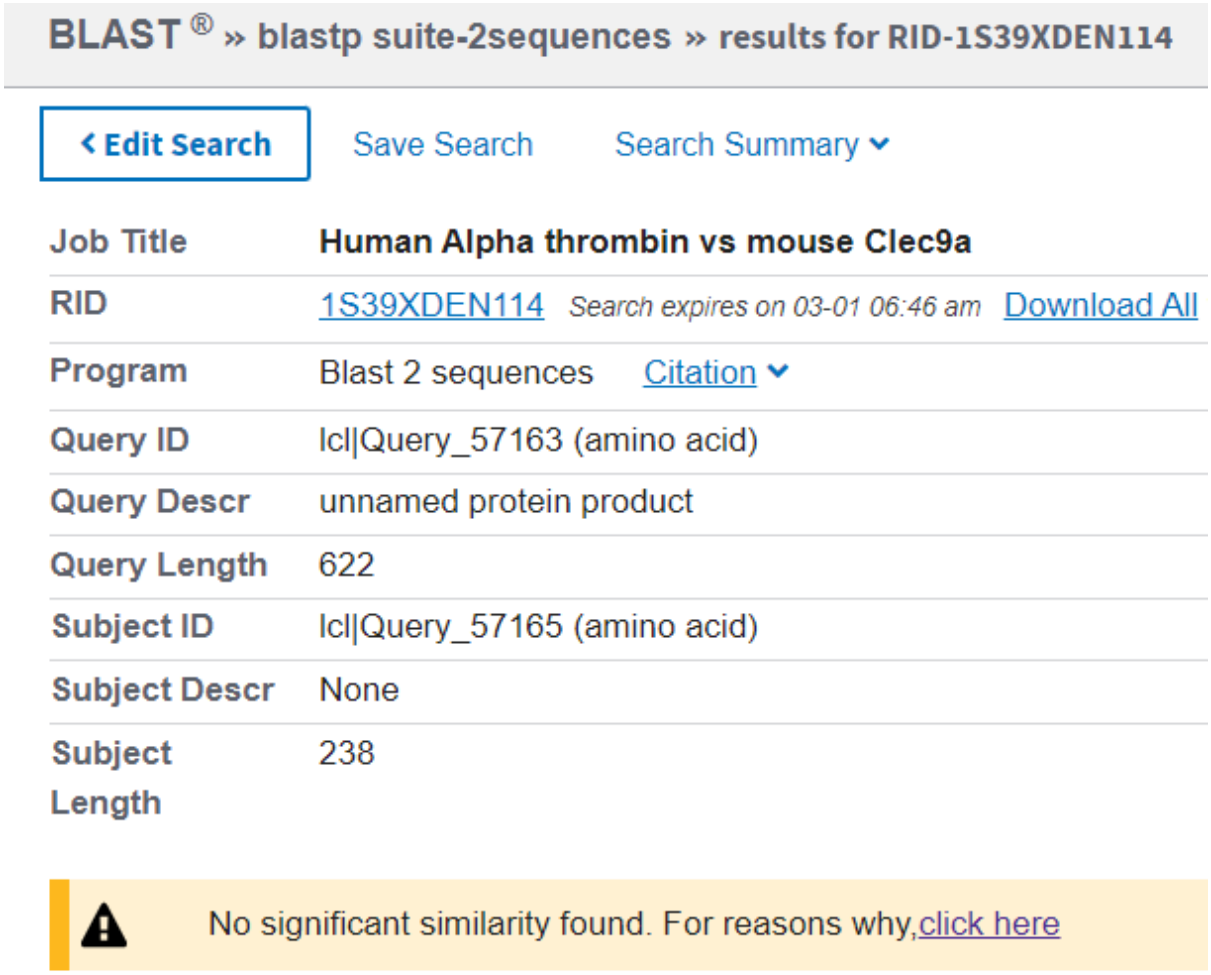

Figure 5.4: BLAST Sequence Alignment of Thrombin and Clec9a.

Appendix 6: Chemicals, Reagents, Consumables and Specialist Equipment and Software

Table 5.2: Table listing the chemicals and reagents used for all experiments

Component	Manufacturer	Catalogue number
10x buffer		
1x tris-acetate-EDTA Trizma® acetate EDTA	Sigma Aldrich, Merck	93337 ED4SS
2-Mercaptoethanol	Gibco™, ThermoFisher Scientific, New Zealand	21985-023
2-Propanol (Isopropanol)	Sigma Aldrich, Merck	67630
Acid rinse	Decon Laboratories™ Fisher Scientific, Thermo Fisher Scientific	DEC#D/0029/21
B220 APC	BD Biosciences, USA	561880
Buffer QX1	Qiagen, New Zealand	20021
Buffer RA1	Takara Bio, USA	740902.250
Buffer RA2	Takara Bio, USA	740902.250
Buffer RA3	Takara Bio, USA	740902.250
Carrier RNA	Takara Bio, USA	740902.250
CD11c Pe-Cy7	BD Biosciences, USA	558079
CD8 BUV395	BD Biosciences, USA	563786
Clec9A PE	BioLegend, USA	743504
Decomatic	Decon Laboratories™, ThermoFisher Scientific, New Zealand	DEC5
Dimethyl sulfoxide	Sigma-Aldrich, Merck, Germany	D2650-5X5ML
DNA clean-up and binding buffer	Monarch®, New England BioLabs, New Zealand	T1030L
DNA gel loading dye	Thermo Scientific™, ThermoFisher Scientific	R0611

DNase	Roche, Sigma-Aldrich, Merck, Germany	104159001
dNTPs		
Ethanol	Sigma-Aldrich, Merch, Germany	E7023
Flow cytometry staining buffer	Gibco™, ThermoFisher Scientific	14190-250 10091-148
Foetal bovine serum	Gibco™, ThermoFisher Scientific	10091148
GeneRuler Low Range DNA Ladder	Thermo Scientific™, ThermoFisher Scientific	SM1193
Gold III chloride trihydrate	Sigma Aldrich, Merck, Germany	520918-5G
HotMasterTaq		
Hydrochloric acid	Sigma Aldrich, Merck, Germany	07104
Igepal®	Sigma Aldrich, Merck	I8896
Iscove's Modified Dulbecco's Medium	Gibco™, ThermoFisher Scientific	31980-030
Liberase	Roche, Sigma-Aldrich, Merck, Germany	54102001
Membrane desalting buffer	Takara Bio, USA	740902.250
MHCII BV421	BD Biosciences, New Zealand	BD 562564
Minimum Essential Medium α	Gibco™, ThermoFisher Scientific	12571063
Nitric acid	Sigma Aldrich, Merck, Germany	438073
NuSieve™ GTG™ Genetic technology grade agarose	Lonza, New Zealand	50081
Pen/Strep	Life Technologies, ThermoFisher Scientific, New Zealand	15070-063
Phosphate buffered saline	Gibco™, ThermoFisher Scientific	10010023

Protein G magnetic beads	New England Biolabs, New Zealand	S1430S
rDNAse	Takara Bio, USA	740902.250
Recombinant mouse Clec9A Fc chimera protein	R&D Systems, In Vitro Technologies, New Zealand	6776-CL-050
Red blood cell lysis buffer	Qiagen, USA	158904
Skim milk	Millipore, Sigma Aldrich, Merck	70166
Sodium acetate	Sigma Aldrich, Merck, Germany	S2889
Sodium bicarbonate	Sigma Aldrich, Merck, Germany	V0T0183
Sodium chloride	Fisher Chemical™, ThermoFisher Scientific	S-3160-53
Sodium hydroxide pellets	Sigma Aldrich, Merck, Germany	S8045
Sodium phosphate	Sigma-Aldrich, Merch, Germany	S9763
Solubilisation and binding buffer (Buffer QG)	Qiagen, New Zealand	19063
Streptavidin magnetic beads	New England Biolabs, New Zealand	S1420S
Superscript enzyme mix	Invitrogen™, ThermoFisher Scientific	11754050
SYBR		
SYBR green qPCR mastermix	Agilent, Integrated Sciences, Australia	600828
Tris(2-carboxyethyl)phosphine	Takara Bio, USA	740902.250
Trisodium citrate dihydrate	Sigma Aldrich, Merck, Germany	W302600
Trypan blue	Gibco™, ThermoFisher Scientific	15250061
TrypLE	Gibco™, ThermoFisher Scientific	12563029

Ultra-Pure H_2O	Invitrogen™, ThermoFisher Scientific	10977015
Ultrapure mouse CD11c microbeads	Miltenyi Biotec, USA	130-125-835
VILO reaction mix	Invitrogen™, ThermoFisher Scientific	11754050
Wash buffer (Buffer PE)	Qiagen, New Zealand	19065
XCR1 (BV421, FR)	BioLegend, USA	148216
Zombie NIR	BioLegend, USA	423105
Trisodium citrate dihydrate	Sigma Aldrich, Merck, Germany	6132-04-3

Table 5.3: Table listing the consumables and equipment used for experiments

Consumable	Manufacturer	Catalogue number
0.2-2 µL pipette	Finnpipette™, Thermo Scientific™, ThermoFisher Scientific, New Zealand	4641010N
0.2-2 µL pipette tips	Interlab, New Zealand	1038-260
0.5 mm Quartz cuvette	SUPRASIL®, Hellma Analytics, Sigma Aldrich, New Zealand	Z800058
1 L Duran® laboratory bottle with cap	Sigma Aldrich, Merck, Germany	Z305200-10EA
1 mL Transfer pipette	Interlab, New Zealand	AP-1-B
1.5 mL Cryogenic vials	Nalgene®, Sigma Aldrich, Merck, Germany	Z359033-500EA
1.5 mL microtube	Axygen®, Bio-Strategy, New Zealand	525-0226
10 mL Serological pipette	Corning, Bio-Strategy, New Zealand	CORN4488
100 mL Erlenmeyer flask	Duran®, Sigma Aldrich, Merck, Germany	DWK212162806
100 mL measuring cylinder	Blaubrand®, Sigma Aldrich, Merck, Germany	Z324353

100 mL Volumetric flask	Pyrex®, Sigma Aldrich, Merck, Germany	CLS5641100
100-1000 µL pipette	Finnpipette™, Thermo Scientific™, ThermoFisher Scientific, New Zealand	4641100N
100-1000 µL pipette tips	Interlab, New Zealand	1019-260
10-100 µL Multichannel Pipette	Finnpipette™, Thermo Scientific™, ThermoFisher Scientific, New Zealand	4662020
1-10 µL Multichannel pipette	Finnpipette™, Thermo Scientific™, ThermoFisher Scientific, New Zealand	4662000
15 mL centrifuge tube	Corning, Bio-Strategy, New Zealand	CORN430791
2 mL microtube	Axygen®, Bio-Strategy, New Zealand	525-0228
20-200 µL pipette	Finnpipette™, Thermo Scientific™, ThermoFisher Scientific, New Zealand	4641080N
20-200 µL pipette tips	Interlab, New Zealand	1030-260
2-20 µL pipette	Finnpipette™, Thermo Scientific™, ThermoFisher Scientific, New Zealand	4641060N
2-20 µL pipette tips	Interlab, New Zealand	1030-260
25 mL Serological pipette	Corning, Bio-Strategy, New Zealand	CORN4489
35 mm Culture dish, Non-treated	Corning®, Sigma Aldrich, Merck, Germany	CLS430588-500EA
5 mL Serological pipette	Corning, Bio-Strategy, New Zealand	CORN4487
50 mL Duran® laboratory bottle with cap	Sigma Aldrich, Merck, Germany	Z305162
50 mL flacon tube	Corning, Bio-Strategy, New Zealand	CORN430829

500 mL Duran® laboratory bottle with cap	Sigma Aldrich, Merck, Germany	Z305197-10EA
6 well plate non-treated, with closure	ThermoFisher Scientific, New Zealand	150239
600 mL microtube	Axygen®, Bio-Strategy, New Zealand	525-0225
70 µM cell strainer	Fisherbrand™, Fisher Scientific, ThermoFisher Scientific, New Zealand	22-363-548
96 well plate non-treated, with closure	ThermoFisher Scientific, New Zealand	M33089
Aluminium spacer	SUPRASIL®, Hellma Analytics, Sigma Aldrich, New Zealand	013-101-71
Amicon Ultracel® 0.5 mL 30kDA cutoff centrifugal filter	Millipore, Sigma Aldrich, Merck, Germany	UFC503024
Amicon® Ultra-0.5 tube	Millipore, Sigma Aldrich, Merck, Germany	UFC503024
Conical flask	Alrdich®, Sigma Aldrich, Merck, Germany	Z723096
CoolCell®	Corning, Australia	432000
Falcon® 5 mL round bottom, polysterine flow cytometry tubes	StemCell Technologies, New Zealand	100-0088
Glass connector	Pyrex®, Sigma Aldrich, Merck, Germany	CLS2360500
Glass leibig condenser with bottom ST joint	Pyrex®, Sigma Aldrich, Merck, Germany	CLS2360500
Goggles	3M™, ThermoFisher Scientific, New Zealand	2720-ASTS
Inverted microscope, Olympus IX51	Olympus, New Zealand	
Kimwipes®	MediRay, Kimtech Science®, New Zealand	KC34120

MagJET separation rack 2 x 1.5 mL	Thermo Scientific™, ThermoFisher Scientific, New Zealand	MR01
Magnetic stirring and heating plate	Cimarec+™, Thermo Scientific, ThermoFisher Scientific, New Zealand	SP88857108
MinElute® spin column	Qiagen, New Zealand	28104
Mini-sub Cell GT gel tank, Gel electrophoresis tank	Bio-Rad, USA	1704487EDU
Nebauer Hemocytometer, Double ruling	Boeco, Germany	BOE 01
Nitrile gloves	LabServ, ThermoFisher Scientific, New Zealand	90202
NucleoSpin centrifugal filter	Takara Bio, USA	740902.250
Nunc™ T175 culture flask, polystyrene	Thermo Scientific™, ThermoFisher Scientific, New Zealand	159910
Nunc™ T25 culture flask, polystyrene	Thermo Scientific™, ThermoFisher Scientific, New Zealand	156367
Nunc™ T75 culture flask, polystyrene	Thermo Scientific™, ThermoFisher Scientific, New Zealand	156499
Pipette gun	Thermo Scientific™, ThermoFisher Scientific, New Zealand	9531
QIAquick PCR purification kit	Qiagen, New Zealand	28104
qPCR 0.1 mL reaction strip tubes and caps	Qiagen, New Zealand	981103
Scalpel	TTR Stores, VUW, New Zealand	
UV transilluminator 2000	Bio-Rad, USA	1708110EDU
See saw rocker		
Rotator		

Table 5.4: Table listing the specialist equipment and software used

Equipment	Manufacturer	Catalogue Number
AutoMACS pro separator	Milteyni Biotec, USA	
BD LSR Fortessa	BD Biosciences, USA	
Chirascan CD spectrophotometer	Applied Photophysics, UK	
Chirascan plus software	Applied Photophysics, UK	
Cytek Aurora Borealis	Cytek, USA	
Dell, Ubuntu 20.04.3 LTS GNU/Linux Bioinformatics computer	Ubuntu, Canonical, UK	
Excel	Microsoft, New Zealand	
FACS Diva software	BD Biosciences, USA	
FASTAptamer	Burke Lab, University of Missouri, USA	
FlaskScrubber, Dishwasher	Labconco, USA	4420321
FlowJo	BD Biosciences, USA	
IBM SPSS analytical software	IBM, USA	
NanoDrop 2000	Thermo Scientific™, ThermoFisher Scientific, New Zealand	ND-2000
OligoAnalyzer	IDT DNA, USA	
Omega Lum G Imaging system	Aplegen, Gel Company, USA	81-12100-00
Primer 3	National Human Genome Research Institute, USA	
QuantStudio3	ThermoFisher Scientific, New Zealand	A28567
Qubit 3.0	Life Technologies, ThermoFisher Scientific, New Zealand	Q33216
Rotor-Gene Rotary Analyzer 6000	Qiagen, New Zealand	11754-050

SPECTROstar Nano Absorbance plate reader	BMG Labtech, Germany
Spectrostar software	BMG Labtech, Germany

REFERENCES

Akerström, B., Brodin, T., Reis, K., & Björck, L. (1985). Protein G: a powerful tool for binding and detection of monoclonal and polyclonal antibodies. *The Journal of Immunology*, *135*(4), 2589-2592.

Alam, K. K., Chang, J. L., & Burke, D. H. (2015). FASTAptamer: a bioinformatic toolkit for high-throughput sequence analysis of combinatorial selections. *Molecular Therapy-Nucleic Acids*, *4*, e230.

Amano, R., Takada, K., Tanaka, Y., Nakamura, Y., Kawai, G., Kozu, T., & Sakamoto, T. (2016). Kinetic and thermodynamic analyses of interaction between a high-affinity RNA aptamer and its target protein. *Biochemistry*, *55*(45), 6221-6229.

Avci-Adali, M., Wilhelm, N., Perle, N., Stoll, H., Schlensak, C., & Wendel, H. P. (2013). Absolute quantification of cell-bound DNA aptamers during SELEX. *Nucleic acid therapeutics*, *23*(2), 125-130.

Bachem, A., Hartung, E., Güttler, S., Mora, A., Zhou, X., Hegemann, A., Plantinga, M., Mazzini, E., Stoitzner, P., & Gurka, S. (2012). Expression of XCR1 characterizes the Batf3-dependent lineage of dendritic cells capable of antigen cross-presentation. *Frontiers in immunology*, *3*, 214.

Backer, R. A., Diener, N., & Clausen, B. E. (2019). Langerin+ CD8+ dendritic cells in the splenic marginal zone: Not so marginal after all. *Frontiers in immunology*, *10*, 741.

Bai, C., Gao, S., Hu, S., Liu, X., Li, H., Dong, J., Huang, A., Zhu, L., Zhou, P., & Li, S. (2020). Self-assembled multivalent aptamer nanoparticles with potential CAR-like characteristics could activate T cells and inhibit melanoma growth. *Molecular Therapy-Oncolytics*, *17*, 9-20.

Bansal, M. (2003). DNA structure: Revisiting the Watson–Crick double helix. *Current Science*, 1556-1563.

Baskerville, S., Zapp, M., & Ellington, A. D. (1995). High-resolution mapping of the human T-cell leukemia virus type 1 Rex-binding element by in vitro selection. *Journal of virology*, *69*(12), 7559-7569.

Bauer, M., Strom, M., Hammond, D. S., & Shigdar, S. (2019). Anything you can do, I can do better: Can aptamers replace antibodies in clinical diagnostic applications? *Molecules*, *24*(23), 4377.

Bayat, P., Nosrati, R., Alibolandi, M., Rafatpanah, H., Abnous, K., Khedri, M., & Ramezani, M. (2018). SELEX methods on the road to protein targeting with nucleic acid aptamers. *Biochimie*, *154*, 132-155.

Beier, R., Boschke, E., & Labudde, D. (2014). New strategies for evaluation and analysis of SELEX experiments. *BioMed research international*, *2014*.

Berezovski, M. V., Lechmann, M., Musheev, M. U., Mak, T. W., & Krylov, S. N. (2008). Aptamer-facilitated biomarker discovery (AptaBiD). *Journal of the American Chemical Society*, *130*(28), 9137-9143.

Berg, K., Lange, T., Mittelberger, F., Schumacher, U., & Hahn, U. (2016). Selection and Characterization of an α6β4 Integrin blocking DNA Aptamer. *Molecular Therapy-Nucleic Acids*, *5*, e294.

Berglund, E. C., Kiialainen, A., & Syvänen, A.-C. (2011). Next-generation sequencing technologies and applications for human genetic history and forensics. *Investigative genetics*, *2*(1), 1-15.

Bittker, J. A., Le, B. V., & Liu, D. R. (2002). Nucleic acid evolution and minimization by nonhomologous random recombination. *Nature biotechnology*, *20*(10), 1024-1029.

Boczkowski, D., Nair, S. K., Snyder, D., & Gilboa, E. (1996). Dendritic cells pulsed with RNA are potent antigen-presenting cells in vitro and in vivo. *The Journal of experimental medicine*, *184*(2), 465-472.

Bonifaz, L. C., Bonnyay, D. P., Charalambous, A., Darguste, D. I., Fujii, S.-I., Soares, H., Brimnes, M. K., Moltedo, B., Moran, T. M., & Steinman, R. M. (2004). In vivo targeting of antigens to maturing dendritic cells via the DEC-205 receptor improves T cell vaccination. *The Journal of experimental medicine*, *199*(6), 815-824.

Borrebaeck, C. A., & Carlsson, R. (2001). Human therapeutic antibodies. *Current opinion in pharmacology*, *1*(4), 404-408.

Bottari, F., Daems, E., de Vries, A.-M., Van Wielendaele, P., Trashin, S., Blust, R., Sobott, F., Madder, A., Martins, J. C., & De Wael, K. (2020). Do aptamers always bind? The need for a multifaceted analytical approach when demonstrating binding affinity between aptamer and low molecular weight compounds. *Journal of the American Chemical Society*, *142*(46), 19622-19630.

Bregy, A., Wong, T. M., Shah, A. H., Goldberg, J. M., & Komotar, R. J. (2013). Active immunotherapy using dendritic cells in the treatment of glioblastoma multiforme. *Cancer treatment reviews*, *39*(8), 891-907.

Brown, M. G., Scalzo, A. A., Matsumoto, K., & Yokoyama, W. M. (1997). The natural killer gene complex: a genetic basis for understanding natural killer cell function and innate immunity. *Immunological reviews*, *155*(1), 53-65.

Bruno, J. G., & Kiel, J. L. (2002). Use of magnetic beads in selection and detection of biotoxin aptamers by electrochemiluminescence and enzymatic methods. *BioTechniques*, *32*(1), 178-183.

Bunka, D. H., Platonova, O., & Stockley, P. G. (2010). Development of aptamer therapeutics. *Current opinion in pharmacology*, *10*(5), 557-562.

Cai, S., Yan, J., Xiong, H., Liu, Y., Peng, D., & Liu, Z. (2018). Investigations on the interface of nucleic acid aptamers and binding targets. *Analyst*, *143*(22), 5317-5338.

Caminschi, I., Proietto, A. I., Ahmet, F., Kitsoulis, S., Shin Teh, J., Lo, J. C., Rizzitelli, A., Wu, L., Vremec, D., & van Dommelen, S. L. (2008). The dendritic cell subtype-restricted C-type lectin Clec9A is a target for vaccine enhancement. *Blood, The Journal of the American Society of Hematology*, *112*(8), 3264-3273.

Carothers, J. M., Oestreich, S. C., Davis, J. H., & Szostak, J. W. (2004). Informational complexity and functional activity of RNA structures. *Journal of the American Chemical Society*, *126*(16), 5130-5137.

Carothers, J. M., Oestreich, S. C., & Szostak, J. W. (2006). Aptamers selected for higher-affinity binding are not more specific for the target ligand. *Journal of the American Chemical Society*, *128*(24), 7929-7937.

Catapano, A., & Papadopoulos, N. (2013). The safety of therapeutic monoclonal antibodies: implications for cardiovascular disease and targeting the PCSK9 pathway. *Atherosclerosis*, *228*(1), 18-28.

Chames, P., Van Regenmortel, M., Weiss, E., & Baty, D. (2009). Therapeutic antibodies: successes, limitations and hopes for the future. *British journal of pharmacology*, *157*(2), 220-233.

Chantret, I., Rodolosse, A., Barbat, A., Dussaulx, E., Brot-Laroche, E., Zweibaum, A., & Rousset, M. (1994). Differential expression of sucrase-isomaltase in clones isolated from early and late passages of the cell line Caco-2: evidence for glucose-dependent negative regulation. *Journal of cell science*, *107*(1), 213-225.

Chatterjee, B., Kalyani, N., Anand, A., Khan, E., Das, S., Bansal, V., Kumar, A., & Sharma, T. K. (2020). GOLD SELEX: a novel SELEX approach for the development of high-affinity aptamers against small molecules without residual activity. *Microchimica Acta*, *187*(11), 1-13.

Chen, A., & Yang, S. (2015). Replacing antibodies with aptamers in lateral flow immunoassay. *Biosensors and bioelectronics*, *71*, 230-242.

Chen, M., Yu, Y., Jiang, F., Zhou, J., Li, Y., Liang, C., Dang, L., Lu, A., & Zhang, G. (2016). Development of cell-SELEX technology and its application in cancer diagnosis and therapy. *International journal of molecular sciences*, *17*(12), 2079.

Chen, P. W., Wang, M., Bronte, V., Zhai, Y., Rosenberg, S. A., & Restifo, N. P. (1996). Therapeutic antitumor response after immunization with a recombinant adenovirus encoding a model tumor-associated antigen. *The Journal of Immunology*, *156*(1), 224-231.

Chivers, C. E., Koner, A. L., Lowe, E. D., & Howarth, M. (2011). How the biotin–streptavidin interaction was made even stronger: investigation via crystallography and a chimaeric tetramer. *Biochemical Journal*, *435*(1), 55-63.

Chu, T. C., Twu, K. Y., Ellington, A. D., & Levy, M. (2006). Aptamer mediated siRNA delivery. *Nucleic acids research*, *34*(10), e73-e73.

Chung, C. H., Mirakhur, B., Chan, E., Le, Q.-T., Berlin, J., Morse, M., Murphy, B. A., Satinover, S. M., Hosen, J., & Mauro, D. (2008). Cetuximab-induced anaphylaxis and IgE specific for galactose-α-1, 3-galactose. *New England Journal of Medicine*, *358*(11), 1109-1117.

Civit, L., Taghdisi, S. M., Jonczyk, A., Haßel, S. K., Gröber, C., Blank, M., Stunden, H. J., Beyer, M., Schultze, J., & Latz, E. (2018). Systematic evaluation of cell-SELEX enriched aptamers binding to breast cancer cells. *Biochimie*, *145*, 53-62.

Cowan, J. A., Ohyama, T., Wang, D., & Natarajan, K. (2000). Recognition of a cognate RNA aptamer by neomycin B: quantitative evaluation of hydrogen bonding and electrostatic interactions. *Nucleic acids research*, *28*(15), 2935-2942.

Cueto, F. J., Del Fresno, C., & Sancho, D. (2020). DNGR-1, a dendritic cell-specific sensor of tissue damage that dually modulates immunity and inflammation. *Frontiers in immunology*, 3146.

Daems, E., Moro, G., Campos, R., & De Wael, K. (2021). Mapping the gaps in chemical analysis for the characterisation of aptamer-target interactions. *TrAC Trends in Analytical Chemistry*, *142*, 116311.

Dao, P., Hoinka, J., Takahashi, M., Zhou, J., Ho, M., Wang, Y., Costa, F., Rossi, J. J., Backofen, R., & Burnett, J. (2016). AptaTRACE elucidates RNA sequence-structure motifs from selection trends in HT-SELEX experiments. *Cell systems*, *3*(1), 62-70.

Davies, B., & Fried, M. (1995). The L19 ribosomal protein gene (RPL19): Gene organization, chromosomal mapping, and novel promoter region. *Genomics*, *25*(2), 372-380.

Demlová, R., Valík, D., Obermannová, R., & ZDRAŽILOVÁ-DUBSKÁ, L. (2016). The safety of therapeutic monoclonal antibodies: implications for cancer therapy including immuno-checkpoint inhibitors. *Physiological research*, *65*.

Dhodapkar, M. V., Sznol, M., Zhao, B., Wang, D., Carvajal, R. D., Keohan, M. L., Chuang, E., Sanborn, R. E., Lutzky, J., & Powderly, J. (2014). Induction of antigen-specific immunity with a vaccine targeting NY-ESO-1 to the dendritic cell receptor DEC-205. *Science translational medicine*, *6*(232), 232ra251-232ra251.

Di Primo, C., & Lebars, I. (2007). Determination of refractive index increment ratios for protein–nucleic acid complexes by surface plasmon resonance. *Analytical biochemistry*, *368*(2), 148-155.

Djordjevic, M. (2007). SELEX experiments: new prospects, applications and data analysis in inferring regulatory pathways. *Biomolecular engineering*, *24*(2), 179-189.

Dobbelstein, M., & Shenk, T. (1995). In vitro selection of RNA ligands for the ribosomal L22 protein associated with Epstein-Barr virus-expressed RNA by using randomized and cDNA-derived RNA libraries. *Journal of virology*, *69*(12), 8027-8034.

Doessegger, L., & Banholzer, M. L. (2015). Clinical development methodology for infusion-related reactions with monoclonal antibodies. *Clinical & translational immunology*, *4*(7), e39.

Drexler, H., Dirks, W., Matsuo, Y., & MacLeod, R. (2003). False leukemia–lymphoma cell lines: an update on over 500 cell lines. *Leukemia*, *17*(2), 416-426.

Dua, P., Kim, S., & Lee, D.-k. (2011). Nucleic acid aptamers targeting cell-surface proteins. *Methods*, *54*(2), 215-225.

Dunand-Sauthier, I., Irla, M., Carnesecchi, S., Seguín-Estévez, Q., Vejnar, C. E., Zdobnov, E. M., Santiago-Raber, M.-L., & Reith, W. (2014). Repression of arginase-2 expression in dendritic cells by microRNA-155 is critical for promoting T cell proliferation. *The Journal of Immunology*, *193*(4), 1690-1700.

Dunand-Sauthier, I., Santiago-Raber, M.-L., Capponi, L., Vejnar, C. E., Schaad, O., Irla, M., Seguín-Estévez, Q., Descombes, P., Zdobnov, E. M., & Acha-Orbea, H. (2011). Silencing of c-Fos expression by microRNA-155 is critical for dendritic cell maturation and function. *Blood, The Journal of the American Society of Hematology*, *117*(17), 4490-4500.

Dyall, J., Latouche, J.-B., Schnell, S., & Sadelain, M. (2001). Lentivirus-transduced human monocyte-derived dendritic cells efficiently stimulate antigen-specific cytotoxic T lymphocytes. *Blood, The Journal of the American Society of Hematology*, *97*(1), 114-121.

Eaton, R. M., Shallcross, J. A., Mael, L. E., Mears, K. S., Minkoff, L., Scoville, D. J., & Whelan, R. J. (2015). Selection of DNA aptamers for ovarian cancer biomarker HE4 using CE-SELEX and high-throughput sequencing. *Analytical and bioanalytical chemistry*, *407*(23), 6965-6973.

Ellington, A. D., & Szostak, J. W. (1990). In vitro selection of RNA molecules that bind specific ligands. *Nature*, *346*(6287), 818-822.

Elvin, J. G., Couston, R. G., & Van Der Walle, C. F. (2013). Therapeutic antibodies: market considerations, disease targets and bioprocessing. *International journal of pharmaceutics*, *440*(1), 83-98.

Famulok, M. (1994). Molecular recognition of amino acids by RNA-aptamers: an L-citrulline binding RNA motif and its evolution into an L-arginine binder. *Journal of the American Chemical Society*, *116*(5), 1698-1706.

Farid, S. S., Baron, M., Stamatis, C., Nie, W., & Coffman, J. (2020). Benchmarking biopharmaceutical process development and manufacturing cost contributions to R&D. MAbs,

Farran, B., Pavitra, E., Kasa, P., Peela, S., Raju, G. S. R., & Nagaraju, G. P. (2019). Folate-targeted immunotherapies: passive and active strategies for cancer. *Cytokine & growth factor reviews*, *45*, 45-52.

Feroze-Merzoug, F., Berquin, I., Dey, J., & Chen, Y. (2002). Peptidylprolyl isomerase A (PPIA) as a preferred internal control over GAPDH and β-actin in quantitative RNA analyses. *BioTechniques*, *32*(4), 776-782.

Figdor, C. G., de Vries, I. J. M., Lesterhuis, W. J., & Melief, C. J. (2004). Dendritic cell immunotherapy: mapping the way. *Nature medicine*, *10*(5), 475-480.

Firer, M. A., & Gellerman, G. (2012). Targeted drug delivery for cancer therapy: the other side of antibodies. *Journal of hematology & oncology*, *5*(1), 1-16.

Fuertes Marraco, S. A., Grosjean, F., Duval, A., Rosa, M., Lavanchy, C., Ashok, D., Haller, S., Otten, L., Steiner, Q.-G., & Descombes, P. (2012). Novel murine dendritic cell lines: a powerful auxiliary tool for dendritic cell research. *Frontiers in immunology*, *3*, 331.

Gilboa, E., Berezhnoy, A., & Schrand, B. (2015). Reducing toxicity of immune therapy using aptamer-targeted drug delivery. *Cancer immunology research*, *3*(11), 1195-1200.

Gold, L., Janjic, N., Jarvis, T., Schneider, D., Walker, J. J., Wilcox, S. K., & Zichi, D. (2012). Aptamers and the RNA world, past and present. *Cold Spring Harbor perspectives in biology*, *4*(3), a003582.

Gopinath, S. C. B. (2007). Methods developed for SELEX. *Analytical and bioanalytical chemistry*, *387*(1), 171-182.

Gordon, B. R. (1995). Immunotherapy basics. *Otolaryngology–Head and Neck Surgery*, *113*(5), 597-602.

Graham, B. S., & Ambrosino, D. M. (2015). History of passive antibody administration for prevention and treatment of infectious diseases. *Current Opinion in HIV and AIDS*, *10*(3), 129.

Haghighi, M., Khanahmad, H., & Palizban, A. (2018). Selection and characterization of single-stranded DNA aptamers binding human B-cell surface protein CD20 by cell-SELEX. *Molecules*, *23*(4), 715.

Hall, B., Micheletti, J. M., Satya, P., Ogle, K., Pollard, J., & Ellington, A. D. (2009). Design, synthesis, and amplification of DNA pools for in vitro selection. *Current protocols in nucleic acid chemistry*, *39*(1), 9.2. 1-9.2. 28.

He, L.-Z., Crocker, A., Lee, J., Mendoza-Ramirez, J., Wang, X.-T., Vitale, L. A., O'Neill, T., Petromilli, C., Zhang, H.-F., & Lopez, J. (2007). Antigenic targeting of the human mannose receptor induces tumor immunity. *The Journal of Immunology*, *178*(10), 6259-6267.

He, M., Chai, Y., Qi, J., Zhang, C. W., Tong, Z., Shi, Y., Yan, J., Tan, S., & Gao, G. F. (2017). Remarkably similar CTLA-4 binding properties of therapeutic ipilimumab and tremelimumab antibodies. *Oncotarget*, *8*(40), 67129.

Heath, W. R., Belz, G. T., Behrens, G. M., Smith, C. M., Forehan, S. P., Parish, I. A., Davey, G. M., Wilson, N. S., Carbone, F. R., & Villadangos, J. A. (2004). Cross-presentation, dendritic cell subsets, and the generation of immunity to cellular antigens. *Immunological reviews*, *199*(1), 9-26.

Hermann, T., & Patel, D. J. (2000). Adaptive recognition by nucleic acid aptamers. *Science*, *287*(5454), 820-825.

Hernandez, I., Bott, S. W., Patel, A. S., Wolf, C. G., Hospodar, A. R., Sampathkumar, S., & Shrank, W. H. (2018). Pricing of monoclonal antibody therapies: higher if used for cancer. *Am J Manag Care*, *24*(2), 109-112.

Hicke, B. J., Marion, C., Chang, Y.-F., Gould, T., Lynott, C. K., Parma, D., Schmidt, P. G., & Warren, S. (2001). Tenascin-C aptamers are generated using tumor cells and purified protein. *Journal of Biological Chemistry*, *276*(52), 48644-48654.

Ho, W. Y., Yee, C., & Greenberg, P. D. (2002). Adoptive therapy with CD8+ T cells: it may get by with a little help from its friends. *The Journal of clinical investigation*, *110*(10), 1415-1417.

Huang, B.-T., Lai, W.-Y., Chang, Y.-C., Wang, J.-W., Yeh, S.-D., Lin, E. P.-Y., & Yang, P.-C. (2017). A CTLA-4 antagonizing DNA aptamer with antitumor effect. *Molecular Therapy-Nucleic Acids*, *8*, 520-528.

Huang, Y.-F., Shangguan, D., Liu, H., Phillips, J. A., Zhang, X., Chen, Y., & Tan, W. (2009). Molecular assembly of an aptamer-drug conjugate for targeted drug delivery to tumor cells. *Chembiochem: a European journal of chemical biology*, *10*(5), 862.

Hughes, P., Marshall, D., Reid, Y., Parkes, H., & Gelber, C. (2007). The costs of using unauthenticated, over-passaged cell lines: how much more data do we need? *BioTechniques*, *43*(5), 575-586.

Huysamen, C., Willment, J. A., Dennehy, K. M., & Brown, G. D. (2008). CLEC9A is a novel activation C-type lectin-like receptor expressed on BDCA3+ dendritic cells and a subset of monocytes. *Journal of Biological Chemistry*, *283*(24), 16693-16701.

Inc., G. M. I. (2021). *Monoclonal Antibodies Market revenue to cross USD 380 Bn by 2027: Global Market Insights Inc.* Notified. Retrieved 03/11/2021 from https://www.globenewswire.com/news-release/2021/06/08/2243267/0/en/Monoclonal-Antibodies-Market-revenue-to-cross-USD-380-Bn-by-2027-Global-Market-Insights-Inc.html

Jayasena, S. D. (1999). Aptamers: an emerging class of molecules that rival antibodies in diagnostics. *Clinical Chemistry*, *45*(9), 1628-1650.

Joffre, O. P., Segura, E., Savina, A., & Amigorena, S. (2012). Cross-presentation by dendritic cells. *Nature Reviews Immunology*, *12*(8), 557-569.

Jørgensen, T., Haase, C., & Michelsen, B. (2002). Treatment of an immortalized APC cell line with both cytokines and LPS ensures effective T-cell activation in vitro. *Scandinavian journal of immunology*, *56*(5), 492-503.

Joshi, N. S., Akama-Garren, E. H., Lu, Y., Lee, D.-Y., Chang, G. P., Li, A., DuPage, M., Tammela, T., Kerper, N. R., & Farago, A. F. (2015). Regulatory T cells in tumor-associated tertiary lymphoid structures suppress anti-tumor T cell responses. *Immunity*, *43*(3), 579-590.

Kalra, P., Mishra, S. K., Kaur, S., Kumar, A., Prasad, H. K., Sharma, T. K., & Tyagi, J. S. (2018). G-quadruplex-forming DNA aptamers inhibit the DNA-binding function of HupB and Mycobacterium tuberculosis entry into host cells. *Molecular Therapy-Nucleic Acids*, *13*, 99-109.

Karimi-Busheri, F., Zadorozhny, V., Carrier, E., & Fakhrai, H. (2013). Molecular integrity and global gene expression of breast and lung cancer stem cells under long-term storage and recovery. *Cell and tissue banking*, *14*(2), 175-186.

Kasahara, S., & Clark, E. A. (2012). Dendritic cell-associated lectin 2 (DCAL2) defines a distinct CD8α− dendritic cell subset. *Journal of leukocyte biology*, *91*(3), 437-448.

Kato, K., Lian, L.-Y., Barsukov, I. L., Derrick, J. P., Kim, H., Tanaka, R., Yoshino, A., Shiraishi, M., Shimada, I., & Arata, Y. (1995). Model for the complex between protein G and an antibody Fc fragment in solution. *Structure*, *3*(1), 79-85.

Kaur, H. (2018). Recent developments in cell-SELEX technology for aptamer selection. *Biochimica et Biophysica Acta (BBA)-General Subjects*, *1862*(10), 2323-2329.

Kenneth Murphy, C. W. (2017). *Janeway's Immunobiology 9th Edition* [Textbook]. Garland Science.

Kerrigan, A. M., & Brown, G. D. (2010). Syk-coupled C-type lectin receptors that mediate cellular activation via single tyrosine based activation motifs. *Immunological reviews*, *234*(1), 335-352.

Khedri, M., Abnous, K., Rafatpanah, H., Nabavinia, M. S., Taghdisi, S. M., & Ramezani, M. (2020). Development and Evaluation of Novel Aptamers Specific for Human PD1 Using Hybrid Systematic Evolution of Ligands by Exponential Enrichment Approach. *Immunological Investigations*, *49*(5), 535-554.

Khedri, M., Rafatpanah, H., Abnous, K., Ramezani, P., & Ramezani, M. (2015). Cancer immunotherapy via nucleic acid aptamers. *International immunopharmacology*, *29*(2), 926-936.

Kilili, G. K., Tilton, L., & Karbiwnyk, C. M. (2016). NaOH concentration and streptavidin bead type are key factors for optimal DNA aptamer strand separation and isolation. *BioTechniques*, *61*(3), 114-116.

Kinghorn, A. B., Fraser, L. A., Liang, S., Shiu, S. C.-C., & Tanner, J. A. (2017). Aptamer bioinformatics. *International journal of molecular sciences*, *18*(12), 2516.

Kohlberger, M., & Gadermaier, G. (2021). SELEX: Critical factors and optimization strategies for successful aptamer selection. *Biotechnology and Applied Biochemistry*.

Kolm, C., Cervenka, I., Aschl, U. J., Baumann, N., Jakwerth, S., Krska, R., Mach, R. L., Sommer, R., DeRosa, M. C., & Kirschner, A. K. (2020). DNA aptamers against bacterial cells can be efficiently selected by a SELEX process using state-of-the art qPCR and ultra-deep sequencing. *Scientific reports*, *10*(1), 1-16.

Komarova, N., Barkova, D., & Kuznetsov, A. (2020). Implementation of High-Throughput Sequencing (HTS) in Aptamer Selection Technology. *International journal of molecular sciences*, *21*(22), 8774.

Komarova, N., & Kuznetsov, A. (2019). Inside the black box: what makes SELEX better? *Molecules*, *24*(19), 3598.

Koressaar, T., & Remm, M. (2007). Enhancements and modifications of primer design program Primer3. *Bioinformatics*, *23*(10), 1289-1291.

Kreutz, M., Tacken, P. J., & Figdor, C. G. (2013). Targeting dendritic cells—why bother? *Blood, The Journal of the American Society of Hematology*, *121*(15), 2836-2844.

Kypr, J., Kejnovská, I., Renčiuk, D., & Vorlíčková, M. (2009). Circular dichroism and conformational polymorphism of DNA. *Nucleic acids research*, *37*(6), 1713-1725.

Ladokhin, A. S., Fernández-Vidal, M., & White, S. H. (2010). CD spectroscopy of peptides and proteins bound to large unilamellar vesicles. *The Journal of membrane biology*, *236*(3), 247-253.

Langer, E. S. (2009). Trends in capacity utilization for therapeutic monoclonal antibody production. MAbs,

Lee, J. F., Stovall, G. M., & Ellington, A. D. (2006). Aptamer therapeutics advance. *Current opinion in chemical biology*, *10*(3), 282-289.

Li, H., & Rothberg, L. (2004). Colorimetric detection of DNA sequences based on electrostatic interactions with unmodified gold nanoparticles. *Proceedings of the National Academy of Sciences*, *101*(39), 14036-14039.

Li, W.-M., Bing, T., Wei, J.-Y., Chen, Z.-Z., Shangguan, D.-H., & Fang, J. (2014). Cell-SELEX-based selection of aptamers that recognize distinct targets on metastatic colorectal cancer cells. *Biomaterials*, *35*(25), 6998-7007.

Li, W., Yang, X., Wang, K., Tan, W., He, Y., Guo, Q., Tang, H., & Liu, J. (2008). Real-time imaging of protein internalization using aptamer conjugates. *Analytical chemistry*, *80*(13), 5002-5008.

Liang, C., Li, D., Zhang, G., Li, H., Shao, N., Liang, Z., Zhang, L., Lu, A., & Zhang, G. (2015). Comparison of the methods for generating single-stranded DNA in SELEX. *Analyst*, *140*(10), 3439-3444.

Liu, K., & Nussenzweig, M. C. (2010). Origin and development of dendritic cells. *Immunological reviews*, *234*(1), 45-54.

López-Colón, D., Jiménez, E., You, M., Gulbakan, B., & Tan, W. (2011). Aptamers: turning the spotlight on cells. *Wiley Interdisciplinary Reviews: Nanomedicine and Nanobiotechnology*, *3*(3), 328-340.

Lozano, T., Soldevilla, M. M., Casares, N., Villanueva, H., Bendandi, M., Lasarte, J. J., & Pastor, F. (2016). Targeting inhibition of Foxp3 by a CD28 2'-Fluro oligonucleotide aptamer conjugated to P60-peptide enhances active cancer immunotherapy. *Biomaterials*, *91*, 73-80.

Lozupone, C., Changayil, S., Majerfeld, I., & Yarus, M. (2003). Selection of the simplest RNA that binds isoleucine. *Rna*, *9*(11), 1315-1322.

Lyu, Y., Chen, G., Shangguan, D., Zhang, L., Wan, S., Wu, Y., Zhang, H., Duan, L., Liu, C., & You, M. (2016). Generating cell targeting aptamers for nanotheranostics using cell-SELEX. *Theranostics*, *6*(9), 1440.

Maduro, M. (2021). *The Maduro Lab, Random Sequence generator*. National Science Foundation. Retrieved 29.11.2021 from http://www.faculty.ucr.edu/~mmaduro/random.htm

Maiorella, B., Winkelhake, J., Young, J., Moyer, B., Bauer, R., Hora, M., Andya, J., Thomson, J., Patel, T., & Parekh, R. (1993). Effect of culture conditions on IgM antibody structure, pharmacokinetics and activity. *Bio/technology*, *11*(3), 387-392.

Mall, C., Sckisel, G. D., Proia, D. A., Mirsoian, A., Grossenbacher, S. K., Pai, C.-C. S., Chen, M., Monjazeb, A. M., Kelly, K., & Blazar, B. R. (2016). Repeated PD-1/PD-L1 monoclonal antibody administration induces fatal xenogeneic hypersensitivity reactions in a murine model of breast cancer. *Oncoimmunology*, *5*(2), e1075114.

Masters, J. R. (2004). Human cell cross-contamination since 1983. *In Vitro Cellular & Developmental Biology*, *40*, 10A.

Mayer, S., Moeller, R., Monteiro, J. T., Ellrott, K., Josenhans, C., & Lepenies, B. (2018). C-type lectin receptor (CLR)–Fc fusion proteins as tools to screen for novel CLR/bacteria interactions: an exemplary study on preselected Campylobacter jejuni isolates. *Frontiers in immunology*, *9*, 213.

Mayordomo, J., Zorina, T., Storkus, W., Zitvogel, L., Celluzzi, C., Falo, L., Melief, C., Ildstad, S., Kast, W. M., & Deleo, A. (1995). Bone marrow-derived dendritic cells pulsed with synthetic tumour peptides elicit protective and therapeutic antitumour immunity. *Nature medicine*, *1*(12), 1297-1302.

McKeague, M., De Girolamo, A., Valenzano, S., Pascale, M., Ruscito, A., Velu, R., Frost, N. R., Hill, K., Smith, M., & McConnell, E. M. (2015). Comprehensive analytical comparison of strategies used for small molecule aptamer evaluation. *Analytical chemistry*, *87*(17), 8608-8612.

McNamara, J. O., Andrechek, E. R., Wang, Y., Viles, K. D., Rempel, R. E., Gilboa, E., Sullenger, B. A., & Giangrande, P. H. (2006). Cell type–specific delivery of siRNAs with aptamer-siRNA chimeras. *Nature biotechnology*, *24*(8), 1005-1015.

Mehrling, T., & Soltis, D. (2018). Challenges in optimising the successful construction of antibody drug conjugates in cancer therapy. *Antibodies*, *7*(1), 11.

Mendonsa, S. D., & Bowser, M. T. (2005). In vitro selection of aptamers with affinity for neuropeptide Y using capillary electrophoresis. *Journal of the American Chemical Society*, *127*(26), 9382-9383.

Meyer, S., Maufort, J. P., Nie, J., Stewart, R., McIntosh, B. E., Conti, L. R., Ahmad, K. M., Soh, H. T., & Thomson, J. A. (2013). Development of an efficient targeted cell-SELEX procedure for DNA aptamer reagents. *PloS one*, *8*(8), e71798.

Mohammadinezhad, R., Jalali, S. A. H., & Farahmand, H. (2020). Evaluation of different direct and indirect SELEX monitoring methods and implementation of melt-curve analysis for rapid discrimination of variant aptamer sequences. *Analytical Methods*, *12*(30), 3823-3835.

Morton, W. R., Agy, M. B., Capuano, S. V., & Grant, R. F. (2008). Specific pathogen-free macaques: definition, history, and current production. *ILAR journal*, *49*(2), 137-144.

Mullard, A. (2021). FDA approves 100th monoclonal antibody product. *Nature reviews. Drug Discovery*.

Murphy, J. F. (2010). Trends in cancer immunotherapy. *Clinical Medicine Insights: Oncology*, *4*, CMO. S4795.

Nagatoishi, S., Isono, N., Tsumoto, K., & Sugimoto, N. (2011). Loop residues of thrombin-binding DNA aptamer impact G-quadruplex stability and thrombin binding. *Biochimie*, *93*(8), 1231-1238.

Nimmerjahn, F., & Ravetch, J. V. (2007). Antibodies, Fc receptors and cancer. *Current opinion in immunology*, *19*(2), 239-245.

Owczarzy, R., Tataurov, A. V., Wu, Y., Manthey, J. A., McQuisten, K. A., Almabrazi, H. G., Pedersen, K. F., Lin, Y., Garretson, J., & McEntaggart, N. O. (2008). IDT SciTools: a suite for analysis and design of nucleic acid oligomers. *Nucleic acids research*, *36*(suppl_2), W163-W169.

Ozer, A., White, B. S., Lis, J. T., & Shalloway, D. (2013). Density-dependent cooperative non-specific binding in solid-phase SELEX affinity selection. *Nucleic acids research*, *41*(14), 7167-7175.

Palucka, K., Ueno, H., Fay, J., & Banchereau, J. (2009). Harnessing dendritic cells to generate cancer vaccines. *Annals of the New York Academy of Sciences*, *1174*, 88.

Pardoll, D. M. (2002). Spinning molecular immunology into successful immunotherapy. *Nature Reviews Immunology*, *2*(4), 227-238.

Parekh, P., Kamble, S., Zhao, N., Zeng, Z., Portier, B. P., & Zu, Y. (2013). Immunotherapy of CD30-expressing lymphoma using a highly stable ssDNA aptamer. *Biomaterials*, *34*(35), 8909-8917.

Patel, D. J., & Suri, A. K. (2000). Structure, recognition and discrimination in RNA aptamer complexes with cofactors, amino acids, drugs and aminoglycoside antibiotics. *Reviews in Molecular Biotechnology*, *74*(1), 39-60.

Pelle, R., & Murphy, N. B. (1993). In vivo UV-cross-linking hybridization: a powerful technique for isolating RNA binding proteins. Application to trypanosome mini-exon derived RNA. *Nucleic acids research*, *21*(10), 2453-2458.

Pica, A., Russo Krauss, I., Parente, V., Tateishi-Karimata, H., Nagatoishi, S., Tsumoto, K., Sugimoto, N., & Sica, F. (2017). Through-bond effects in the ternary complexes of thrombin sandwiched by two DNA aptamers. *Nucleic acids research*, *45*(1), 461-469.

Plach, M., & Schubert, T. (2019). Biophysical characterization of aptamer-target interactions. *Aptamers in Biotechnology*, 1-15.

Pollard, J., Bell, S. D., & Ellington, A. D. (2000). Design, synthesis, and amplification of DNA pools for construction of combinatorial pools and libraries. *Current protocols in molecular biology*, *52*(1), 24.22. 21-24.22. 24.

Porgador, A., & Gilboa, E. (1995). Bone marrow-generated dendritic cells pulsed with a class I-restricted peptide are potent inducers of cytotoxic T lymphocytes. *The Journal of experimental medicine*, *182*(1), 255-260.

Potty, A. S., Kourentzi, K., Fang, H., Jackson, G. W., Zhang, X., Legge, G. B., & Willson, R. C. (2009). Biophysical characterization of DNA aptamer interactions with vascular endothelial growth factor. *Biopolymers: Original Research on Biomolecules*, *91*(2), 145-156.

Prante, M., Schüling, T., Roth, B., Bremer, K., & Walter, J. (2019). Characterization of an Aptamer directed against 25-hydroxyvitamin D for the development of a competitive aptamer-based Assay. *Biosensors*, *9*(4), 134.

Raghavendra, P., & Pullaiah, T. (2018). Pathogen identification using novel sequencing methods. *Advances in Cell and Molecular Diagnostics; Academic Press: London, UK*, 161-199.

Reichert, J. M., Rosensweig, C. J., Faden, L. B., & Dewitz, M. C. (2005). Monoclonal antibody successes in the clinic. *Nature biotechnology*, *23*(9), 1073-1078.

Riedl, T., van Boxtel, E., Bosch, M., Parren, P. W., & Gerritsen, A. F. (2016). High-throughput screening for internalizing antibodies by homogeneous fluorescence imaging of a pH-activated probe. *Journal of biomolecular screening*, *21*(1), 12-23.

Rizzo, J. M., & Buck, M. J. (2012). Key principles and clinical applications of “next-generation” DNA sequencing. *Cancer prevention research*, *5*(7), 887-900.

Rosch, J. C., Neal, E. H., Balikov, D. A., Rahim, M., & Lippmann, E. S. (2020). CRISPR-mediated isogenic cell-SELEX approach for generating highly specific aptamers against native membrane proteins. *Cellular and Molecular Bioengineering*, *13*(5), 559-574.

Ruso, J. M., & Piñeiro, Á. (2013). *Proteins in solution and at interfaces: methods and applications in biotechnology and materials science* (Vol. 8). John Wiley & Sons.

Samaranayake, H., Wirth, T., Schenkwein, D., Räty, J. K., & Ylä-Herttuala, S. (2009). Challenges in monoclonal antibody-based therapies. *Annals of medicine*, *41*(5), 322-331.

Sambuy, Y., De Angelis, I., Ranaldi, G., Scarino, M., Stammati, A., & Zucco, F. (2005). The Caco-2 cell line as a model of the intestinal barrier: influence of cell and culture-related factors on Caco-2 cell functional characteristics. *Cell biology and toxicology*, *21*(1), 1-26.

Sancho, D., Joffre, O. P., Keller, A. M., Rogers, N. C., Martinez, D., Hernanz-Falcón, P., Rosewell, I., & e Sousa, C. R. (2009). Identification of a dendritic cell receptor that couples sensing of necrosis to immunity. *Nature*, *458*(7240), 899-903.

Sancho, D., Mourão-Sá, D., Joffre, O. P., Schulz, O., Rogers, N. C., Pennington, D. J., Carlyle, J. R., & e Sousa, C. R. (2008). Tumor therapy in mice via antigen targeting to a novel, DC-restricted C-type lectin. *The Journal of clinical investigation*, *118*(6), 2098-2110.

Santulli-Marotto, S., Nair, S. K., Rusconi, C., Sullenger, B., & Gilboa, E. (2003). Multivalent RNA aptamers that inhibit CTLA-4 and enhance tumor immunity. *Cancer research*, *63*(21), 7483-7489.

Sassanfar, M., & Szostak, J. W. (1993). An RNA motif that binds ATP. *Nature*, *364*(6437), 550-553.

Savina, A., & Amigorena, S. (2007). Phagocytosis and antigen presentation in dendritic cells. *Immunological reviews*, *219*(1), 143-156.

Savory, N., Nzakizwanayo, J., Abe, K., Yoshida, W., Ferri, S., Dedi, C., Jones, B. V., & Ikebukuro, K. (2014). Selection of DNA aptamers against uropathogenic Escherichia coli NSM59 by quantitative PCR controlled Cell-SELEX. *Journal of microbiological methods*, *104*, 94-100.

Schilling-Loeffler, K., Rodriguez, R., & Williams-Woods, J. (2021). Target Affinity and Structural Analysis for a Selection of Norovirus Aptamers. *International journal of molecular sciences*, *22*(16), 8868.

Schmittgen, T. D., & Livak, K. J. (2008). Analyzing real-time PCR data by the comparative CT method. *Nature protocols*, *3*(6), 1101-1108.

Schuler, G., Schuler-Thurner, B., & Steinman, R. M. (2003). The use of dendritic cells in cancer immunotherapy. *Current opinion in immunology*, *15*(2), 138-147.

Sefah, K., Meng, L., Lopez-Colon, D., Jimenez, E., Liu, C., & Tan, W. (2010). DNA aptamers as molecular probes for colorectal cancer study. *PloS one*, *5*(12), e14269.

Seguín-Estévez, Q., Dunand-Sauthier, I., Lemeille, S., Iseli, C., Ibberson, M., Ioannidis, V., Schmid, C. D., Rousseau, P., Barras, E., & Geinoz, A. (2014). Extensive remodeling of DC function by rapid maturation-induced transcriptional silencing. *Nucleic acids research*, *42*(15), 9641-9655.

Shangguan, D., Bing, T., & Zhang, N. (2015). Cell-SELEX: Aptamer selection against whole cells. In *Aptamers selected by cell-SELEX for theranostics* (pp. 13-33). Springer.

Shangguan, D., Li, Y., Tang, Z., Cao, Z. C., Chen, H. W., Mallikaratchy, P., Sefah, K., Yang, C. J., & Tan, W. (2006). Aptamers evolved from live cells as effective molecular probes for cancer study. *Proceedings of the National Academy of Sciences*, *103*(32), 11838-11843.

Shaughnessy, A. F. (2012). Monoclonal antibodies: magic bullets with a hefty price tag. *Bmj*, *345*.

Shigdar, S., Qiao, L., Zhou, S.-F., Xiang, D., Wang, T., Li, Y., Lim, L. Y., Kong, L., Li, L., & Duan, W. (2013). RNA aptamers targeting cancer stem cell marker CD133. *Cancer letters*, *330*(1), 84-95.

Shigdar, S., Ward, A. C., De, A., Yang, C. J., Wei, M., & Duan, W. (2011). Clinical applications of aptamers and nucleic acid therapeutics in haematological malignancies. *British journal of haematology*, *155*(1), 3-13.

Shrimpton, R. E., Butler, M., Morel, A.-S., Eren, E., Hue, S. S., & Ritter, M. A. (2009). CD205 (DEC-205): a recognition receptor for apoptotic and necrotic self. *Molecular immunology*, *46*(6), 1229-1239.

Soldevilla, M., Villanueva, H., & Pastor, F. (2016). Aptamers: a feasible technology in cancer immunotherapy. *Journal of immunology research*, *2016*.

Song, W., Kong, H.-L., Carpenter, H., Torii, H., Granstein, R., Rafii, S., Moore, M. A., & Crystal, R. G. (1997). Dendritic cells genetically modified with an adenovirus vector encoding the cDNA for a model antigen induce protective and therapeutic antitumor immunity. *The Journal of experimental medicine*, *186*(8), 1247-1256.

Srinivasan, J., Cload, S. T., Hamaguchi, N., Kurz, J., Keene, S., Kurz, M., Boomer, R. M., Blanchard, J., Epstein, D., & Wilson, C. (2004). ADP-specific sensors enable universal assay of protein kinase activity. *Chemistry & biology*, *11*(4), 499-508.

Suh, S. H., Dwivedi, H. P., Choi, S. J., & Jaykus, L.-A. (2014). Selection and characterization of DNA aptamers specific for Listeria species. *Analytical biochemistry*, *459*, 39-45.

Svobodová, M., Pinto, A., Nadal, P., & O'Sullivan, C. (2012). Comparison of different methods for generation of single-stranded DNA for SELEX processes. *Analytical and bioanalytical chemistry*, *404*(3), 835-842.

Swanson, J. A., & Watts, C. (1995). Macropinocytosis. *Trends in cell biology*, *5*(11), 424-428.

Tabrizi, M., Bornstein, G. G., & Suria, H. (2010). Biodistribution mechanisms of therapeutic monoclonal antibodies in health and disease. *The AAPS journal*, *12*(1), 33-43.

Takahashi, M., Sakota, E., & Nakamura, Y. (2016). The efficient cell-SELEX strategy, Icell-SELEX, using isogenic cell lines for selection and counter-selection to generate RNA aptamers to cell surface proteins. *Biochimie*, *131*, 77-84.

Tang, Z., Shangguan, D., Wang, K., Shi, H., Sefah, K., Mallikratchy, P., Chen, H. W., Li, Y., & Tan, W. (2007). Selection of aptamers for molecular recognition and characterization of cancer cells. *Analytical chemistry*, *79*(13), 4900-4907.

Tao, X., He, F., Liu, X., Zhang, F., Wang, X., Peng, Y., & Liu, J. (2020). Detection of chloramphenicol with an aptamer-based colorimetric assay: critical evaluation of specific and unspecific binding of analyte molecules. *Microchimica Acta*, *187*(12), 1-11.

Theisen, D., & Murphy, K. (2017). The role of cDC1s in vivo: CD8 T cell priming through cross-presentation. *F1000Research*, *6*.

Thevendran, R., & Citartan, M. (2022). Assays to Estimate the Binding Affinity of Aptamers. *Talanta*, *238*, 122971.

Thiel, W. H., Bair, T., Peek, A. S., Liu, X., Dassie, J., Stockdale, K. R., Behlke, M. A., Miller Jr, F. J., & Giangrande, P. H. (2012). Rapid identification of cell-specific, internalizing RNA aptamers with bioinformatics analyses of a cell-based aptamer selection.

Thiviyanathan, V., & Gorenstein, D. G. (2012). Aptamers and the next generation of diagnostic reagents. *PROTEOMICS–Clinical Applications*, *6*(11-12), 563-573.

Thornton, B., & Basu, C. (2011). Real-time PCR (qPCR) primer design using free online software. *Biochemistry and Molecular Biology Education*, *39*(2), 145-154.

Tokoyoda, K., Hauser, A. E., Nakayama, T., & Radbruch, A. (2010). Organization of immunological memory by bone marrow stroma. *Nature Reviews Immunology*, *10*(3), 193-200.

Tolle, F., Wilke, J., Wengel, J., & Mayer, G. (2014). By-product formation in repetitive PCR amplification of DNA libraries during SELEX. *PloS one*, *9*(12), e114693.

Tuerk, C., & Gold, L. (1990). Systematic evolution of ligands by exponential enrichment: RNA ligands to bacteriophage T4 DNA polymerase. *Science*, *249*(4968), 505-510.

Tullett, K. M., Tan, P. S., Park, H.-Y., Schittenhelm, R. B., Michael, N., Li, R., Policheni, A. N., Gruber, E., Huang, C., & Fulcher, A. J. (2020). RNF41 regulates the damage recognition receptor Clec9A and antigen cross-presentation in mouse dendritic cells. *eLife*, *9*, e63452.

Uemachi, H., Kasahara, Y., Tanaka, K., Okuda, T., Yoneda, Y., & Obika, S. (2021). Hybrid-Type SELEX for the Selection of Artificial Nucleic Acid Aptamers Exhibiting Cell Internalization Activity. *Pharmaceutics*, *13*(6), 888.

Valencia, C. A., Pervaiz, M. A., Husami, A., Qian, Y., & Zhang, K. (2013). Sanger Sequencing Principles, History, and Landmarks. In *Next Generation Sequencing Technologies in Medical Genetics* (pp. 3-11). Springer.

Van Der Burg, S. H., Visseren, M., Brandt, R., Kast, W. M., & Melief, C. (1996). Immunogenicity of peptides bound to MHC class I molecules depends on the MHC-peptide complex stability. *The Journal of Immunology*, *156*(9), 3308-3314.

Velázquez-Campoy, A., Ohtaka, H., Nezami, A., Muzammil, S., & Freire, E. (2004). Isothermal titration calorimetry. *Current protocols in cell biology*, *23*(1), 17.18. 11-17.18. 24.

Wang, A. Z., & Farokhzad, O. C. (2014). Current progress of aptamer-based molecular imaging. *Journal of Nuclear Medicine*, *55*(3), 353-356.

Wang, P., Wang, X., Wang, L., Hou, X., Liu, W., & Chen, C. (2015a). Interaction of gold nanoparticles with proteins and cells. *Science and technology of advanced materials*.

Wang, Y., Wu, J., Chen, Y., Xue, F., Teng, J., Cao, J., Lu, C., & Chen, W. (2015b). Magnetic microparticle-based SELEX process for the identification of highly specific aptamers of heart marker--brain natriuretic peptide. *Microchimica Acta*, *182*(1), 331-339.

Wengerter, B. C., Katakowski, J. A., Rosenberg, J. M., Park, C. G., Almo, S. C., Palliser, D., & Levy, M. (2014). Aptamer-targeted antigen delivery. *Molecular Therapy*, *22*(7), 1375-1387.

Werner, R. G. (2004). Economic aspects of commercial manufacture of biopharmaceuticals. *Journal of Biotechnology*, *113*(1-3), 171-182.

Winnard, P. T., Pathak, A. P., Dhara, S., Cho, S. Y., Raman, V., & Pomper, M. G. (2008). Molecular imaging of metastatic potential. *Journal of Nuclear Medicine*, *49*(Suppl 2), 96S-112S.

Yamada, T. (2011). Therapeutic monoclonal antibodies. *The Keio journal of medicine*, *60*(2), 37-46.

Yazdian-Robati, R., Ramezani, M., Khedri, M., Ansari, N., Abnous, K., & Taghdisi, S. M. (2017). An aptamer for recognizing the transmembrane protein PDL-1 (programmed death-ligand 1), and its application to fluorometric single cell detection of human ovarian carcinoma cells. *Microchimica Acta*, *184*(10), 4029-4035.

Zarganes-Tzitzikas, T., Konstantinidou, M., Gao, Y., Krzemien, D., Zak, K., Dubin, G., Holak, T. A., & Dömling, A. (2016). Inhibitors of programmed cell death 1 (PD-1): a patent review (2010-2015). *Expert opinion on therapeutic patents*, *26*(9), 973-977.

Zhang, F., & Liu, J. (2021). Label-Free Colorimetric Biosensors Based on Aptamers and Gold Nanoparticles: A Critical Review. *Analysis & Sensing*, *1*(1), 30-43.

Zhang, J.-G., Czabotar, P. E., Policheni, A. N., Caminschi, I., San Wan, S., Kitsoulis, S., Tullett, K. M., Robin, A. Y., Brammananth, R., & van Delft, M. F. (2012). The dendritic cell receptor Clec9A binds damaged cells via exposed actin filaments. *Immunity*, *36*(4), 646-657.

Zhao, F., Zhou, J., Su, X., Wang, Y., Yan, X., Jia, S., & Du, B. (2017). A Smart Responsive Dual Aptamers-Targeted Bubble-Generating Nanosystem for Cancer Triplex Therapy and Ultrasound Imaging. *Small*, *13*(20), 1603990.

Zhao, N., Pei, S.-n., Parekh, P., Salazar, E., & Zu, Y. (2014). Blocking interaction of viral gp120 and CD4-expressing T cells by single-stranded DNA aptamers. *The international journal of biochemistry & cell biology*, *51*, 10-18.

Zhao, N., Pei, S.-N., Qi, J., Zeng, Z., Iyer, S. P., Lin, P., Tung, C.-H., & Zu, Y. (2015). Oligonucleotide aptamer-drug conjugates for targeted therapy of acute myeloid leukemia. *Biomaterials*, *67*, 42-51.

Zhou, J., & Rossi, J. (2017). Aptamers as targeted therapeutics: current potential and challenges. *Nature reviews Drug discovery*, *16*(3), 181-202.

Zhu, J., & Paul, W. E. (2008). CD4 T cells: fates, functions, and faults. *Blood, The Journal of the American Society of Hematology*, *112*(5), 1557-1569.

Zimmermann, G. R., WICK, C. L., SHIELDS, T. P., JENISON, R. D., & PARDI, A. (2000). Molecular interactions and metal binding in the theophylline-binding core of an RNA aptamer. *Rna*, *6*(5), 659-667.

Zong, C., & Liu, J. (2019). The arsenic-binding aptamer cannot bind arsenic: critical evaluation of aptamer selection and binding. *Analytical chemistry*, *91*(16), 10887-10893.

Zwaagstra, J. C., Sulea, T., Baardsnes, J., Radinovic, S., Cepero-Donates, Y., Robert, A., O'Connor-McCourt, M. D., Tikhomirov, I. A., & Jaramillo, M. L. (2019). Binding and functional profiling of antibody mutants guides selection of optimal candidates as antibody drug conjugates. *PloS one*, *14*(12), e0226593.